Analysis of vaccine

Structure, storage, moisture, and classification by infrared technology

Zheng, Yiwu

Publication date:
2006

Document Version
Publisher's PDF, also known as Version of record

Analysis of vaccine:
Structure, storage, moisture, and classification by infrared technology

Ph.D. Thesis by

Yiwu Zheng

2006

BioCentrum-DTU

Section of Biochemistry and Nutrition

Technical University of Denmark

Building 224, Sølvtofts Plads

2800 Kgs. Lyngby

Denmark

Preface

This thesis has been submitted as partial fulfilment of the requirement for a Ph.D. degree at the Technical University of Denmark. The work has been done at Biochemistry and Nutrition Group, BioCentrum-DTU and ALK-Abelló A/S. I would like to thank my supervisors Susanne Jacobsen and Henning Løwenstein for giving me the opportunity to do this project and for all the work they have done for me.

I specially wish to thank Ib Søndergaard, Henrik Ipsen, and Jørgen Nedergaard Larsen for enthusiastic discussions and the comments on the project and the thesis. If I were not with them, I would need a couple of more years to finish this Ph.D. project. I also would like to thank Charlotte Hejl for bridging the communication between the company and me when I worked at DTU. And also thank her for the helpful suggestion on the project. I want to thank Helene Henmar for the introduction of CD technique and the help on the experiments and data analysis. Mercedes Ferreras are greatly appreciated for the great discussion and references.

I want to thank Marianne K. Pertersen, Ljljana Nesic, Gitte Nordskov Hansen, and Lotte Friberg for the help in the labs. Susanne Warng Bruun is greatly appreciated for discussions of the same interest—infrared and that we have been able to support each other. I would like to thank all the people in the research department, ALK-Ablleó A/S and at Biochemistry and Nutrition Group, BioCentrum-DTU for kind help and the beautiful working environment. And also thank all the Danish and Chinese friends for your help during these years.

At last, but not the least, I would like to thank my pretty wife Xuxin and my lovely daughter Xinyi for all your love and supports.

Yiwu Zheng

June 2006, Denmark

Summary

Aims of this thesis

The research described in this thesis is to extend our knowledge on the properties of vaccines and antigens using fast and cheap infrared techniques. FTIR-ATR spectroscopy is applied to elucidate the structural changes when antigen is adsorbed by aluminium hydroxide and when it is subsequently released. The structural stability during the storage and heating process is investigated as well. The alterations of other parameters, such as adsorption, release, and pH are also investigated during the storage. FT-NIR is applied as a fast and non-destructive method to determine the residual moisture content in lyophilized vaccines and to classify and identify different vaccine products.

Organization of this thesis

In **Chapter I,** the background of the project and the introductions to infrared spectroscopy as well as chemometrics are given respectively. In **Chapter II**, the current techniques for protein structure analysis have been discussed, especially the FTIR-ATR method.

In **Chapter III,** the structural changes of two model antigens are investigated when they are adsorbed by aluminium hydroxide and the structures refold to their native state when they are released from adjuvant. The mechanism of the adjuvant enhancing the immune response is discussed in this chapter too.

Chapter IV describes the structural stability of adsorbed model antigens in thermal and aging process in comparison to the antigens in solutions. The results indicate that aluminium hydroxide can protect the structure of antigens against aggregation at high temperature and/or after long period storage. It is more pronounced for BSA. Further study is required to confirm if the protection is protein specific.

Chapter V gives the alterations of model vaccines during storage at two different temperatures. It demonstrates that the change of adsorption capacity by aluminium hydroxide during the storage is protein specific. The release of adsorbed protein from adjuvant decreases as a function of storing time. The pH and NIR absorbance also change. The aging effects undergo faster modification at 37 ºC than 4 ºC during the storage. The rotation effects when preparing vaccines are also discussed in this chapter as well.

NIR method for determination of residual moisture content of lyophilized allergen vaccines is

introduced in **Chapter VI**. Five different allergen vaccines are analyzed. Acceptable calibration model (RMESEP 10.20 µg H_2O / vial with 2 PLS factors) is obtained for multi-products data. The models based on product-specific data are slightly better (**Appendix B**). However, a general multi-products model is more attractive since one model can predict all samples. The reference data which are measured by Karl Fischer titration are presented in **Appendix A**.

NIR spectroscopy is applied to classify and identify five different allergen vaccines (the information of samples in **Appendix C**) at different concentrations of antigens and different batches in **Chapter VII**. The results show that NIR spectroscopy can be used to classify different allergen vaccines at highest antigen concentration (100,000 SQ) without api. The highest concentration products can be separated from other low concentrations. The discrimination of different batches may also be possible but need further experiments to confirm this. All SIMCA results are given in **Appendix C** to **Appendix S.**

Resumé

Hensigt med afhandlingen

Forskningsarbejdet, beskrevet i denne afhandling, skal øge vores viden om vacciners og antigeners egenskaber ved hjælp af hurtige og billige infrarød-teknikker. FTIR-ATR spektroskopi benyttes til bestemmelse af strukturændringer, når antigen adsorberer til aluminium hydroxid, og når det efterfølgende frigives. Den strukturelle stabilitet under opbevaringen og under opvarmningsprocessen undersøges ligeledes. Desuden undersøges ændringer i andre parametre, såsom adsorption, frigivelse og pH, under opbevaringen. FT-NIR benyttes som en hurtig og ikke-destruktiv metode til at bestemme resterende fugtindhold i frysetørrede vacciner og til at klassificere og identificere forskellige vaccineprodukter.

Organisering af afhandlingen

I **kapitel I** er baggrunden for projektet samt introduktion til infrarød spektroskopi og kemometri beskrevet. I **kapitel II** er de nuværende teknikker til protein-struktur-analyse, især FTIR-ATR metoden, blevet diskuteret.

I **kapitel III** er undersøgt strukturændringer af to model antigener ved adsorption til aluminium hydroxid samt deres foldning tilbage til nativ tilstand ved frigivelse fra adjuvanten. Mekanismen for den immunfremmende effekt af adjuvanten er ligeledes diskuteret.

Kapitel IV beskriver strukturel stabilitet af adsorberet modelantigen i termiske- og aldringsprocesser sammenlignet med antigener i opløsning. Resultaterne indikerer at aluminium hydroxid kan beskytte strukturen af antigenet mod aggregeringen ved høj temperatur og/eller lang tids opbevaring. Dette er mest udtalt for BSA. Yderligere studier kræves for at bekræfte om denne beskyttelse er protein-specifik.

Kapitel V omhandler ændringen af modelvacciner under opbevaring ved to forskellige temperaturer. Det demonstrerer at ændringen i aluminium hydroxids adsorptionskapacitet under opbevaring er protein-specifik. Frigivelse af adsorberet protein fra adjuvanten nedsættes som funktion af opbevaringstid. Ligeledes ændres pH og NIR-absorbansen. Aldringseffekterne gennemgår hurtigere modifikationer med opbevaringstiden ved 37 ^{o}C end ved 4 ^{o}C. Rotationseffekter under fremstilling af vacciner diskuteres også i kapitlet.

NIR-metoden til bestemmelse af resterende fugtindhold i frysetørrede allergenvacciner introduceres i kapitel **VI**. Fem forskellige allergenvacciner analyseres. Acceptable kalibreringsmodeller (RMSEP

10.20 µg H_2O/ flaske med 2 PLS faktorer) er opnået for multi-produkt data. Modellerne baseret på produktspecifikke data er lidt bedre (**Appendiks B**). Imidlertid er en generel multiprodukt-model mere attraktiv idet en enkelt model kan forudsige alle prøverne. Referencedataene som måles ved Karl Fischer-titrering præsenteres i **Appendiks A**.

NIR spektroskopi benyttes til at klassificere og identificere fem forskellige allergenvacciner (information om prøverne ses i **Appendiks C**) ved forskellige koncentrationer af antigener og forskellige batcher i **kapitel VII**. Resultaterne viser at NIR spektroskopi kan benyttes til at klassificere forskellige allergen vacciner ved højeste antigenkoncentration (100,000 SQ) uden api. Produkter ved den højeste koncentration kan adskilles fra produkter ved lave koncentrationer. Diskrimineringen af forskellige batcher kan også være mulig. Dette mangler dog at blive bekræftet. Alle SIMCA-resultater gives i **Appendiks C** til **Appendiks S**.

Publications include in this thesis

1. Yiwu Zheng, Xuxin Lai, Henrik Ipsen, Jørgen Nedergaard Larsen, Henning Løwenstein, Ib Søndergaard and Susanne Jacobsen. Characterization of the structural changes of model antigens using FTIR-ATR. Submitted to Vaccine 2006.
2. Yiwu Zheng, Xuxin Lai, Henrik Ipsen, Jørgen Nedergaard Larsen, Henning Løwenstein, Ib Søndergaard and Susanne Jacobsen. The structural stability of model antigens adsorbed by aluminium hydroxide in heating and aging processes in comparison to the antigens in solutions. Submitted to Vaccine 2006.
3. Yiwu Zheng, Xuxin Lai, Henrik Ipsen, Jørgen Nedergaard Larsen, Henning Løwenstein, Ib Søndergaard and Susanne Jacobsen. Stability of model vaccines during storage analysed by NIR spectroscopy. Submitted to Vaccine.
4. Yiwu Zheng, Xuxin Lai, Henrik Ipsen, Jørgen Nedergaard Larsen, Henning Løwenstein, Ib Søndergaard and Susanne Jacobsen. Determination of residual moisture content of lyophilized allergen vaccines by NIR spectroscopy. Will be submitted to Applied Spectroscopy 2006.

Abbreviation list

3D, three dimensional;
ACA, aluminium-contained adjuvants;
ADT, accelerated degradation test;
ATR, attenuated total reflection;
BSA, bovine serum albumin;
BLG, β-Lactoglobulin;
CD, circular dischroism;
EMSC, extended multiplicative scatter correction;
FT, Fourier transform;
FTIR, Fourier transform infrared spectroscopy;
FSD, Fourier self-deconvolution;
KF, Karl Fischer;
MIR, mid infrared;
MSC, multiplicative scatter correction;
MVA, multivariate data analysis;
NIR, near infrared;
NMR, multidimensional nuclear magnetic resonance;
PCs, principal components
PCA, principal component analysis;
PCR, principal component regression;
PBS, phosphate buffer;
PLS, partial least squares;
RMC, residue moisture content;
RMSE, root mean square average;
RMSED, root mean square error of deviation;
RMSEP, root mean square error of prediction;
SIMCA, soft independent modelling of class analogy;
SIT, allergen-specific immunotherapy;
SNR, signal to noise ratio;
SNV, standard normal variate.

Table of contents

Chapter I: Background of the project and the introductions to infrared technology and chemometrics

This chapter describes the background and purpose of this study, as well as infrared technology and chemometrics, which are the core technologies used in this work.

1 Background

Two public health interventions, clean water and vaccines, have had the greatest impact on the world's health. Vaccines prevent disease or death for millions of individuals every year [1]. Vaccine manufacturers and public authorities, e.g. World Health Organization (WHO), have established ambitious goals for enhancing present vaccines and for developing new ones. New vaccine candidates have emerged over the past years against allergic, infectious, autoimmune diseases, and for cancer and fertility treatment as well [2].

In the case of allergy, the prevalence of hypersensitivity reactions increases rapidly, especially in developed countries. Allergic diseases concern approximately 30% of the population, thus they become a serious clinical and social problem [3]. Allergic diseases such as asthma, atopic dermatitis, allergic rhinitis and conjunctivitis belong to inflammatory disorders, which can be treated using anti-inflammatory drugs. Although efficient in symptom control, this treatment is not a causal method and the WHO recommends combination treatment considering immunotherapy [4]. The conventional allergen-specific immunotherapy (SIT) protocol was introduced by Noon and Freeman in 1911 [5], when they injected an extract of grass pollen to a person whose allergic symptoms coincided with the pollination of grass. Since then, controlled studies have shown that SIT is effective in patients with allergic diseases. SIT involves repeated administration of gradually increasing quantities of specific allergens to an allergic patient until a dose is reached that will raise the patient's tolerance to the allergen. Among the current approaches in allergy therapy, SIT is the only treatment that may affect the course of allergic diseases and it also may prevent the development of asthma in patients with allergic rhinitis [4]. The mechanisms of SIT have been reviewed elsewhere [4]. A successful SIT is dependent on the use of high quality allergen vaccines that are properly standardized and can be manufactured consistently.

Vaccine is produced by maximum adsorption of antigens onto adjuvants. Beginning in the early 20th century, researchers experimented with a wide variety of organic and inorganic compounds including aluminium salts, mineral oil, and killed mycobacteria to improve the immunogenicity of vaccines, but most of these concepts were never accepted for routine vaccination because of safety

concerns, e.g. acute toxicity and the possibility of delayed side effects [2]. These compounds are called adjuvants, which derived from the Latin verb adjuvare meaning "to help" [2, 6-8]. In brief, an adjuvant is a substance that, when mixed with an antigen and injected with it, enhances the immunogenicity of that antigen. Adjuvants are often used to boost the immune response when an antigen has low immunogenicity or when only small amounts of an antigen are available [9].

Aluminium-contained adjuvants (ACA), first described in 1926 [10], are the only immunologic adjuvants used in human vaccines licensed in the United States, and are also present in many veterinary vaccines. They have been administered to hundreds of millions of people with only rare reports of serious local reactions [11]. Vaccines containing ACA are prepared by two principal methods [12, 13]: 1) Antigens are adsorbed by aluminium hydroxide or aluminium phosphate. Such products are termed adsorbed vaccines. The commercial products are prepared by this method. 2) Antigen solutions are mixed with a solution of $KAl(SO_4)_2.12H_2O$. These products are termed alum precipitated vaccines. The alum precipitated vaccines are not applied today, because such preparations could be highly heterogeneous [12].

Although adjuvants have been used for many years to enhance, accelerate and prolong the specific immune response towards the desired response to vaccine antigens, the mechanism by which adjuvant can enhance the immune response and/or exert their activities is still not clear [9]. A few hypotheses have been proposed elsewhere [2, 6, 9, 12, 14-18], which are briefly introduced here.

- The first hypothesis is known as the "depot effect". It is based on the lower solubility of aluminium-protein complex compared to the free protein solution. Vaccine antigen is released slowly after administration, which results in a sufficient time to induce a significant immune response [2, 6, 9, 12, 14-18].
- The physical appearance of the antigen is defined by the adjuvants in the vaccine [2].
- Adjuvant may target the distribution of antigens to specific cells. And it may regulate both quantitatively and qualitatively aspects of the ensuing immune responses [2].
- Adjuvant itself can stimulate immune response since it is associated with *e.g.* cytokine production [12, 14].
- The particles of size from 5 to 10 μm are more easily phagocytosed by macrophages, dendritic cells, and neutrophils, than other particles. These are the size for most aluminium-protein complexes [9, 14, 15].
- Protein may be destabilized by adsorption of adjuvants. The adsorbed protein, once inside cells, would be more prone to degradation than the free protein. In this way the protein is

processed faster and thereby quickly reaches the outer membrane of antigen presenting cells [15].

- Adjuvants can protect the antigen from degradation and elimination [2].

Thus, adjuvants may enhance the immune response as a result of multiple factors. Individual antigens vary in their physical, biological and immunogenic properties and thus antigens may have different needs for help from an adjuvant [2]. Whatever the case, the structure of protein antigen is of great importance because it results in the functions of protein. It may also important to stimulate an immune response. There is little knowledge about the structure when protein antigen is adsorbed by ACA and after it is released, as well as on the stability of adsorbed protein antigens during storage and the effect of temperature variation. However, the stability of proteins has become recognized as a major problem in the past decades. Denatured and/or aggregated protein will not only be therapeutically inactive, but also may cause unpredictable side effects, such as acute toxicity [19, 20].

1.1 Objective of the project

In order to produce high quality vaccines and manufacture consistently and to well understand antigens and vaccines, the study focuses on the structures of model antigens when they are adsorbed by aluminium hydroxide and when they are subsequently released. The mechanism of ACA enhancement of immune responses is also discussed. The stability of vaccines is investigated during storage and temperature variation. And finally, a fast, non-destructive method is also introduced for the determination of the residual moisture content and classification of lyophilized allergy vaccines.

2 Introduction to infrared spectroscopy

The human eyes only respond to electromagnetic radiation within a range of wavelengths between 400-700 nm, i. e. the visible spectrum. However, the electromagnetic spectrum extends from the extremely short wavelength of gamma radiation to the long wavelength of radio waves. Infrared refers to that part of the electromagnetic spectrum between the visible and the microwave regions. The infrared region is divided into three regions: near, mid, and far infrared. Near infrared (NIR) radiation is in the wavelength range of 780-2500 nm or 12,821- 4,000 cm^{-1}, and the mid-infrared (MIR) radiation is in regions from 2500 nm to 25000 nm or 4000- 400 cm^{-1}. MIR chemists prefer to use the wavenumber (cm^{-1}) designation, whereas in NIR, most people use wavelength in nanometers (nm).

The NIR radiation was discovered in 1800 by Herschel [21], who separated the electromagnetic

spectrum with a glass prism and found that the temperature increased markedly beyond the red, i.e. in the region that is called NIR today. Coblentz [22] recorded the first MIR spectrum in 1900, and the first commercial IR spectrometer emerged in the 1950s. From then on, MIR spectroscopy has been accepted as a research tool and structure-elucidation techniques in the industrial as well as the academic environment, especially from the availability of the first commercial Fourier transform infrared (FTIR) spectrometer in 1970 [23]. A number of NIR experiments were carried out in the early 1920s. The general attitude was that the NIR region was too confusing with many weak bands and overlapping peaks of numerous overtone and combination bands. Compared with the MIR absorption, NIR features were very weak and because of the overall complexity, baselines were hard to define. The seemingly hopeless results led to neglect of NIR. The re-birth of the NIR occurred in the early 1970s when Norris coupled a spectrometer to a computer and employed it to unravel the reflectance spectra of cereals [24]. In recent years, with the personal computers and new optical techniques rapidly developing, NIR spectroscopy has become an indispensable tool for academic research and industrial quality control in a wide field of applications ranging from chemistry to agriculture and from life science to environmental analysis. More detailed information on the applications of NIR spectroscopy in chemistry, polymers and textiles, agricultural and foodstuff, medical sciences, industrial process control, as well as pharmaceutical industry can be found elsewhere [25, 26]

2.1 Theory

Unless stated otherwise, the description of theory is taken from the handbooks or from personal experience. The detailed information also can also be found in these books [27-29].

NIR and MIR are closely related technologies. Both analyze functional group vibrations of organic molecules by monitoring their absorption of radiation as a function of frequency in the infrared spectrum [23]. Infrared radiation is absorbed by the sample when the frequency corresponds to its molecular vibrational transitions. Molecular vibrations give rise to absorption fundamental bands generally located in the MIR range. The NIR region contains adsorption bands corresponding to overtone and combinations of fundamental bands. The difference between NIR and MIR is only the frequency of these vibrations.

The frequency of a bond can be approximated by Hooke's law. In this approximation, two atoms and the connecting bond can be treated as a simple harmonic oscillator composed of two atoms joined by a spring. According to Hooke's law, the frequency of the vibration of the spring is related to the mass and the force constant of the spring, by the following formula (Eq. 1.1):

$$\nu = \frac{1}{2\pi}\sqrt{\frac{k}{\mu}} \qquad \text{Eq. 1.1}$$

where ν is the frequency of the vibration; k is the force constant; μ is the reduced mass and can be given by:

$$\mu = \frac{mM}{m+M} \qquad \text{Eq. 1.2}$$

where *m* and *M* are masses of atoms.

In the classical harmonic oscillator, vibrational energy can be given as follow formula:

$$E = h\nu \qquad \text{Eq. 1.3}$$

Where *h* is Planck's constant, 6.6×10^{-34} Js.

However, vibrational motion is quantized, and must follow the rules of quantum mechanics.

$$E = (n + \frac{1}{2})h\nu \qquad \text{Eq. 1.4}$$

where n is the quantum number: 0, 1, 2, 3…

Therefore, the lowest energy level is $E_0 = \frac{1}{2}h\nu$. At ambient temperature, most molecules are at this ground level E_0, and the most observed transition is from this level to the next level. The transitions with $\Delta n = 1$ are called fundamental transitions, which match the energy of radiation in the MIR region. The occasional transitions with $n = 2,\ 3$, or higher are observed, which are designated as 'hot bands'.

However, a molecule is actually an anharmonic oscillator. Transition with $n = \Delta 2$, $\Delta 3$ or higher are possible in this anharmonic oscillator. These correspond to bands called overtones in the NIR region. The vibrational energy levels become more closely spaced with increasing interatomic distance in the anharmonic oscillator. The allowed transitions become smaller in terms of energy. Thus, overtones can be lower in energy than predicted by the harmonic oscillator theory. The energy level can be expressed as following formula:

$$E = hv(n + \frac{1}{2}) - hvx(n + \frac{1}{2})^2, n = 0,1,2,.... \qquad \text{Eq. 1.5}$$

where *x* is the anharmonicity constant, which is from 0.01 to 0.05, and it accounts for dissociation of atoms and repulsion between atoms.

For most chemical bonds the frequency of overtones can be estimated from their fundamental vibrations with the anharmonicity constant by following equation:

$$\nu_x = \Delta n \nu_0 (1 - \Delta n x) \quad \text{Eq. 1.6}$$

Where ν_x is frequency of x overtone; ν_0 is frequency of fundamental vibration; x is the anharmonicity constant.

Combination band appear between 1900 nm to 2500 nm in NIR region. It is the result of fundamental vibration interactions, i.e. when the energy of an adsorbed photon is shared by two or more fundamental transitions. The frequency of a fundamental band is the sum of multiples of each interacting frequency.

It should be noted that bonds which do not involve hydrogen do not have absorption in NIR region. It is because hydrogen atom is the lightest and thus exhibits the largest vibrations and greatest deviations from harmonic behaviour. Another reason is that most X-H fundamentals absorb at wavelength < 5000 nm, which results in their first overtone appear in NIR region. Some polar bonds, However, such as C-O, C=O, and C-F, have intense fundamental bands in the MIR region resulting from their absorption at wavelength > 5000 nm. The absorption bands of these bonds in the NIR region are very weak and can be neglected due to the intensity loss. NIR absorption bands are typically broad, overlapping and 10-100 times weaker than their corresponding fundamental MIR absorption bands, since the probabilities of overtone and combination transitions are low. The low absorption coefficient in NIR, however, permits high penetration depth, which allows direct analysis of strongly absorbing and highly scattering samples and makes sample preparation unnecessary.

Despite their common fundamental basis, the instrumentation used in the two fields has traditionally been quite different.

2.2 Sample presentation

Sample presentation is one of the important factors affecting measurements using infrared spectroscopy. The sample presentation methods for NIR and MIR are different due to the different extinction coefficients. NIR cannot be used for trace analysis as the mid-IR. However, this disadvantage becomes important when considering process analysis. The strong light source and weak absorbance allow NIR radiation to penetrate further into the sample, which make it possible to measure intact solid samples. An appropriate sample presentation improves the accuracy, precision and sensitivity of the spectroscopic measurements, especially when measuring solid sample due to scatter effects. Selecting the sample presentation for infrared spectroscopic analysis mainly depends on the physical conditions of samples and target parameters. Although there are some general

guidelines for sample presentation, the proper method is a case by case decision.

2.2.1 NIR sample presentation

A detailed description of NIR sample presentation can be found elsewhere [26, 30-32].

Transmittance

In this case, the light source and the detector are positioned opposite of each other and the incident light has to pass through the whole sample to be detected. Therefore, the light intensity should be high enough to penetrate the sample, which depends on the absorption coefficient of the sample and the sample thickness. In general, it is widely applied for the liquids, solutions, and can also be used for suspensions, or some solids such as tablets and capsules. Limitations are observed with very thick solid samples [26].

Diffuse reflectance

Diffuse reflectance mode is used for solid samples and requires a different spectrometer configuration comparing to transmittance mode. The light source and the detector are on the same side in an angle of 45 ºC to each other. The configuration minimizes the contribution to measurement of the specular reflectance, which contains little information about composition of samples. The incident light reaches the surface of the sample. It penetrates some millimeters depending on structure, particle size and other properties of the sample. Some light is absorbed by the sample and the rest is reflected, but only a part reaches the detector. Therefore, for low concentration applications, one can use a larger or multi-channel detector to increase the sensitivity.

Transflectance

Transflectance was originally developed by Technicon for the Infraanalyzer, which combines transmittance and reflectance. Incident light is transmitted through the sample and then scattered back from a reflector, which is normally made of ceramic or aluminium. Since the incident light has to pass through the sample twice, the limitations mentioned under transmittance measurements are especially relevant.

Interaction

In the case of interaction, a fibre optic probe having a concentric outer ring of illuminator and an inner portion of receptor is usually used. The end of the probe should be on or near (depends on the applications) the surface of the sample. This mode can be used for online analysis.

2.2.2 MIR sample presentation

The techniques of MIR sample presentation have been developed allowing the analysis of samples in any physical phase: solid, liquid or gas. The most common methods are transmittance

experiments with pressed disks; diffuse reflectance experiments with powder samples, and attenuated total reflectance (ATR) measurements with aqueous solutions and hydrated suspensions. These presentation methods are briefly discussed here focusing on structural analysis of proteins. Different methods may not provide the same information about protein structures. Weet and co-workers [33] demonstrated the effect of sampling methods on the protein conformation.

Transmittance

This is the simplest and most common method of FTIR measurement. Solid samples are diluted to 1-2% in a medium (usually KBr) and made into a disk with a certain pressure. The final sample is a thin, clear disk that is placed perpendicular to the infrared beam. Water must be removed from the system; thus, samples are heated to remove as must water as possible prior to dilution. Although the high-pressure affects the structure of proteins in aqueous solution [34, 35], the current established procedures for producing KBr-pellets does not induce protein structural changes [36-38]. For sample solution, the spectra can be measured in a special liquid cell with CaF_2 windows. The pathlength has to be approximately 6 μm to allow for precise subtraction of the strong water band around 1640 cm^{-1} which overlaps the protein amide I bands. Experiments measured in transmission can provide quantitative information more easily than other sampling methods, since Beer-Lambert Law is directly applicable. The pathlength is known. However, heating samples during water removing may lead to structural changes in the sample.

Diffuse reflectance

This technique is only suited for powder samples. Measurements can be conducted for raw samples (without dilution) or diluted with non-absorbing matrix such as KBr. Samples do not need to be pressed into a disk as measured in transmission, but can be packed directly onto the sample holder. This avoids the high-pressure during the pellet preparation. However, samples have to necessarily ground with a mortar and pestle to avoid large particles that may distort the spectrum. Regardless of the sample preparation, the diffuse reflectance spectra are different from the data which are collected in transmission mode experiments. Peak intensities at higher wave number are typically compressed, and all peaks tend to be rather rounded compared with sharp peaks from pressed disks. This can be solved using a mathematical correction known as the Kubelka-Munk equation, which is usually available from the software used to control the FTIR. One thing that has to be noted is that samples should be dried and may need to be diluted with a matrix if the absorption is overloaded.

ATR

ATR (also called internal reflection element or briefly IRE) is a versatile and powerful technique

for MIR sampling. Minimal or no sample preparation is usually required for rapid analysis. ATR is ideal for those materials which are strongly absorbing. In addition, ATR is a useful technique for providing information about the surface properties or conditions of the material. Materials which are either too thick or too strongly absorbing to be analyzed by transmission spectroscopy can be routinely analyzed using ATR. With the ATR technique, it is possible to measure a wide range of samples. Basic details of ATR are reviewed elsewhere [39, 40].

When using ATR, it is important to have the sample in intimate contact with the crystal. For solids, it is important to use a pressure device which presses the sample against the crystal. Paste or slurry samples are problematic, but the analysis becomes easy when measuring films by evaporating the solvent from the samples. The intimate contact is easily achieved with most liquids since they wet the surface of the ATR crystal. In addition, a clear advantage of ATR spectra of solutions is the reproducibility of the pathlength comparing to the transmission experiments, in which a very thin cell (6 μm) is applied to deal with a reasonable absorbance in transmission experiments. Such small pathlength is difficult to reproduce with sufficient accuracy. Liquid samples can also be analyzed as films by evaporating the solvent, which minimize the effect of water absorption [41].

The FTIR-ATR spectra depend on the following parameters: wavelength of the incident radiation, refractive indices of the internal reflection element and the sample, angle of incidence and efficiency of the contact between sample and the crystal. In particular, strongly distorted spectra result from an unwise choice of the incidence angle, from the nature of the internal reflection element and from the thickness of the sample (pathlength).

Since the ATR spectra depend on the refractive index, the spectra may be distinctly different from the absorption bands. How much the band shapes and intensities are different from absorption spectra depend on the experimental conditions. However, these differences are due to the particular nature of the reflection spectrum and should not be confused with distortion of a true spectrum. Furthermore, it is a possibility to quantify concentrations even for components which are not absorbing within the spectral range of investigation [42]. A disadvantage, which should be noted, is that the spectrum may be affected by the adsorption by the ATR crystal [43] and the anomalous dispersion of sample on the surface of ATR [44, 45].

2.3 Quantitative analysis using infrared spectroscopy

In transmission mode, the basic theory of quantitative analysis results from the Beer-Lambert Law (Eq. 1.7). It says that the absorbance of a homogeneous sample (with an extinction coefficient ε) is proportional to the concentration c and pathlength l. The law is defined only for transmittance

measurements on homogeneous samples using data that has been corrected for non-absorption effects.

$$A = \log(1/T) = \varepsilon c l \qquad \text{Eq. 1.7}$$

The theory of reflectance is not clear, because people have not found a way to determine the pathlength followed by the radiation energy in the sample. In addition, we do not yet have a good model for the way radiation interacts with the sample at particle interfaces. What we know is that reflection is non-linear with respect to the constituent concentrations. However, even though the theory of reflectance is not clear, it is widely applied in infrared spectroscopic measurements.

3 Introduction to Chemometics

Infrared spectra are typically composed of broad overlapping bands, and the absorption bands contain both chemical and physical information of all sample components. The interesting information is always multivariate in nature, and thus, hardly selective [46]. The spectral data always contain more variables than samples and have correlated variables. The classical multiple linear regressions are not suitable in this case [47]. Therefore, Cheometrics (also known as multivariate data analysis, MVA) is required to extract useful information and reduce the irrelevant information. Cheometrics can be defined as the development and application of mathematical and statistical methods to extract useful chemical information from chemical measurements [48, 49]. Chemometircs was emerged in the late of 1960s and developed during 1970s and was introduced to spectroscopic data in this period [49]. The whole idea of chemometrics is that the data contain redundant information and can be reduced substantially. The reduced data are easier to understand and have more stability and residuals contain noise and less useful information [50]. The new latent variables in the reduced data set provide an overview of the main variation in the raw data. The outliers can be identified and the noise can be separated from the signal as well [51].

In the following sections, the basic methods of Chemometrics and some methods for pre- treatments of mathematical data are briefly introduced. These methods are used throughout this work for analysis of NIR and MIR spectroscopic data.

3.1 Data pre-treatment

Visualization of data has always been very important in Chemometrics and it is impossible to discuss Chemometrics without showing plots of data [50]. However, raw data often need prior treatment to mathematically remove defects due to light scattering, path length variations and random noise. Careful selection of the method of pre-treatments can significantly improve the

robustness of the final calibration model. The most commonly used methods in this thesis are briefly discussed with respect to the effect they are able to correct. The detailed description is available in textbooks [52] and in the introduction to the Unscrambler software.

Standard normal variate (SNV)

SNV removes the multiplicative interference of scatter and particle size. The method removes slope variations for individual spectra. Each spectrum is transformed independently as the function of:

$$x_{i,snv} = \frac{x_i - \bar{x}}{\sqrt{\sum (x_i - \bar{x})^2 / (n-1)}} \quad \text{Eq. 1.8}$$

Where, $x_{i,snv}$ is the transformed spectrum; x_i is the original spectral; $\bar{x}$ is the average value of the variable; and n is the number of the variables in the spectrum. In other words, SNV transformation is row centring followed by row scaling [53].

Multiplicative scatter correction (MSC)

MSC is used to correct for the significant light scattering problems. It is used based on the assumption that all samples have same scatter coefficient for all variables. A mean spectrum of the dataset is applied to estimate the scatter of the spectra. Other spectra are corrected to have the same scatter level as this mean spectrum. Each spectrum is shifted and rotated to fit as closely as possible to the mean spectrum. The fit for each spectrum is obtained by least squares as the following function:

$$x_i = 1a_i + b_i \overline{x_i} + \varepsilon_i \quad \text{Eq. 1.9}$$

Where, x_i is individual spectrum. $\overline{x_i}$ is the mean spectrum of the dataset, and ε_i is the residual spectrum, which ideally represents the chemical information in the spectrum. The fitted constants a_i (offset, intercept) and b_i (slope) are used to correct each value of the spectrum i (Eq. 1.10) and they reflects additive and multiplicative light scattering effects, respectively.

$$x_{i,MSC} = \frac{x_i - 1a_i}{b_i} \quad \text{Eq. 1.10}$$

A disadvantage of MSC is that the obtained parameters may be affected by the chemical variations, since the mean spectrum is simply used as the ideal chemical spectrum.

Extended multiplicative scatter correction (EMSC)

This method is an extension to conventional MSC and is used to remove unwanted physical information resulting from light scattering, pathlength variations, and baseline drifts [54]. It allows a separation of physical light scattering effects from chemical light absorbance in the spectra. The

sample spectra are expressed as ideal chemical spectra modified by various physical effects. In the case of EMSC, Eq. 1.9 is extended with correction for linear and quadratic wavelength effects, i. e. the wavelength-dependent scatters. It is given in Eq. 1.11, where λ represents the wavelength range; $x_{i,chem}$ is the ideal chemical spectrum.

$$x_i = 1a_i + d_i\lambda + e_i\lambda^2 + b_i x_{i,chem} + \varepsilon_i \qquad \text{Eq. 1.11}$$

The parameters in Eq. 1.11 are used to correct each value of the spectrum using Eq. 1.12. The baseline and pathlength variations as well as wavelength-dependent spectral effect will be removed, yielding corrected spectra with only chemical absorbance information left.

$$x_{i,corrected} = (x_i - 1a_i - d_i\lambda - e_i\lambda^2)/b_i \qquad \text{Eq. 1.12}$$

Derivatives

Derivatives have been described in detail by Mark and Workman [55-58]. They are an approach to addressing two of the basic problems with infrared spectra: overlapping peaks and removing large baseline shifts. Derivatives are used for MIR spectra as a resolution-enhancement method (see Chapter II, III, and IV). The effect of derivatives is most clearly seen with the second derivative of a spectrum, which is able to separate overlapping absorption bands because it is slated to curvature and has the same sign as the curvature of a spectrum. Second derivative can be used to remove the baseline shifts, because the curvature of a straight line is zero, the derivative of a spectrum-plus-a-straight-line-baseline will be the same as the derivative of the spectrum. The first derivative also has these two effects, but to a lesser extent, and has a geometric interpretation as the slope of the spectrum at each wavelength. Higher-order derivatives have the same two basic functions as second derivative, and will resolve overlapping adsorption bands more effectively than the lower-order derivatives. They will remove gently curved background as well as linear background shifts. However, they are more sensitive to noise and generate more artefacts than the lower-order derivatives. Higher-order derivatives do not easily give rise to get visual geometric interpretation and have not been widely applied in infrared spectra. They have not been shown to give great advantages in calibration or validation.

There are three common methods to calculate derivatives: Savitzky-Golay, finite-difference, and Fourier transform. The Savitzky-Golay method fits the spectrum with a polynomial and then takes the derivative of that polynomial. It is most useful with very sharp absorption bands and with high noise spectra.

The drawback of the derivative is that it amplifies noise. Therefore, sometimes, it is necessary to

smooth the data beforehand.

Smoothing

Smoothing is used to reduce the noise in the data. Savitzky-Golay is an averaging algorithm that fits a polynomial to the data points. The value to be averaged is then predicted from this polynomial equation. The number of variables or points has to be chosen in the averaging segment. If the variable number in the segment is large, it will give a smoother shape to the sample, but if the segment is too large, sharp peaks may be removed and the remaining bands are distorted [59]. It should be noted that after the operation the data will be slightly truncated at both ends. If n is the number of variables in the averaging segment, the first and last n variables will be zero. The order of the polynomial to be fitted is also important. Typically, a second- or third-order polynomial is used [58]. A second-polynomial means that a second-degree equation will be used to fit the data points.

Normalization

Normalization is used to get all data in approximately the same scaling or to get a more even distribution of the variances and the average values. Normalization of a sample is accomplished by dividing each variable by a constant. It reduces systematic variation, but normalization may remove important concentration information.

It is a row-oriented transformation, that is to say the contents of a cell are likely to be influenced by its horizontal neighbours. There are three types of normalization: 1) mean normalization; 2) maximum normalization; 3) range normalization. Mean normalization is the standard normalization. Maximum normalization is a normalization that "polarizes" the spectra. The peaks of all spectra with positive values touch +1, while spectra with values of both signs touch -1. Range normalization involves scaling all samples to a common range, for example between 0 and +1. Thus each axis in a plot of range-scaled data is adjusted such that the data fill the region of the plot in all directions.

Baseline transformation

Baseline transformation includes baseline offset and linear baseline correction. The formula for the baseline offset can be written as in Eq. 1.13, where x_i is a variable and X denotes all selected variables for a spectrum. For each sample, the value of the lowest point in the spectrum is subtracted from all the variables. The result of this is that the minimum value is set as zero and the rest are positive values.

$$x_{i,offset} = x_i - \min(X) \quad \text{Eq. 1.13}$$

Linear baseline correction transforms a sloped baseline into a horizontal baseline. The technique is performed by pointing out two variables which are set as zero and as a new baseline. The rest of the variables are transformed according to this with linear interpolation or extrapolation.

3.2 Principal component analysis (PCA)

The further details of PCA are available elsewhere [50, 60-62]. A brief introduction is given here based on spectral data. PCA is the basis of multivariate data analysis. The most important use of PCA is to represent a multivariate data set as a low dimensional space to find interesting phenomena, often without prior knowledge. As a result, outliers, clustering of objects and gradients between clusters may be detected [50].

PCA is a mathematical procedure that resolves the data into orthogonal components whose linear combination approximates the original data. The original data matrix *X*, consisting of *i* spectra and each spectrum having *j* variables (data-points), is described by two smaller matrices called score *T (i, R)* and loading *P (j, R)* as shown in Eq. 1.14. *R* is the principal components (PCs) of the PCA model, which expresses the complexity of the observed variations in the data. The matrices *T* and *P* can be calculated by nonlinear iterative partial least square (NIPALS). The matrix *E (i, j)* consists of the difference between the values in the data matrix and the values obtained from the multiplication of *T* and L^T. It is called residual matrix or error matrix [63].

$$X = TP^T + E \quad \text{Eq. 1.14}$$

The obtained scores and loadings can be used in *scores plots* that allow an efficient interpretation of the whole data space [50].To discriminate several different materials, score vectors are plotted against each other. If the vectors form different clusters which are clearly separated from each other, identification is possible.

3.3 Multivariate calibration for quantitative analysis

The PCs from the PCA are found by successively reducing the residual sums of squares of X (e.g. NIR spectra) with no consideration to interest Y (e.g. concentration); there is no predictive optimality that will subsequently be used for regression onto Y. Thus, PCA cannot be used for quantitative analysis. The multivariate calibration methods most frequently used in quantitative analysis are principal component regression (PCR) and partial least squares regression (PLSR) [64]. They are the most successful applications of the combinations of Chemometrics with spectral data

[50]. PCR uses the PCs provide by PCA to perform regression on sample property. PLS finds the direction of greatest variability by comparing both spectral (X) and target property (Y) information with the new axes, called PLS components or PLS factors. The main difference between these two methods is that the first PC or factor. In PCR, the first factor represents the largest variations in the spectrum, whereas in PLS it presents the most relevant variations showing the best correlation with the target property. Therefore, to reach an ideal regression model, PCR needs more PCs than PLS.

PLS relates two data matrices, X and Y, to each other by a linear multivariate model. It models both X and Y matrices simultaneously to find latent variables in X that will predict the latent variables in Y. No direct closed mathematical description can be made for PLSR [65], but it may be simply given in Eq. 1.15. *B* is the regression coefficients, which is helpful in spectroscopic analyses and band assignment [66]. The detailed algorithm of PLS can found elsewhere [67].

$$Y = XB + F \qquad \text{Eq. 1.15}$$

3.4 Soft independent modelling of class analogy (SIMCA)

The detailed theory of SIMCA has already been extensively discussed by others [67-69]. The idea behind this method is that objects in one class or group show similar behaviour and this approach allows the objects to display intrinsic individualities as well as their common patterns, but only common properties of the class are modelled. SIMCA is based on making a PCA model for each class in the training set. Each class is modelled separately with a certain number of significant PCs. The number of PCs is normally selected by cross-validation automatically. This can be described in Eq. 1.16 for one class or group (c) [69].

$$X_c = \overline{X_c} + T_{c(iR)} P^T_{c(jR)} + E_{c(ij)} \qquad \text{Eq. 1.16}$$

Where $\overline{X_c}$ is the mean centred data matrix, $T_{c(iR)}$ is the score matrix obtained for *i* objects and *R* selected PCs. $P^T_{c(jR)}$ is the loading matrix obtained for *R* selected PCs and *j* variables and $E_{c(ij)}$ is the residual matrix.

After the PCA models have been contrasted, the distances between classes e.g. $RMSE(X)_c$ can be calculated as in Eq. 1.17, and also the distance from an object to the specified class e.g. $RMSE(X)_{i,c}$ can be calculated as in Eq. 1.18.

$$RMSE(X)_c = \sqrt{\{\sum RMSE(X)^2_{i,c} / N\}} \qquad \text{Eq. 1.17}$$

$$RMSE(X)_{i,c} = \sqrt{\{e_{i,c,R} e'_{i,c,R} / (j - R)\}} \qquad \text{Eq. 1.18}$$

Where, RMSE is the root-mean-square average. *N* is the sample size of class *c*. *R* is the selected

PCs, and j is the number of variables of X, The X-residual vector is $e_{i,cR}$.

The class modes are cross-classified and evaluated. Then a new unknown sample can be classified by checking if it falls inside the boundaries of any class models and assigned to classes according to its analogy to the training samples. The detailed methodology of SIMCA is described in [68].

References

1. http://www.vaclib.org/news/vaccinelicense.htm Feb. 2006.
2. Guideline on adjuvants in vaccines for human use. The European Medicines Agency. http://www.emea.eu.int. Feb. 2006.
3. Grzela K, Lazarczyk M, Dziunycz P, Milewski L, Niderla J, Grzela T. Molecular therapy versus standard treatment in allergy. International Journal of Molecular Medicine, 2004; 14:3-22.
4. Bousquet J, Lockey RF, Malling HJ. WHO position paper. Allergen immunotherapy: therapeutic vaccines for allergic diseases. Allergy 1998; 53: 1-43.
5. Noon L. Prophylactic inoculation against hay fever. Lancet, 1911; 1:1572-1573.
6. Rogan D, Babiuk LA. Animal health: biologics/biopharmaceutics- novel vaccines from biotechnology. Revue Scientifique et Technique – Office International des Epizooties, 2005; 24: 159-174.
7. Matheis W, Zott A, Schwanig M. The role of the adsorption process for production and control combined adsorbed vaccines, Vaccine, 2000; 20: 67-73.
8. Gupta RK, Siber GR. Adjuvants for human vaccines—current status, problems and future prospects, Vaccine, 1995; 14: 1263-1276.
9. Goldsby RA, Kindt TJ, Osborne BA, Kuby J. Immunology, 5th edition, W.H. Freeman Company. New York, 2003, p66
10. Glenny AT, Pope CG, Waddington H, Wallace UJ. The antigen value of toxoid precipitated by potassium alum, Journal of Pathology and Bacteriology, 1926; 29:31-40.
11. Gupta RK, Rost BE, Relyveld E, Siber GR. Adjuvant properties of aluminium and calcium compounds. In: Powell MF, Newman MJ, editors. Vaccine design: the subunit and adjuvant approach. New York: Plenum Press, 1995, p229-148.
12. Lindblad EB, Aluminium adjuvants—in the retrospect and prospect, Vaccine, 2004; 22: 3658-3668.
13. Shirodkar S, Hutchinson RL, Perry DL, White JL, Hem SL. Aluminium compounds used as adjuvants in vaccines, Pharmaceutical Research, 1990; 7: 1282-1288.
14. Morten JM, Rasmus LK. Adsorption of proteolytic enzymes to the adjuvant aluminium hydroxide, Master's thesis, BioCentrum-DTU, 2005.

15. Jones LS, Peek LJ, Power J, Markham A, Yazzie B, Middaugh CR. Effect of adsorption to aluminium salt adjuvants on the structure and stability of model protein antigens. The Journal of Biological Chemistry, 2005: 280: 13406-13414.
16. HogenEsch H. Mechanisms of stimulation of the immune response by aluminium adjuvants, Vaccine, 2002; 20: 34-39.
17. Cox JC, Coulter AR. Adjuvants—a classification and review of their modes of action, Vaccine, 1997; 15: 248-256.
18. Alexander J, Brewer JM, Adjuvants and their modes of action, Livestock Production Science, 1995; 42: 153-162.
19. Weet MVD, Hennink W, Jiskoot W. Protein instability in poly (lactic-co-glycolic acid) microparticles. Pharmaceutical Research, 2000; 17: 1159-1167.
20. Cleland JL, Powell MF, Shire SJ. The development of stable protein formulations: a close look at protein aggregation, deamidation, and oxidation. Critical Reviews in Therapeutic Drug Carrier System, 1993; 10: 307-377.
21. Pasquini C. Near infrared spectroscopy: fundamentals, practical aspects and analytical applications. Journal of the Brazilian chemical Society, 2003; 14: 198-219.
22. Burns DA. Historical development. In: Burns DA. Ciurczak EW (Eds.), Handbook of near-infrared analysis. Marcel Dekker Inc. New York, 1992, p 1-6.
23. Doyle WM. Near-IR and mid-IR process analysis – a critical comparison. Axiom Analytical Inc. www.gozxiom.com/an_911.html.
24. Williams PC, Norris KH, Zarowski WS. Influence of temperature on estimation of protein and moisture in wheat by near-infrared reflectance. Cereal Chemistry, 1982; 59: 473-480.
25. Siesler HW, Ozaki Y. Kawata S, Heise HM (Eds.). Near-infrared spectroscopy: principles, instruments, Applications.WILEY-VCH Verlag GmbH, Germany, 2002 p179-328.
26. Reich G. Near-infrared spectroscopy and imaging: basic principles and pharmaceutical applications. Advanced Drug Delivery Reviews 2005; 57: 1109-1143.
27. Bokobza L. Origin of near-infrared absorption bands. In: Siesler HW, Ozaki Y. Kawata S, Heise HM (Eds.), Near-infrared spectroscopy: principles, instruments, applications. WILEY-VCH Verlag GmbH, Germany, 2002, p11-41.
28. Olinger JM, Griffiths PR, Burger T. Theory of diffuses reflection in the NIR region, in: Burns DA, Ciurczak EW. (Eds.), Handbook of near-infrared analysis, 2nd edition, Marcel Dekker Inc., New York, 2001, pp 75-84.

29. Osborne BG, Fearn T, Hindle PH. Practical NIR spectroscopy with applications in food and beverage analysis. Longman Scientific & Technical. Harlow, England, 1993, p13-35.
30. Kawano S. Sampling and sample presentation. in: Siesler HW, Ozaki Y. Kawata S, Heise HM (Eds.). Near-infrared spectroscopy: principles, instruments, Applications.WILEY-VCH Verlag GmbH, Germany, 2002, p115-124.
31. Sukowski L. NIR based process analytical technology: In-line residual moisture determination for a complete batch inspection of lyophilized end-products. PhD thesis, University of Basel, Deutschland, 2003.
32. Pasquini C. Near infrared spectroscopy: fundamentals, practical aspects and analytical applications. Journal of the Brazilian Chemical Society, 2003; 14: 198-219.
33. Weet MVD, Haris PI, Hennink WE, Crommelin DJA. Fourier Transform infrared spectrometric analysis of protein conformation: effect of sampling method and stress factors. Analytical Biochemistry, 2001; 297: 160-169.
34. Prehoda KE, Mooberry ES, Markley JL. Pressure denaturation of proteins: evaluation of compressibility effects. Biochemistry, 1998; 37: 5785-5790.
35. Tanaka N, Nishizawa H, Kunugi S. Structure of pressure-induced denatured state of human serum albumin: a comparison with the intermediate in urea-induced denaturation. Biochimica et Biophysica Acta, 1997; 1338: 13-20.
36. Carpenter JF, Prestrelski SJ, Arakawa T. Separation of freezing- and drying-induced denaturation of lyophilized proteins using stress-specific stabilization. I: enzyme activity and calorimetric studies. Archives of Biochemistry and Biophysics, 1993; 303: 456-464.
37. Costantino HR, Nguyen TH, Hsu CC. Fourier-transform infrared spectroscopy demonstrates that lyophilization alters the secondary structure of recombinant human growth hormone. Journal of Pharmaceutical Sciences, 1996; 2: 229-232.
38. Costantino HR, Carrasquillo KG, Cordero RA, Mummenthaler M, Hsu CC, Griebenow K. The effect of excipients on the structure and stability of lyophilized recombinant human growth hormone. Journal of Pharmaceutical Sciences, 1998; 87: 1412-1420.
39. Goormaghtigh E, Raussens V, Ruysschaer JM. Attenuated total reflection infrared spectroscopy of proteins and lipids in biological membranes. Biochimica et Biophysica Acta, 1999; 1422: 105-185.
40. Chittur KK. FTIR/ATR for protein adsorption to biomaterial surfaces. Biomaterials, 1998; 19: 375-369.

41. de Jongh HHJ, Goormaghtigh E, Ruysschaert JM. The different molar absorptivities of the secondary structure types in the amide I region: an attenuated total reflection infrared study on globular proteins. Analytical Biochemistry, 1996; 242: 95-103.
42. Muller G, Abraham K, Schaldach M. Quantitative ATR spectroscopy: some basic considerations, Applied Optics, 1981; 20: 1182-1190.
43. Oberg KA, Fink AL. A new attenuated total reflectance Fourier transform infrared spectroscopy method for the study of proteins in solution. Analytical Biochemistry, 1988; 256: 92-106.
44. Hancer M, Sperline RP, Miller JD. Anomalous dispersion effects in the IR-ATR spectroscopy of water. Applied Spectroscopy, 2000; 54: 138-143.
45. Max JJ, Chapados C. Influence of anomalous dispersion on the ATR spectra of aqueous solutions. Applied Spectroscopy, 1999; 53: 1045-1053.
46. Reich G. Near-infrared spectroscopy and imagine: Basic principles and pharmaceutical applications. Advanced Drug Delivery Reviews, 2005; 57: 1109-1143.
47. Murry I. Scattering information: philosophy and practice of near infrared spectroscopy. In: Davies AMC, Garrido-Varo A (Eds.) Near infrared spectroscopy: proceedings of the 11th international conference. NIR publications, Chichester, England, 2004. pp 1-12.
48. Barton FE, Kays SE. Analytical application to fibrous foods and commodities. In: Williams P, Norris K (Eds.), Near-infrared technology in the agricultural and food industries. American Association of Cereal Chemists, Inc. St. Paul, Minnesota, USA. 2001, p215-231.
49. Martens H, Martens M. Multivariate analysis of quality; an introduction. John Wiley & Sons, LTD. 2001, p3-23.
50. Geladi P. Chemometrics in spectroscopy. Part 1: Classical chemometrics. Spectrochimica Acta Part B, 2003; 58: 767-782.
51. Wold S. Sjostrom M. Eriksson L. PLS-regression: a basic tool of chemometrics. Chemometrics and Intelligent Laboratory System, 2001; 58: 109-130.
52. Hesise HM, Winzen R. Chemometrics in Near-infrared spectroscopy, in: Siesler HW, Ozaki Y. Kawata S, Heise HM (Eds.). Near-infrared spectroscopy: principles, instruments, Applications.WILEY-VCH Verlag GmbH, Germany, 2002, p125-162.
53. Pravdova V, Walczak B, Massart DL, Kawano S, Toyoda K, Tsenkova R. Calibration of somatic cell count in milk based on NIR spectroscopy. Analytica Chimica Acta, 2001; 450: 131-141.

54. Martens H, Nielsen JP, Engelsen SB. Light scattering and light absorbance separated by extended multiplicative signal correction. Application to near-infrared transmission analysis of powder mixture. Analytical Chemistry, 2003; 75: 394-404.
55. Mark H., Workman JJ. Derivatives in spectroscopy Part I- The behavior of Derivative. Spectroscopy 2003; 4: 32-37.
56. Mark H., Workman JJ. Derivatives in spectroscopy Part II- the true derivative. Spectroscopy 2003; 9: 25-28.
57. Mark H., Workman JJ. Derivatives in spectroscopy Part III- Computing the derivative. Spectroscopy 2003; 12: 106-111.
58. Mark H., Workman JJ. Derivatives in spectroscopy Part IV-Calibrating with derivatives. Spectroscopy 2004, 1: 44-51.
59. Beebe K, Pell RJ, Seasholts MB. Chemometrics: A practical guide. John Wiley & Sons, INC. New York, 1998; p 33.
60. Martens H, Martens M. Multivariate analysis of quality. An introduction. John Wiley & Sons, LTD. 2001, p93-109.
61. Howard M. Data analysis: multilinear regression and principal component analysis, in: Burns DA, Ciurczak EW (Eds.), Handbook of near-infrared analysis, 2nd edition, Marcel Dekker Inc., New York/Basel, 2001, p 129-184.
62. Esbensen KH, Multivariate data analysis --in practice. 4th edition, CAMO ASA, 2000, p19-97.
63. Kramer K, Ebel S. Application of NIR reflectance spectroscopy for the identification of pharmaceutical excipients, Analytical chimica Acta, 2000; 420: 155-161.
64. Naes T, Isaksson T, Fearn T, Davies T. A user friendly guide to multivariate calibration and classification. NIR publication, Chichester, 2002, 27-54.
65. Andersson CA. Exploratory multivariate data analysis with applications in food technology. PhD thesis, the Royal Veterinary and Agricultural University, Denmark. 2000, 15-16.
66. Šašić S, Ozaki Y. Band assignment of near-infrared spectra of milk by use of partial least-squares regression. Applied Spectroscopy, 2000; 54: 1327-1338.
67. Esbensen KH. Multivariate data analysis – in practice: an introduction to multivariate data analysis and experimental design. 5th Edition. CAMO ASA/ CAMO Process AS. 2001; p145.

68. Martens H, Martens M. Multivariate analysis of quality: an introduction. John Wiley & Sons, Ltd. England, 2001; p163-169.
69. Candolfi A, Maesschalck, Massart DL, Hailey PA, Harrington ACE. Identification of pharmaceutical excipients using NIR spectroscopy and SIMCA. Journal of Pharmaceutical and Biomedical Analysis, 1999; 19: 923-935.

Chapter II: Protein structure and protein structure analysis

This chapter briefly introduces protein structures and the methods used for protein structure analysis. The main focus of the chapter is on protein structures when adsorbed onto surfaces and FTIR spectroscopy.

1 Protein structures

The primary structure of a segment of a polypeptide chain or of a protein is the amino-acid sequence of the polypeptide chain, without regard to spatial arrangement [1]. The secondary structure of a segment of polypeptide chain is the local spatial arrangement of its main-chain atoms without regard to the conformation of its side chains or to its relationship with other segments [1]. The secondary structures are formed through certain patterns of hydrogen bonding of the peptide backbone. There are three common secondary structures in proteins, namely α-helix, β-sheet, and turns. Those segments, which cannot be classified as one of the standard three classes is usually grouped into a category called 'other' or 'random coil' [1].

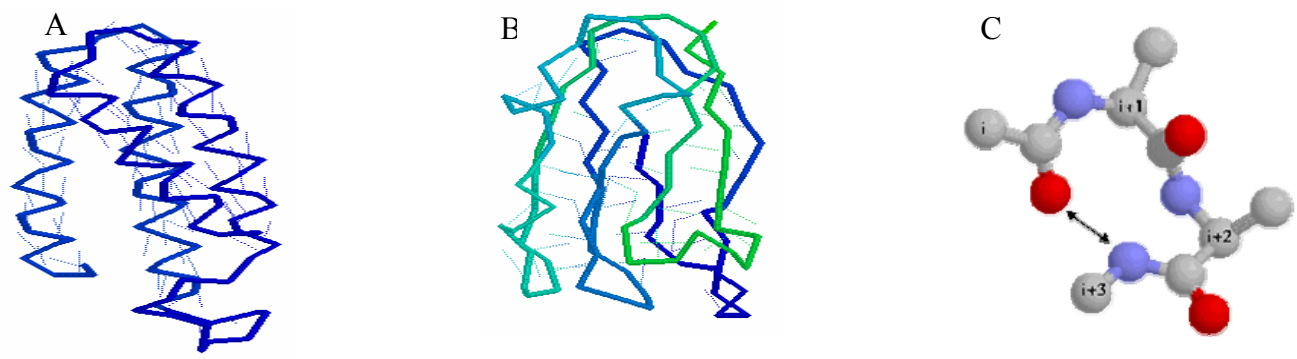

Fig. 2.1 The secondary structures of protein: A, α-helix; B, β-sheet; and C, turns [2, 3].

The α-helix is characterized by hydrogen bonds along the chain, almost co-axial (Fig. 2.1A) [2]. An α-helix is an element of secondary structure adopting a right handed helical conformation with approximately 3.6 residues per turn. In a perfect α-helix, there is a repeating pattern of hydrogen bonds from the carbonyl oxygen of residue *i* to the amide hydrogen of residue *i+4*. Favourable dipole interactions stabilize the α-helix. Side chains that are perpendicular to the helix axis may interact with each other, which also stabilize the helix structure. Another helix structure which is called 3_{10} helix has entirely different hydrogen bonding pattern, i. e. from *i* to *i+3*. It accounts about 12% of all protein helices. Beta-sheet is composed of two or more different regions of stretches of

at least 5 to 10 amino acids, which are stabilized by hydrogen bonds crossing between chains (Fig. 2.1B) [2]. Beta-sheets include parallel and anti-parallel forms and also the mixture of both β-sheets. In parallel sheets adjacent peptide chains proceed in the same direction; *i.e.* the direction of N-terminal to C-terminal is the same. In anti-parallel sheets adjacent chains are aligned in opposite directions. The third type of secondary structures is turns. Turns involve 4 amino acid residues which form a loop. A hydrogen bond is formed between the carbonyl oxygen of residue *i* and the amide nitrogen of *i+3* (Fig. 2.1C) [3].

The tertiary structure of a protein molecule is the arrangement of all its atoms in space, without regards to its relationship with neighbouring molecules. The quaternary structure of a protein molecule is the arrangement of its subunits in space and the ensemble of its inter-subunit contacts and interactions, without regards to the internal geometry of the subunits.

2 Protein structure analysis

Protein structure analysis has gained increasing interests in recent years. The information of protein structures is important for the understanding of protein function and facilitates pharmaceutical drug development [4]. The function and activity of proteins depends on their three-dimensional (3D) structure. However, the 3D structures of proteins do not only depend on the protein molecules themselves, but result from van der Walls, electrostatic and hydrophobic interactions between the various amino acids residues and surrounding molecules, as well as the formation of hydrogen and disulfide bonds [5]. Protein molecules are amphoteric, i.e. they contain both acidic and basic moieties, and they are amphiphilic molecules, i.e. they contain both hydrophilic and hydrophobic moieties. This chemical character causes proteins to be easily adsorbed by a wide rage of different surfaces.

The adsorption of proteins by material surfaces is not only a fundamental phenomenon but is also a key to several important and novel applications. For examples, the applications of protein purification and protein analysis by chromatography rely on the protein adsorption [6, 7]. Protein adsorption is the first step in the integration of an implanted material with tissue [8]. The adsorption of serum proteins can influence the adhesion of leukocytes, macrophages or platelets, and ultimately lead to fibrous encapsulation [9]. In pharmaceuticals, vaccines are formulated by protein antigens adsorbed onto adjuvants to enhance the immune response. Several reviews are available on physicochemical aspects of the adsorption of proteins onto biomaterials [10-12]. The structure of protein is often thought to be changed after they are adsorbed by biomaterial surface. The protein-surfaces interaction involves a large number of dynamic steps, *e.g.,* transport (diffusion) of proteins

toward to the surface, reversible attachment, structural rearrangement, irreversible adsorption, and desorption from the surfaces of adsorbents [13-15]. Direct observation of protein-surface interaction is presently impossible [5], but progress has been made toward determining protein structure on a surface and useful structural information can be obtained. Many available techniques have been introduced [16]. A number of common methods are briefly discussed in this thesis with regard to the advantages, limitations, sample requirements and especially the application of measurement of protein adsorption by adsorbents.

X-ray crystallography

This method yields information on the three-dimensional structure of protein molecules [17-19]. However, the main challenges of this method are to form a well ordered single crystals and pure protein is required, thus, it is not suitable to study the structure of the adsorbed protein, since a two-dimensional crystal is difficult to obtain [20]. Furthermore, a question arises as to whether the relatively 'static' structure in single crystal adequately represents the protein conformation in a complex and dynamic environment. Moreover, data interpretation is also complex and time-consuming.

Multidimensional nuclear magnetic resonance (NMR) spectroscopy

This is another method which can provide full three-dimensional structural determination [21, 22]. NMR is used for measuring sample in solution; the concentration of protein is normally from 2 to 20 mg/ml. This technique is only suitable for the small proteins (~15-30 kDa), since interpretation of the NMR spectra of large proteins is very complex, and the assignment of inter-proton distances generated by the NMR experiment is not always feasible [23]. The method for the study of adsorbed proteins is also severely limited by experimental difficulties; only a few applications have been reported on protein structural changes and the adsorption of protein on a solid interface [24, 25].

Circular Dischroism (CD) spectroscopy

This is a good method to monitor the secondary and tertiary structure of proteins in solution [26, 27]. Far-UV CD (170-250 nm) spectroscopy is a good tool to obtain overall information on the secondary structure, *i.e.,* the relative amount of α-helix, β-sheet, turns and random coil. The amount of α-helix or β-sheet can be estimated after fitting the Far-UV CD spectra to the corresponding spectra with known secondary structures [28]. The tertiary structure can be measured using near-UV CD spectroscopy (250 -300 nm), where the spectral characteristics of the aromatic amino acids are dependent on solvent exposure. Since the aromatic residues tryptophan and tyrosine are also

fluorescent, near-UV CD spectroscopy is complementary to the intrinsic fluorescence spectroscopy. CD spectroscopy has been applied to study the conformation of adsorbed protein both on colloidal suspension adsorbent and solid macroscopic interfaces. Usually, concentrations of protein in the range of 0.05 to 1mg/ml are used [25]. The particles of adsorbents should not significantly absorb in the UV band and should have a refractive index that is close to that of water.

Circular dichroism together with fluorescence spectrometry and Fourier transform infrared spectroscopy, which will be introduced later, provide global insight into the overall secondary structure of proteins without being able to establish a precise three-dimensional structure.

Fluorescence spectrometry:

Steady state fluorescence and quenching of fluorescence are useful tools for determination of secondary and tertiary structure [29-31], although one should be aware that these methods only reflect local changes in the environments of the fluorophore. Most measurements focus on the fluorescent amino acid residue, tryptophan. Tyrosine and phenylalanine can also be measured; however, the intensity is often low. Some proteins contain either no or many trytophan residues, thus limiting its use to provide detailed structural information. Fluorescence spectroscopy is not necessarily restricted to the fluorescence of intrinsic fluorophores. Specific residues on the protein can be labeled with a fluorescent group [32], but this modification of a protein may lead to structural change. For intrinsic fluorescence measurements, the concentration of protein is usually above 50 μg/ml.

Fluorescence spectroscopy can be used to measure the system in which suspended adsorbent particles provide an interface for protein adsorption [32, 33]. In contrast to CD, the wavelengths used are higher and the concentration of protein and adsorbent used are lower. This drastically reduces the effect of light scattering in fluorescence spectroscopy compared to CD spectroscopy. In addition, fluorescence spectroscopy is more sensitive than CD spectroscopy.

3 Protein structure determination using Fourier transforms infrared spectroscopy (FTIR)

The application of FTIR spectroscopy to protein analysis is based on the assessment of the amide bands. FTIR is a good method to determine the secondary structure of globular proteins [34-36]. Kumosinski *et al.* [37] demonstrated that the secondary structures of 14 proteins from FTIR spectroscopy was in excellent agreement with the values calculated from X-ray crystallographic data. Structural analysis using FTIR offers many advantages over other spectroscopy techniques. The major advantage is the lack of dependence on the physical state of the sample. Samples may be

gas, aqueous or organic solution, hydrated film, inhomogeneous suspension, or solid. The use of FTIR spectroscopy to analyze the structure of proteins has been extensively reviewed [36, 38-41]. FTIR is particularly suitable for the analysis of adsorbed proteins [42, 43]. It was applied to track the loss of secondary structure during insulin unfolding on a model lipid-water interface [44], proteins adsorb to silica surfaces [45-47], different clay surfaces [48], oil-water interface [49], air-water interface [50], and brushite [51]. The conformation of adsorbed protein depends on properties of the surface.

3.1 FTIR spectrum of protein

FTIR absorption bands are particularly sensitive to bond angles and hydrogen bands, theoretically, any specific alteration, peak shifts or intensity change, is caused by the changes in secondary structure of protein. Each type of secondary structure is thought to absorb at a specific frequency in FTIR spectrum [38]. The amide groups of polypeptides or proteins exhibit nine vibrational modes in the infrared region, giving rise to the amide bands A, B, and I-VII [40, 52]. However, due to the very low intensities, the amide IV-VII bands are not important in mid-infrared region. Only the amide I, amide II and amide III can be applied to determine secondary structure of proteins [53].

Amide I

The amide I vibration present as an infrared band from 1600 to 1700 cm^{-1}, around 1650 cm^{-1}, arises mainly from the C=O stretching vibration with minor contributions from the out-of-phase CN stretching vibration, the CNN deformation and the NH in-plane bend [34, 52]. About 70-85 % of the band intensity is from C=O stretching and 10-20 % is from CN stretching [34]. The amide I band is hardly affected by the nature of the amino acid side-chain. It only depends on the secondary structure of the backbone. Thus, it is best suited to determine the secondary structure of proteins.

Amide II

Amide II vibration is from 1500 to 1600 cm^{-1}, around 1550 cm^{-1}. Amide II is the out-of-phase combination of the NH in-plane bending (40-60 %) and the CN stretching vibration (18-40 % with smaller contributions from the CO in-plane bend and the CC and CN stretching vibrations [34]. As amide I, amide II is hardly affected by side-chain vibrations. However, the correlation between secondary structure and frequency is less straightforward as compared to the amide I region.

Amide III

Amide III vibration can be seen in the infrared region from 1200 to 1400 cm^{-1}. It is the in-phase combination of the NH bending and the CN stretching vibration with small contribution from the CN in-plane bending and CC stretching vibration [34]. Therefore, the amide III band is affected by

side-chain, and the backbone vibrations vary considerably, which makes the amide III vibration less suitable for secondary structure analysis. However, amide III vibration also has an advantage for secondary structure analysis of protein because of the reduced water effect. Previous studies also showed that the amide III region can be used to calculate the secondary structures for various proteins [54-57], although the amide III is much weaker than the amide I band. However, better band separation allows for curve-fitting without the need of employing resolution-enhancement methods. Griebenow and Klibanov found that the amide III results and X-ray data were in good agreement for most proteins [58].

3.2 The correspondence between protein secondary structure and amide bonds

A critical step in the interpretation of infrared spectra of proteins is to assign the component bands to different types of secondary structures. Theoretical and experimental attempts have been made to correlate FTIR absorption bands of protein to the secondary structure of protein either in aqueous state or in solid state. Briefly, bands in the range 1650-1658 cm^{-1} is generally associated with the presence of α-helix conformers in aqueous environments. Nevertheless, intensity increase in this region of the spectrum is hardly assigned to increase in α-helical structure alone, since α-helical structures overlap significantly with those from random or unordered structure (1645-1652 cm^{-1}) [59] and loops (1658-1665 cm^{-1}) [60]. When helical proteins are associated with membranes, the band appears in the range 1656 to 1658 cm^{-1}, whereas in soluble proteins this band occurs at the lower wave numbers, approximately 1650 to 1655 cm^{-1} [61].

The β-sheet vibration has been shown in region 1620 to 1640 cm^{-1}. The exact position is affected by varying strengths of the hydrogen bonding and transition dipole coupling in different β-strands [59]. The possibility of distinguishing between parallel and anti-parallel β-sheets was investigated in a previous study [62]. Bands around 1662-1690 cm^{-1} has been assigned as β-turn or turn. Beta-turns appear at a broad region in the amide I region due to the diversity of its geometries. Moreover, β-turn with internal hydrogen bonds gives rise to absorption band around 1638-1646 cm^{-1} [63]. Like the amide I, the amide II region is also used for investigation of the secondary structure of protein, but the correspondence between FTIR absorption bands and secondary structure is more complex than in the amide I region. Bands in the amide II region have not been well studied. Generally, bands in the range 1540-1550 cm^{-1} are regarded as α-helix. The β-sheet vibration is at the range 1520-1530 cm^{-1} [64, 65]. Beta-turns are assigned around 1568 cm^{-1} [66, 67].

In the amide III region, the protein absorption bands have not been fully understood due to the low intensity and high contribution from side chain vibrations. Cai and Singh [56] have reported that α-

helix bands usually appear in range 1295-1340 cm^{-1}; β-turns gives rise to bands around 1270-1295 cm^{-1}; random structure is at 1250-1270 cm^{-1}; and β-sheet is assigned from 1220 to 1250 cm^{-1}. The assignments of FTIR bands are given in Tab. 2.1.

Tab. 2.1 Band assignments in the amide I region of FTIR spectrum.

FTIR region	Wavenumbers (cm^{-1})	Secondary structure	References
Amide I	1620-1640	β-sheet	[59]
	1645-1652	Random or unordered	[59]
	1650-1658	α-helix	[59]
	1662-1690	β-turn	[59, 63]
Amide II	1520-1530	β-sheet	[64, 65]
	1540-1550	α-helix	[64, 65]
	1568	β-turn	[66, 67]
Amide III	1220-1250	β-sheet	[56]
	1250-1270	Random	[56]
	1270-1295	β-turn	[56]
	1295-1340	α-helix	[56]

3.3 Water absorption in FTIR spectrum

The absorption bands of a specific component can also be influenced by the contribution of other compounds. These contributions need to be removed before further analysis of the spectrum. The most common interfering substance is liquid water, which has three prominent bands centred at 3360 cm^{-1} (H-O stretching band), 2130 cm^{-1} (water association band) and at 1640 cm^{-1} (the H-O-H bending vibration) [43]. The amide I band for proteins absorption bands overlap directly with a water bending vibational band at 1640 cm^{-1}. The intensity of the water band at 1640 cm^{-1} is about an order of magnitude larger than the amide I bands of proteins and yet precise subtraction of the water band is possible because of the frequency precision in FTIR spectra.

Techniques have been developed to automatically subtract the water band to obtain information from the protein. The objective of these techniques is to eliminate the possible individual bias and uncertainty in the selection of the scale factor due to baseline variations. Powell and co-workers [68] approached the water subtraction problem through analysis of the change in the region from 1900 to 1790 cm^{-1} in the protein spectrum as the scale factor for the water spectrum is changed.

Dousseau *et al*. [69] assume that 2125 cm^{-1} water association band is not affected by the presence of protein. This assumption works for most proteins except when they are highly charged. The accuracy of subtraction of the very large water band at 1640 cm^{-1} is always a concern, but studies have shown that the positions and intensities of the bands are maintained even with deliberate over or under subtraction of the water peak [70]. A simple and practical method is to subtract the water band until the region from 1900 to 1740 cm^{-1} is flat. This method works well with most proteins and surface combinations if applied consistently.

3.4 Resolution-enhancement

Compared to NIR spectra, the peaks of MIR spectra are not that broad and overlapped, but it is still difficult to perform a straightforward analysis of the spectra, especially for complicated samples, *e.g.* proteins. Resolution-enhancement methods are applied to solve this problem. However, this terminology is misleading. Resolution is an instrumental parameter that cannot be changed after the spectra are collected. These mathematical techniques are more correctly referred to as band-narrowing procedures.

Fourier self-deconvolution (FSD) and derivation have been used for many years to allow visualization of overlapping bands [71-74].

FSD requires knowledge of the number of bands, their shapes and parameters, such as position, band width and intensity. For example, if the chosen band width is greater than the width of the peak being studied, the result will be side-lobes at the edges of the deconvoluted bands, which can lead to problems with visualization of weaker neighbouring bands. On the other hand, if the chosen band width is too small, the deconvoluted spectra will appear unaltered and no additional information will be gained. Moreover, if the bands are highly overlapped, the results obtained may be ambiguous and largely dependent on the initial parameters [75]. FSD also reduces the width of water vapour absorption and enhance noise, producing very sharp peaks with even minimal deconvolution. Noise and water vapour can very quickly become a problem in deconvoluted spectra. Thus, FSD should only be performed on spectra with a high signal-to-noise ratio (SNR) and a low contribution from water vapour [38]. A spectrum may be judged to be water vapour-free if no sharp absorption is seen from 1700 to 1800 cm^{-1}.

Derivative spectroscopy was introduced by Dong *et al.* [76], who analyzed the secondary structure of proteins in aqueous solution. It is mainly employed to identify the number of bands and their position. The derivative spectra are applied rarely for quantitative studies. The pitfalls that apply to FSD are also applicable to derivation. Furthermore, derivation suffers from the fact that relative

integrated intensities are not maintained. In addition, significant edge effects are possible in derivative spectra [38, 77]. If the spectrum has a significant slope at the edges of the peak to which derivation is to be performed, distortions will be introduced at the edges of the derivative spectrum. This is easily avoided by choosing a wider spectral region for derivative calculation, and the features at the edges of the extended region should be ignored.

3.5 Disadvantages of FTIR for protein structure analysis

As mentioned above, FTIR cannot provide full three-dimensional structural information of proteins. The spectrum of a protein may be influenced by water and other components. It also should be noted that high protein concentration (10-20% w/w) is normally needed for FTIR measurements for obtaining the SNR necessary for conformational analyses. This is due to the use of small path length in FTIR measurements [78, 79].

References

1. http://www.friedli.com/herbs/phytochem/proteins.html. Feb, 2006.
2. http://bmbiris.bmb.uga.edu/wampler/tutorial/prot2.html. Feb, 2006.
3. http://www.med.unibs.it/~marchesi/proteins.html. Feb, 2006.
4. Zhang C, Kim SH. Overview of structural genomics: from structure to function. Current Opinion in Chemical Biology, 2003; 7: 28-32.
5. Weert MVD, Hennink WE, Jiskoot W. Protein instability in poly (lactic-co-glycolic acid) microparticles. Pharmaceutical Research, 2000; 17: 1159-1167.
6. Chase HA, Purification of proteins from feedstocks containing particulate material by adsorption chromatography in expended beds, Trends Biotechnology, 1994; 12: 296-303.
7. Regnier FE. Chromatography of complex protein mixtures. Journal of Chromatography, 1987; 418: 115-143.
8. Horbett TA, Biological activity of adsorbed proteins. Surfactant Science Series, 2003; 110: 393-413.
9. Shen M, Martinson L, Wagner MS, Castner DG, Ratner BD, Horbett TA, PEO-like plasma polymerized tetraglyme surface interaction with leukocytes and proteins: in vitro and in vivo studies. Journal of Biomaterials Science, Polymer Edition, 2002; 13: 367-390.
10. Gray JJ: The interaction of proteins with solid surface. Current Opinion in Structural Biology, 2004; 14: 110-115.
11. Nakanishi K, Sakiyama T, Imamura K. On the adsorption of proteins on solid surfaces, a common but very complicated phenomenon. Journal of Bioscience and Bioengineering, 2001; 91: 233-244.
12. Malmsten M. Formation of adsorbed protein layers. Journal of Colloid and Interface Science, 1998; 207: 186-199.
13. Urano H, Fukuzaki S. Conformation of adsorbed bovine serum albumin governing its desorption behavior at alumina-water interfaces, Journal of Bioscience and Bioengineering, 2000; 90: 105-111.
14. McGuire J, Krisdhasima V. Surface chemical influences on protein adsorption kinetics. Food Technology, 1991; 45: 92-96.
15. Wahlgren M, Arnebrant T. Protein adsorption to solid surfaces. Trends in Biotechnology, 1991; 9: 201-208.

16. Herron J, Jikoot W, Crommelin DJA (Edts.). Physical methods to characterize pharmaceutical proteins. Plenum Pub Corp, New York, 1995.
17. Pusey ML, Liu ZJ, Termpel W, Praissman J, Lin D, Wang BC, Gavira JA, Ng JD. Life in the fast lane for protein crytalliztion and X-ray crystallography. Progress in Biophysics and Molecular Biology, 2005; 88: 359-386.
18. Jean-Philippe C, Hartmut L. X-ray crystallographic analysis of lipid-protein interactions in the bacteriorhodopsin purple membrane. Annual Review of Biophysics and Biomolecular Structure, 2003, 32: 285-310.
19. Tsuda S. Modern NMR spectroscopy and x-ray crystallography: a different approach to study the structure and its functions of a protein. Journal of the Crystallographic Society of Japan, 1996; 38: 84-88.
20. Hasler L, Heymann JB, Engel A, Kistler J, Walz T. 2D crystallization of membrane proteins: rationales and examples. Journal of Structural Biology, 1998; 121: 162-171.
21. Jahnke W, Widmer H. Protein NMR in biomedical research. Cellular and Molecular Life Science, 2004; 61: 580-599.
22. Mierlo CPMV, Steensma E. Protein folding and stability investigated by fluorescence, circular dichroism (CD), and nuclear magnetic resonance (NMR) spectroscopy: the flavodoxin story. Journal of Biotechnology, 2000; 79: 281-298.
23. Surewicz WK, Mantsch HH, Chapman D. Determination of protein secondary structure by Fourier transform infrared spectroscopy: A critical assessment, Biochemistry, 1993; 32: 389-394.
24. Conejero LF, ParradoJ, Lazuaga A, Smith RAG, Ponting CP, Dobson CM. Stability of the three domains of streptokinase studied by circular dichroism and nuclear magnetic resonance. Protein Science, 1996; 5: 2583-2591.
25. Engel MFM. Detailed characterized of adsorption-induced protein unfolding. Ph.D thesis. http://library.wur.nl/wda/dissertations/dis3563.pdf. Oct, 2005.
26. Bulone D, Martorana V, Biagio PLS. Effects of intermediates on aggregation of native bovine serum albumin. Biophysical Chemistry, 2001; 91: 61-69.
27. Itri R, Caetano W, Barbosa LRS, Baptista MS. Effect of urea on bovine serum albumin in aqueous and reverse micelle environments investigated by small angle X-ray scattering, fluoresecence and circular dichroism. Brazilian Journal of Physics, 2004; 34: 58-63.

28. Greenfield NJ. Methods to estimate the conformation of proteins and polypeptides from circular dichroism data. Analytical Biochemistry, 1996; 235: 1-10.
29. Castelain C, Genot C. Conformational changes of bovine serum albumin upon its adsorption in dodecane-in-water emulsions as revealed by front-face steady-state fluorescence. Biochimica et Biophysica Acta, 1994; 1199: 59-64
30. Gelamo EL, Tabak M. Spectroscopic studies on the interaction of bovine and human serum albumins with ionic surfactants. Spectrochimica Acta Part A, 2000; 56: 2255-2271.
31. Gelamo EL, Silva CHTP, Imassato H, Tabak M. Interaction of bovine (BSA) and human (HAS) serum albumins with ionic surfactants: spectroscopy and modeling. Biochimca et Biophysica Acta, 2002; 1954: 84-99.
32. Tan J, Martic P. Protein adsorption and conformational changes on small polymer particles, Journal of Colloid Interface Science, 1990; 136: 415-431.
33. Clark SP, Billsten P, Elwing H. A fluorescence technique for investigating protein adsorption phenomena at a colloidal silica surface. Colloid Surf. B-Biointerfaces 2, (1994) 457-461.
34. Barth A, Zscherp C. What vibrations tell us about proteins. Quarterly Reviews of Biophysics, 2002; 35: 369-430.
35. Byler DM, Susi H. Examination of the secondary structure of proteins by deconvolved FTIR spectra. Biopolymers, 1986; 25: 469-487.
36. Surewicz WK, Mantsch HH. New insight into protein secondary structure from resolution-enhanced infrared spectra. Biochemica et Biophysica Acta, 1988; 952: 115-130.
37. Kumosinki TF, Unruh JJ. Quantization of the global secondary structure of globular proteins by FTIR spectroscopy: comparison with X-ray crystallographic structure. Talanta, 1996; 43: 199-219.
38. Jackson M, Mantsch HH. The use and misuse of FTIR spectroscopy in the determination of protein structure. Critical Reviews in Biochemistry and Molecular Biology, 1995; 30: 95-120.
39. Surewicz WK, Mantsch HH, Chapman D. Determination of protein secondary structure by Fourier transform infrared spectroscopy: A critical assessment. Biochemistry, 1993; 32: 389-394.
40. Bandekar J. Amide modes and protein conformation. Biochimica et Biophysica Acta, 1992; 1120: 123-143.

41. Braiman MS, Rothschild KJ. Fourier-transform infrared techniques for probing membrane protein structure. Annual Review of Biophysics and Biophysical Chemistry, 1988; 17: 541-570.
42. Gray J. The interaction of protein with solid surface. Current Opinion in Structural Biology, 2004; 14: 110-115.
43. Chittur KK. FTIR/ATR for protein adsorption to biomaterial surfaces. Biomaterials, 1998; 19: 357-369.
44. Sharp JS, Forrest JA, Jones RA. Surface denaturaration and amyloid fibril formation of insulin at model lipid-water interface. Biochemistry, 2002; 41: 15810-15819.
45. Tunc S, Maitz MF, Steiner G, Vázquez L, Pham MT, Salzer R. In situ conformational analysis of fibrinogen adsorbed on Si surfaces. Colloids and Surfaces B: Biointerfaces, 2005; 42: 219-225.
46. Giacomelli CE, Bremer MGEG, Norde W. ATR-FTIR study of IgG adsorbed on different silica surface. Journal of Colloid interface Science, 1999; 220: 13-23.
47. Tarasevich YI, Monakhova LI. Interaction between globular proteins and silica surfaces. Colloid Journal, 2002, 64: 482-487.
48. S-Noinville S, Revault M, Quiquampoix H, Baron MH. Journal of Colloid and Interface Science, 2000; 221: 273-283.
49. Fang Y, Dalgleish DG. Conformation of β-lactoglobulin studied by FTIR: effect of pH, temperature, and adsorption to the oil-water interface. Journal of Colloid and Interface Science, 1997; 196: 292-298.
50. Meinders MBJ, Bosch GGM, Jongh HHJ. Adsorption properties of proteins at and near the air/water interface from IRRAS spectra of protein solutions. European Biophysics Journal, 2001; 30: 256-267.
51. Xie J, Riley C, Kumar M, Chittur K. FTIR/ATR study of protein adsorption and brushite transformation to hydroxyapatite. Biomaterials, 2002; 23: 3609-3626.
52. Krimm S., Bandekar J., Vibrational spectroscopy and conformation of peptides, polypeptides, and proteins. Advances in Protein Chemistry, 1986; 38: 181-364.
53. Griebenow K, Santos AM, Carrasquillo KG. Secondary structure of proteins in the amorphous dehydrated state probed by FTIR spectroscopy. The Internet Journal of Vibrational Spectroscopy, http://www.Ijvs.com/volume3/edition1/section3. Nov, 2005.

54. Cai S, Singh BR. A distinct utility of the amide III infrared band for secondary structure estimation of aqueous protein solution using partial least squares methods. Biochemistry, 2004; 43: 2541-2549.
55. Cai S, Singh BR. Theory and basic principles- Determination of the secondary structure of proteins from amide I and amide III infrared bands using partial least square method. ACS Symposium Series, 2000; 750: 117-131.
56. Cai S, Singh BR. Identification of beta-turn and random coil amide III infrared bands for secondary structure estimation of proteins. Biophysical Chemistry, 1999; 80: 7-20.
57. Fu FN, Deoliveira DB, Trumble WR, Sarkar HK, Singh BR. Secondary structure estimation of proteins using the amide III region of Fourier transform infrared spectroscopy: application to analyze calcium-banding-induced structural changes in calsequestrin. Applied Spectroscopy, 1994; 48: 1432-1441.
58. Griebenow K, Klibanov AM. Lyophilization-induced reversible structural changes of proteins. Proceedings of the National Academy of Science, 1995: 92: 10969-10976.
59. Haris PI, Severcan F. FTIR spectroscopic characterization of protein structure in aqueous and non-aqueous media. Journal of Molecular Catalysis B: Enzymatic, 1999; 7: 207-221.
60. Khurana R, Fink AL. Do parallel beta-helix proteins have a unique Fourier transform infrared spectrum. Biophysical Journal, 2000; 78: 994-1000.
61. Buijs J, Norde W. Changes in the secondary structure of adsorbed IgG and $F(ab)_2$ studied by FTIR spectroscopy. Langmuir, 1996; 12: 1605-1613.
62. Oberg KA, Ruysschaert JM, Goormaghtigh E. The optimization of protein secondary structure determination with infrared and circular dichroism spectra. European Journal of Biochemistry, 2004; 271: 2937-2948.
63. Mantsch HH, Perczel A, Hollosi M, Fasman GD. Characterization of beta-turns in cyclic hexapeptides in solution by Fourier-transform IR spectroscopy. Biopolymers, 1993; 33: 201-207.
64. Tamm LK, Tatulian SA. Infrared spectroscopy of proteins and peptides in lipids bilayers, Quarterly reviews of biophysics, 1997; 30: 365-429.
65. Speare JO, Rush TS. IR spectra of cytochrome c denatured with deuterated guanidine hydrochloride show increase in β sheet. Biopolymers, 2003; 72: 193-204.

66. Lacey DJ, Wellner N, Beaudoin F, Napier JA, Shewry PR. Secondary structure of oleosins in oil bodies isolated from seeds of safflower (Carthamus tinctorius L.) and sunflower (Helianthus annuus L.). Biochemical Journal, 1998: 334: 469-477.
67. Krimm S. Bandekar J. Vibrational spectroscopy and conformation of peptides, polypeptides, and proteins. Advances in Protein Chemistry, 1986; 38: 181-364.
68. Powell JR, Wasacz FM, Jacobsen RJ. An algorithm for the reproducible spectral subtraction of water from the FTIR spectra of proteins in dilute solutions and adsorbed monolayers. Applied Spectroscopy, 1986; 40: 339-344.
69. Dousseau F, Therrien M, Pezolet M. On the spectral subtraction of water from the FTIR spectra of aqueous solution of proteins. Applied Spectroscopy, 1989; 43: 538-542.
70. Lenk TJ. Infrared studies of protein adsorption and transitions on polyurethanes. PhD dissertation, University of Washington Chemical Engineering, 1994
71. Cameron DG, Moffatt DJ. A generalized approach to derivative spectroscopy. Applied Spectroscopy, 1987; 41: 539-544.
72. Cameron DG, Moffatt DJ. Deconvolution, derivation and smoothing of spectra using Fourier transforms. Journal of Testing & Evaluation, 1984; 12: 78-85.
73. Kauppinen JK, Moffatt DJ, Mantsch HH, Carmeron DG. Fourier transforms in the computation of self-deconvolution and first-order derivative spectra of overlapped band contours. Analytical Chemistry, 1981; 53: 1454-1457.
74. Kauppinen JK, Moffatt DJ, Mantsch HH, Cameron DG. Fourier self-deconvolution: a method for resolving intrinsically overlapped bands. Applied Spectroscopy, 1981; 35: 271-276.
75. Czarnecki MA, Ozaki Y. Determination of integrated intensities of overlapped IR bands by curve-fitting, Fourier self-deconvolution and combination of both methods, Spectroshimica Acta Part A, 1996; 52: 1593-1601.
76. Dong A, Huang P, Caughy W. Protein secondary structures in water from second-derivative amide I infrared spectra. Biochemistry, 1990; 29: 3303-3308.
77. Moffatt DJ, Mantsch HH. Fourier resolution enhancement of infrared spectral data. Methods in Enzymology, 1992; 210: 192-200.
78. Haris PI, Severcan F. FTIR spectroscopic characterization of protein structure in aqueous and non-aqueous media. Journal of Molecular Catalysis B: Enzymatic, 1999; 7: 207-221.

79. Jackson M, Mantsch HH. The use and misuse of FTIR spectroscopy in the determination of protein structure. Critical Reviews in Biochemistry and Molecular Biology, 1995; 30: 95-120.

Chapter III: Characterization of the structural changes of model antigen when it is absorbed onto and released from aluminium hydroxide using FTIR-ATR

Abstract

Aluminium hydroxide is often used as adjuvant in specific immunotherapy, i.e. allergy vaccination. Structural integrity of antigens upon adsorption and release is not only important for investigating vaccine immunogenicity, but also for the epitope specificity of the resulting immune response and hence therapeutic efficacy. However, it is also important for understanding the mechanism of how adjuvants can enhance the immune response. However, little is known about an antigen's structure when it is adsorbed and subsequently released from aluminium adjuvants. In this study, the structural changes of two model antigens, bovine serum albumin (BSA) and β-lactoglobulin (BLG), were investigated using Fourier transform infrared – attenuated total reflection (FTIR-ATR) spectroscopy. The secondary structures of both model antigens change when absorbed to aluminium hydroxide. The structural perturbation depends on the amount of the adsorbed protein. Maximal adsorption gives a more native-like structure than lower protein adsorption. This may indicate that protein is adsorbed by aluminium hydroxide by different mechanisms depending on the concentration. The adsorbed model antigens are released using phosphate buffer (PBS) pH 7.4 with final concentrations between 5 mM and 200 mM. The maximum antigen recovery is 80% after 40 min in the presence of phosphate buffer (PBS). The recovery curves of both proteins also indicated two different adsorption modes. FTIR-ATR and circular dischroism (CD) spectroscopy yield similar results suggesting that the antigens refold to their native state after release. Released BSA regains its native structure more complete than BLG.

1 Introduction

Antigens are proteins capable of inducing specific immune responses when injected to humans. The molecular properties of antigens and the way in which these properties contribute to immune activation are central to determine the outcome of vaccination treatments. All four levels of protein organization—primary, secondary, tertiary, and quaternary—affect its immunogenicity [1]. The structural information of the antigen is not only important for investigating its immunogenicity; it is also important to understanding of the interaction between antigen and adjuvant and the mechanism of how adjuvant can enhance the immune response. In general, proteins have a very fragile three-dimensional structure [2, 3], and this structure may easily change in different environments, such as binding to membranes, at air-water interfaces, under pressure, or even during drying and storage. Protein adsorption processes are believed to cause structural changes in the protein. Previous studies have shown that the adsorption of a protein onto interfaces or solid surfaces induces structural changes in the protein [4-8]. These structural changes during absorption may lead to irreversible aggregate formation, inactivate the ability to induce an immune response, or even cause serious side-reactions. Protein aggregation is difficult to control and hampers precise prediction of the release profile of the protein. Furthermore, protein aggregates can be immunogenic and may potentially constitute risk patients.

Aluminium adsorbed vaccines have been safely used for many years. However, the structure of the antigen when adsorbed to aluminium-containing adjuvants, have not been well characterized. Two studies have addressed the structure of aluminium adsorbed proteins [9, 10], but a major obstacle is the lack of experimental techniques allowing structural information to be obtained directly on this complex system. Hem and white demonstrated that a slight deformation of the structure of pepsin occurred when adsorbed by aluminium hydroxide using infrared spectroscopy. They regarded this an example of ligand exchange [9]. Jones *et al.* [10] studied the structures of model antigens as a function of temperature by FTIR-ATR spectroscopy in order to investigate vaccine stability. To our knowledge, there is no available structural information of released antigens from aluminium-containing adjuvants.

FTIR spectroscopy is a good method to determine the secondary structure of globular proteins. It offers many advantages over other spectroscopic techniques [11, 12]. A major advantage is the lack of dependence on the physical state of the sample. Sample can be gas, aqueous or organic solution, hydrated film, inhomogeneous suspension, or solid. FTIR is particularly suitable for the analysis of proteins adsorbed by other materials, especially when an ATR crystal is used. FTIR was applied to

study the loss of secondary structure during insulin unfolding in a lipid-water interface model [13] and protein adsorption by silica, polysulfone, and other biomaterials [14-17].

CD spectroscopy is a suited method to monitor the secondary and tertiary structure of proteins in solution [18]. Far-UV CD (170-250 nm) spectroscopy is a good tool to obtain the overall information of the secondary structure. However, the analyses involve complex calculations using a standard set of reference proteins as a basis for estimation and thus yield only indirect measures [19]. Moreover, CD spectroscopy is not a suitable technique for measuring the adsorbed protein in suspension because light cannot pass through such high density samples.

Protein	α-helix	β-sheet	Random
BSA	66	03	31
BLG	06	46	48

Tab. 3.1 Secondary structures content in two model proteins [21].

In this study, FTIR-ATR and CD spectroscopy were applied to investigate the structural changes of model antigens. The model antigens were adsorbed by aluminium hydroxide and subsequently released using phosphate buffer (PBS) at pH 7.4. PBS was chosen because phosphate anions easily adsorb onto the surface of aluminium hydroxide through ligand exchange displacing the antigens from the aluminium adjuvant [20]. Bovine serum albumin (BSA) and β-lactoglobulin (BLG) were used as model antigens because their structures have been well studied. They are α-helix-rich and β-sheet-rich proteins, respectively. BSA consists of 66% α-helix and BLG contains 46% β-sheet as shown in Tab. 3.1[21]. BSA is made up of 100 acidic side chains with 41 Asp and 59 Glu residues and 99 basic side chains with 23 Arg, 59 Lys, and 17 His. The isoelectric point of BSA is 4.8 [22]. BSA is a small globular protein with a molecular weight of approximate 66.4 kDa. BLG has a well-known structure containing one very short helix segment and eight strands of anti-parallel β-sheet, which wrap to form an anti-parallel β-barrel. BLG exists at neutral pH as a dimmer in its native state. Each monomer constituted by identical 162 amino acids, with one free thiol group and two disulphide bridges. The isolectric point of BLG is 6.5 and the molecular weight is approximately 18.3 kDa [23, 24].

2 Materials and methods

2.1 Materials

Clinical reagent grade BSA (reference L84960) and approximate 90% pure BLG (reference L3908)

were purchased from ICN biomedical Inc and Sigma respectively. Both proteins were used directly without further purification. Aluminium hydroxide adjuvant was purchased from Superfos Biosector A/S (Denmark) and used without further treatment. Other chemicals were all of analytical grade and obtained from commercial sources.

2.2 Adsorption experiments

Sample preparation

A protein stock solution (10 mg/ml) was prepared by dissolving protein in Milli-Q water. Working samples were prepared by mixing the appropriate amount of protein stock solution and aluminium hydroxide and subsequently diluted to 1 ml using Milli-Q water. The final calculated aluminium concentration was 3.4 mg/ml for all samples; the final protein concentrations were from 1mg/ml to 5mg/ml, with final pH 6.5. Samples were mixed gently by end-over-end rotation for 30 min to obtain the maximum protein adsorption before FTIR measurement.

FTIR-ATR measurement

Spectra were collected using a FTIR spectrometer (PerkinElmer Spectrum One), which was mounted with a three bounces ZnSe ATR crystal (PerkinElmer). An 8 µl sample was deposited onto ATR crystal and by evaporating the solvent to obtain a film. The calculated amount of aluminium hydroxide for a film was 27.2 µg; and the calculated value of protein was from 8 µg to 40 µg, respectively. Spectra were directly recorded on the film by co-adding 128 scans with a resolution of 4 cm^{-1} at a scan speed 0.2 cm/s. Control spectra were collected from the samples which contained the same components except protein at same experimental conditions. All samples were analyzed at least in duplicate.

2.3 Release experiments

Sample preparation

Samples were prepared as described for the adsorption experiments. The final concentration of aluminium hydroxide was 3.4 mg/ml for each sample; final protein concentration was 4 mg/ml for BSA and 3 mg/ml for BLG. The samples were gently rotating by end-over-end at room temperature for one hour, and stored at 4 ºC overnight. Adsorbed proteins were released by adding PBS pH 7.4 to a final concentration between 5 and 200 mM at room temperature. Samples were incubated for 40 min before measurement.

FTIR-ATR measurements

FTIR measurements were performed on the same instrument as mentioned for the adsorption experiments. Measuring films were made in either of two ways: by evaporating the complex of protein and aluminium hydroxide; or by measuring released protein alone after centrifugation at 6800 × g for 10 min. Blank samples contained the same components except protein at same condition. All samples were measured at least in duplicate.

CD measurements

Adsorbed protein was released using PBS pH 7.4 at a final concentration of 150 mM for 40 min. Control samples were in prepared using the same components except protein. Free protein solutions were prepared by dissolving appropriate amounts of protein in the supernatant which was obtained from the control experiment.

CD measurements were carried out using an Olis spectropolarimeter (On-line instrument systems, Inc. USA), equipped with a temperature control system. Protein solutions were scanned in a 0.1 cm quartz cuvette five times at 15 ºC. In order to compare the CD spectra of the free protein and the released protein, protein concentrations were identical. Free protein solutions were also measured from 15 ºC to 90 ºC, with 5 ºC interval. At each temperature, the sample was incubated for 2 min before scanning.

Ultraviolet spectrophotometry (UV) measurements

After 40 minutes release, the samples were centrifuged at 6800 × g for 10 min, and the supernatants were measured using an UV/VIS spectrophotometer (Lamda 800, PerkenElmer instruments) at 280 and 320 nm. The protein recovery from aluminium hydroxide was calculated from the following equation (Eq. 3.1):

$$R = \frac{\frac{A'_{280} - A'_{320}}{\varepsilon} - \frac{A_{280} - A_{320}}{\varepsilon}}{AC} \times 100\% \qquad \text{Eq. 3.1}$$

Where R is protein recovery, ε is extinction coefficient, AC is adsorption capacity, A_{280} is the absorbance of protein at 280 nm in MilliQ water. A'_{280} is absorbance at 280 nm in the presence of PBS. So are the A_{320} and A'_{320}.

2.4 Data analysis

FTIR data

All FTIR spectra were analyzed using Unscrambler Ver. 9.2 software (Camo process AS). The replicated spectra of the same sample were averaged first. The spectrum of a corresponding blank

sample was subtracted from the spectrum of adsorbed proteins. A flat baseline from 1900 to 1740 cm^{-1} was obtained for each spectrum after background subtraction. A window size of 23-point Savitsky-Golay smoothing function was applied to each spectrum. The second derivative spectra were calculated using a window size of 11-point Savitsky-Golay function from 1750 to 1220 cm^{-1}. The inverted second derivative spectra were obtained by multiplying with -1 for convenient interpretation. Finally, the spectra were baseline corrected, mean normalized, transferred into Excel file and plotted.

CD data

Before analysis, a CD spectrum of control sample, which contained all components except protein, was subtracted from each CD spectrum.

3 Results and discussion

3.1 Protein adsorption by aluminium hydroxide

Typical FTIR spectra of BSA and BLG adsorbed by aluminium hydroxide and recorded on films are shown in Fig. 3.1. For comparison, the spectrum of pure aluminium hydroxide is also presented in same figure. It is seen that amide I (1700-1600 cm^{-1}) and amide II (1600-1500 cm^{-1}) bands are not affected by the absorption of aluminium hydroxide enabling to the aluminium hydroxide background subtraction. The subtracted spectra in the region from 1800 cm^{-1} to 1200 cm^{-1} are given in Fig. 3.2. Subtraction of background is dangerous. Over or under subtraction of the spectra may damage the final spectra. A simple and practical method is to subtract background until the region from 1900 to 1740 cm^{-1} is flat. This method works well with most proteins when adsorbed by other materials, if it is applied consistently. However, studies also have shown that the positions and intensities of the bands are maintained even with deliberate over or under subtraction of the background spectrum [25]. In this study, potential alterations of the secondary structure of model antigens are monitored in the amide I and amide II region of the final inverted 2^{nd} derivative FTIR spectra.

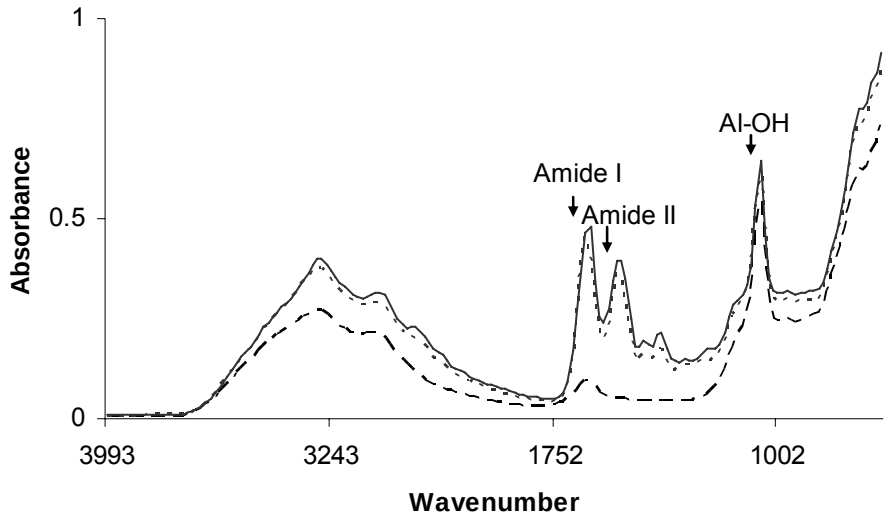

Fig. 3.1 Typical FTIR spectra of protein adsorbed by aluminium hydroxide measured on films: absorbed BSA (dotted line), adsorbed BLG (solid line), and aluminium hydroxide alone (dashed line)

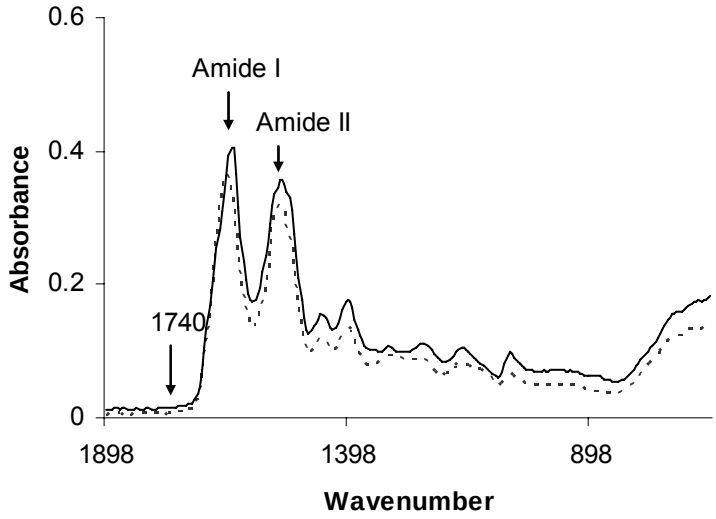

Fig. 3.2 The subtracted spectra of protein: BSA (dotted line) and BLG (solid line).

The inverted 2nd derivative FTIR spectra of free BSA, adsorbed BSA and aggregated BSA are given in Fig. 3.3. Except when specifically mentioned, in this paper free protein means pure protein; adsorbed protein means that protein adsorbed to aluminium hydroxide; and the aggregated protein is the protein that has been preheated at 90 ºC for 30 min. The spectra present that there are band-broadening and induction of new peak for adsorbed BSA in amide I and amide II regions. A novel

peak at 1646 cm^{-1} is induced and can be assigned to random structure. Another band at 1653 cm^{-1} decreases in intensity, which ascribes to α-helix. In other words, adsorbed BSA loses its α-helix but gains random structure in amide I range. In amide II region, two new bands are induced at 1549 cm^{-1} and 1533 cm^{-1}. Bands around 1570 cm^{-1} and 1513 cm^{-1} increase in intensity during adsorption. The significant difference in the spectra of adsorbed BSA and free BSA indicates that the secondary structure of BSA changes when adsorbed to aluminium hydroxide. Noinville *et al.* [26] had studied BSA adsorbed by montmorillonite and concluded that all unfolding processes involve about 20% of the backbone.

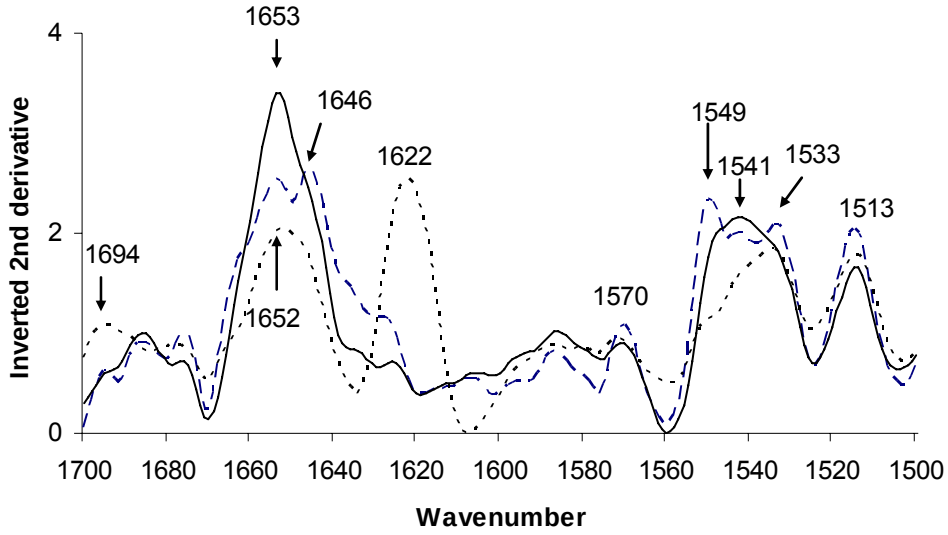

Fig. 3.3 Inverted 2nd derivative spectra of BSA in amide I and amide II region: free BSA (solid line), adsorbed BSA (dashed line) and aggregated BSA (dotted line).

In order to compare the structural difference of adsorbed protein and the aggregated protein, BSA was preheated at 90 ºC for 30 min and the spectrum was recorded under identical experimental condition at room temperature. The final inverted 2nd derivative spectrum of aggregated BSA is also shown in Fig. 3.3 for comparison. For aggregated BSA, there are two novel bands around 1622 cm^{-1} and 1694 cm^{-1} in the amide I region. The band at 1622 cm^{-1} is extremely strong. These two bands relate to intermolecular anti-parallel β-sheet formation. The result agrees with other heat-denatured protein aggregates [27-29]. In the amide II range, aggregated BSA loses intensities at 1549 cm^{-1} and 1541 cm^{-1} compared to adsorbed and free BSA. These significant differences indicate that the adsorption-induced secondary structural change is not the same as observed for protein aggregation.

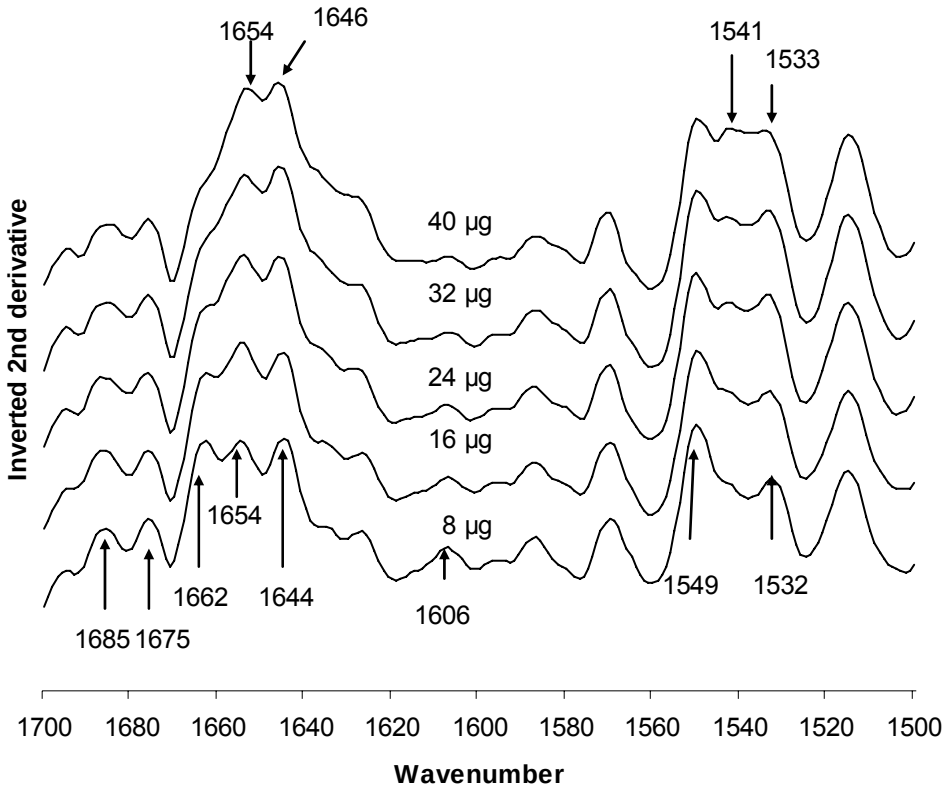

Fig. 3.4 Inverted 2nd derivative spectra of different amount of BSA adsorbed by same amount of aluminium hydroxide in amide I and amide II region.

Protein adsorption capacity by aluminium adjuvants has well been studied. Aluminium hydroxide can adsorb different amounts of protein depending on the protein. Adsorption of different amounts of protein may not result in same structural changes. To elucidate the absorption level effect, we investigated the structures at different ratios for protein adsorption by aluminium hydroxide.

Five amounts of BSA, from 8 µg to 40 µg with 8 µg interval, were adsorbed by same amount of aluminium hydroxide (27.2µg), and measured under identical experimental condition. The inverted 2nd derivative spectra are given in Fig. 3.4. The spectra were significantly different in the amide I and amide II regions due to the intensity changes and peak shifts. For low ratio of adsorbed BSA, *e.g.* 8 µg, bands in amide I region increase in intensity around 1685, 1675, 1662, and 1606 cm^{-1}. On the other hand, in the spectra of high ratio of adsorbed BSA, *e.g.* 40 µg, bands increase around 1654 and 1646 cm^{-1}, which are the α-helix and random structure. In the amide II region, high ratio of adsorbed protein loses intensities at 1549 and 1532 cm^{-1}, but the band at 1941 cm^{-1} increase. The band at 1532 cm^{-1} shifts to 1533 cm^{-1} for a low ratio of adsorbed BSA. Therefore, the structure of

adsorbed protein depends on how much protein is adsorbed by the aluminium adjuvant. A high ratio of adsorbed BSA gives a native-like structure.

In the case of BLG, the experiments were performed using the same experimental condition as for BSA. Fig. 3.5 presents the inverted 2nd derivative spectra of free BLG, adsorbed BLG and aggregated BLG. The spectral difference between adsorbed BLG and free BLG are due to peak shifts and band broadening in the amide I region, and intensity changes in the amide II region. The broadest band widens and shifts from 1630 to 1636 cm^{-1} for adsorbed BLG, which can be ascribed to β-sheet. A shoulder peak is induced at 1644 cm^{-1}, which can be assigned to random structure. Another difference in the amide I range is the intensity of the band at 1665 cm^{-1}; adsorbed BLG has a stronger absorption. In the amide II region, the intensities of three peaks increase considerably around 1551, 1533, and 1514 cm^{-1} for adsorbed BLG. These significant spectral alterations indicated that the secondary structure of BLG is dramatically modified when adsorbed by aluminium hydroxide, revealing a strong effect of the aluminium adjuvant on BLG. The results is excellent an agreement with other study, in which BLG rearranged when adsorbed to dimyristoyphosphatidylglycerol (DMPG) [30].

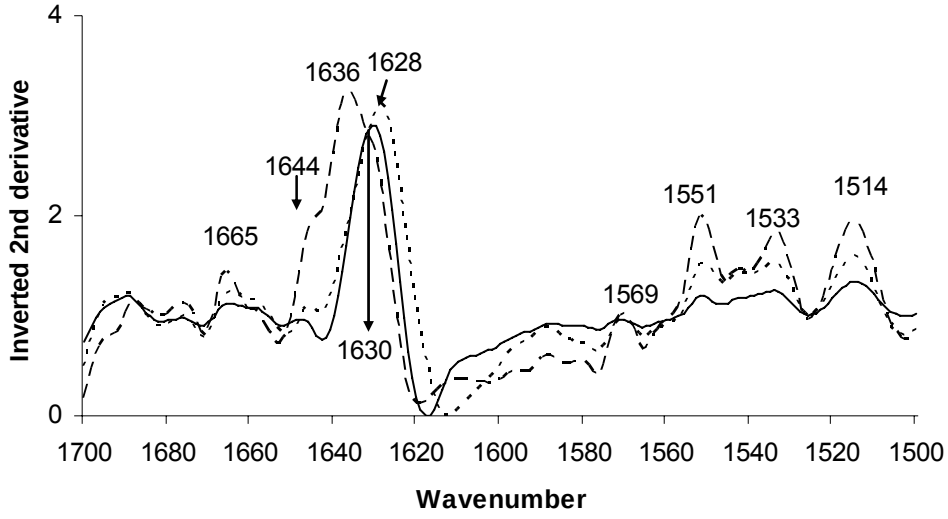

Fig. 3.5 Inverted 2nd derivative spectra of BLG in amide I and amide II region: free BLG (solid line), adsorbed BLG (dashed line) and aggregated BLG (dotted line).

In order to compare the adsorption-modified structure and the heat-induced structure, Heat induced aggregation of BLG was also investigated in this work. Fig. 3.6 presents the spectrum of aggregated BLG. It has been preheated at 90 ºC for 30 min and measured under identical experimental conditions. The spectrum of aggregated BLG differs from free BLG by band-broadening and band

shift from 1630 to 1628 cm^{-1} in amide I region. In contrast, this band of adsorbed BLG shifts to high wavenumber, 1636 cm^{-1}. In the amide II range, the intensities of three bands around 1551, 1533 and 1514 cm^{-1} increase for both aggregated BLG and adsorbed BLG. Surprisingly, adsorbed BLG has stronger absorption for these three bands than aggregated BLG. This is an indication that BLG is not extensively unfolded at this heat process or that the unfolded structure refold when retuning to room temperature. However, the structure is dramatically modified by adsorption onto aluminium hydroxide.

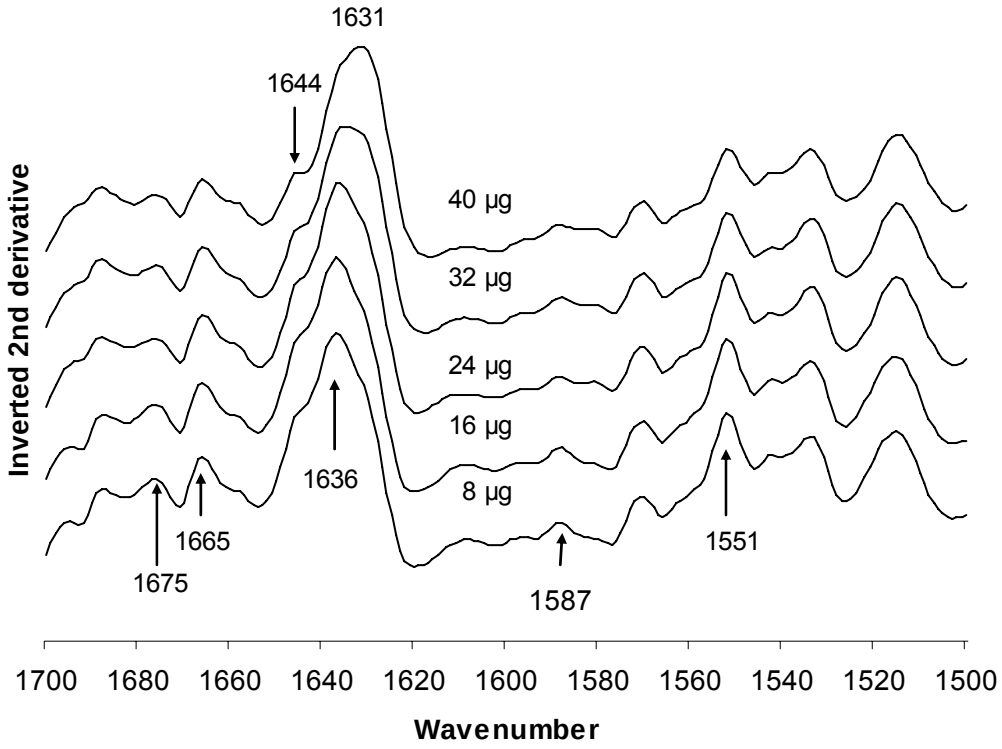

Fig. 3.6 Inverted 2nd derivative spectra of different amount of BLG adsorbed by same amount of aluminum hydroxide in amide I and amide II region.

Five concentrations of BLG, from 8 to 40 µg with an 8 µg interval, were adsorbed by 27.2 µg aluminium hydroxide, respectively. FTIR spectra were collected at identical conditions. The inverted 2nd derivative spectra are shown in Fig. 3.6. Spectral differences are mainly due to band shifts and intensity changes. The β-sheet band shifted from 1636 cm^{-1} to 1631 cm^{-1} according to protein adsorption increasing, *e.g.* from 8 µg to 40 µg. The band at 1644 cm^{-1}, which is random structure, loses intensity for a high ratio of adsorbed BLG, *e.g.* 40 µg. This phenomenon is different from was observed with adsorbed BSA.

Two bands at 1675 and 1665 cm^{-1} have stronger absorption at a low ratio adsorbed of BLG. In the amide II range, a low ratio of adsorbed BSA has a stronger absorption at 1551 cm^{-1}. Therefore, the structures differ as a function of amount of adsorbed BLG. The more BLG adsorbed, the more native-like the structure is. Interference from free BLG in the adsorbed sample can not be excluded in this case, as BLG can not be totally adsorbed by aluminium hydroxide even at very low concentrations. Free protein may affect the final spectra, especially for high amount of protein adsorption such as 40 μg.

Antigen adsorption is believed resulting from the electrostatic attraction between protein and aluminium adjuvant. When antigen is adsorbed onto aluminium surface, the resulting intermolecular electrostatic interaction may weaken the intramolecular forces that stabilize the protein native structure. It may be the reason of adsorption-induced structural changes in the antigens.

The manner by which the structural changes depends on the adsorbed amount of protein, which is in agreement with other studies [31, 32]. Urano *et al.* [31] demonstrated that BSA was adsorbed on the Al_2O_3 surface by formation of a monomolecular layer. A model of BSA adsorption was proposed according to which protein was adsorbed in two different configurations depending on the amount of adsorbed protein. Nevertheless, Urano *et al*. [31] did not conclude that protein structure changes due to adsorption using potentiometric titration. It is probably because the conformation of adsorbed protein depends on the prosperities of the aluminium hydroxide surface [33, 34]. In this study, two model proteins are adsorbed by aluminium hydroxide resulting in different conformations. Small amounts of protein are strongly adsorbed by aluminium hydroxide. The protein molecules form a monomolecular layer on aluminium hydroxide and secondary structure becomes more denatured. On the other hand, the structural perturbation of the protein becomes smaller when the degree of banding decreases. A high ratio of adsorbed protein is weakly adsorbed via few linking points. The protein molecules are oriented perpendicular onto the aluminium hydroxide, which results in a native-like structure. This model is illustrated in Fig. 3.7. However, structural changes of the proteins when adsorbed on the ATR crystal cannot be excluded. Previous study showed that the changes in protein structure may occur upon adsorption onto ATR surface [35].

Fig. 3.7 The model of protein adsorbed by aluminium hydroxide: large cure presents the molecule of aluminium hydroxide; and small cures present the molecules of protein. The direction of arrow shows the protein concentration increasing.

The mechanism of how aluminium adjuvants can enhance the immune response is still poorly understood. Jones *et al.* [10] proposed that protein structure became destabilized upon adsorption by aluminium adjuvants. These physical changes of adsorbed antigens made them more susceptible to proteolytic processing by the immune system, resulting in an enhanced antigen presentation. According to this hypothesis, vaccines with low ratio of protein adsorption should induce stronger or similar immune response as compared to high ratio adsorption, since it has a more destabilized structure. This hypothesis is confirmed by Lund *et al.* (unpublished data). Lund and co-workers studied the immune response after immunisation of mice using different ratios of antigen and aluminium hydroxide. They concluded that low protein adsorption give rise to similar immune response as did maximal protein adsorption. In this study, the different structures resulting from different amount protein adsorption may give the explanation of this phenomenon. Moreover, denatural proteins may be pharmaceutically inactive for its treating purposes, but it may be the reason why it causes immunogenicity, which was regarded as side effect in other fields [36, 37].

3.2 Release of protein from aluminium hydroxide

PBS is capable of replacing pre-adsorbed BSA and BLG from aluminium hydroxide. The protein recovery (amount of released proteins / adsorbed protein) at different PBS concentration is shown Fig. 3.8. Protein release from aluminium hydroxide is quite fast; recovery is around 80% within 40 minutes both for BSA and BLG. These high values indicate that pH 7.4 PBS is a good candidate for replacement of protein from aluminium hydroxide. Some surfactants have also been used for protein release from aluminium adjuvant [38, 39]. The recovery of protein is proportional to the concentration of buffer, especially for BLG. The amount of released BSA decreases after at PBS exceeding 130 mM. Both for BSA and BLG, adsorbed protein can not be totally released from aluminium hydroxide. Incomplete release may associate with aggregation. The aggregated protein can not be released from aluminium hydroxide. Protein recoveries do not increase significantly

even when increasing the final PBS concentration from 50 mM to 100 mM. The curves have two platens lat stages. It may indicate that proteins have different adsorption conformations on the aluminium hydroxide.

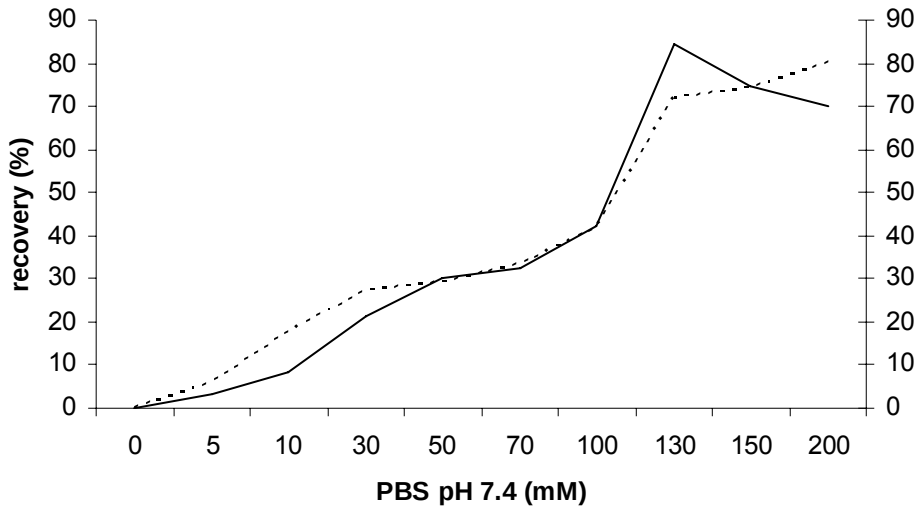

Fig. 3.8 Recovery of proteins that are first adsorbed by aluminium hydroxide and subsequently released using pH 7.4 PBS at different concentrations. The incubation time in the presence of PBS is 40 min. The recovery was calculated by the released amount / adsorbed protein.

The structure of released protein was measured by FTIR spectroscopy in two ways, either using the complex of protein and aluminium hydroxide or using only the released protein without adjuvant after centrifugation. Fig. 3.9 shows the inverted 2nd derivative spectra of released BSA in the amide I and the amide II regions. For comparison, the adsorbed BSA and free BSA are also shown in same figure. In the amide I range, released BSA loses random structure at 1646 cm^{-1} and regains α-helix structure at 1654 cm^{-1}. In the amide II range, band at 1546 cm^{-1} shifts from 1549 cm^{-1} comparing to adsorbed BSA, and a band is lost at 1533 cm^{-1}. All makes the spectrum of released BSA look like the spectrum of free one. This may be an indication that released BSA again regains the native structure. This meets to the study of Engel *et al.* [39]. They showed that released bovine α-lactalbumin (BLA) from polystyrene nanospheres had native spectroscopic properties. The structure of adsorbed BLA refolded to its native state upon release from the surface. There is a small spectral difference between released BSA when measured in complex of the released protein and aluminium and when measured on the released protein alone. This can be explained by the former sample

having 20 % adsorbed BSA, which cannot be released.

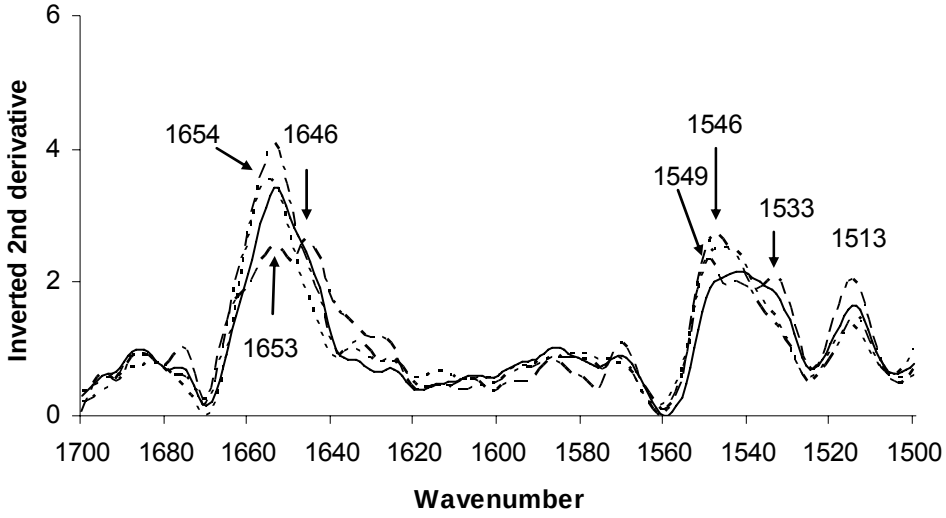

Fig. 3.9 Inverted 2nd derivative spectra of BSA in amide I and amide II region: free BSA (solid line), adsorbed BSA (dashed line), released BSA which measured on the complex of protein and aluminium hydroxide (dotted line), and released BSA which measured on protein alone after centrifugation (dash-dotted line).

The refolding procedure was studied by investigating the release using different final PBS concentrations, from 5 mM to 200 mM. The spectra were recorded on the complex sample of protein and aluminium hydroxide. For low PBS concentration the sample has more adsorbed protein, whereas, there is more released protein in sample containing high PBS concentration. Fig. 3.10 presents the inverted 2nd derivative spectra of released BSA. It is seen that in amide I range, Band at 1646 cm^{-1}loses, and the band at 1653 cm^{-1} becomes stronger with increasing PBS concentration. Random structure is lost and the amount of α-helix increases. In amide II region, bands at 1569, 1549, 1533 and 1514 cm^{-1} lose intensity, and the band at 1543 cm^{-1} increases. These structural alterations make the spectrum more native-like if increasing PBS concentration.

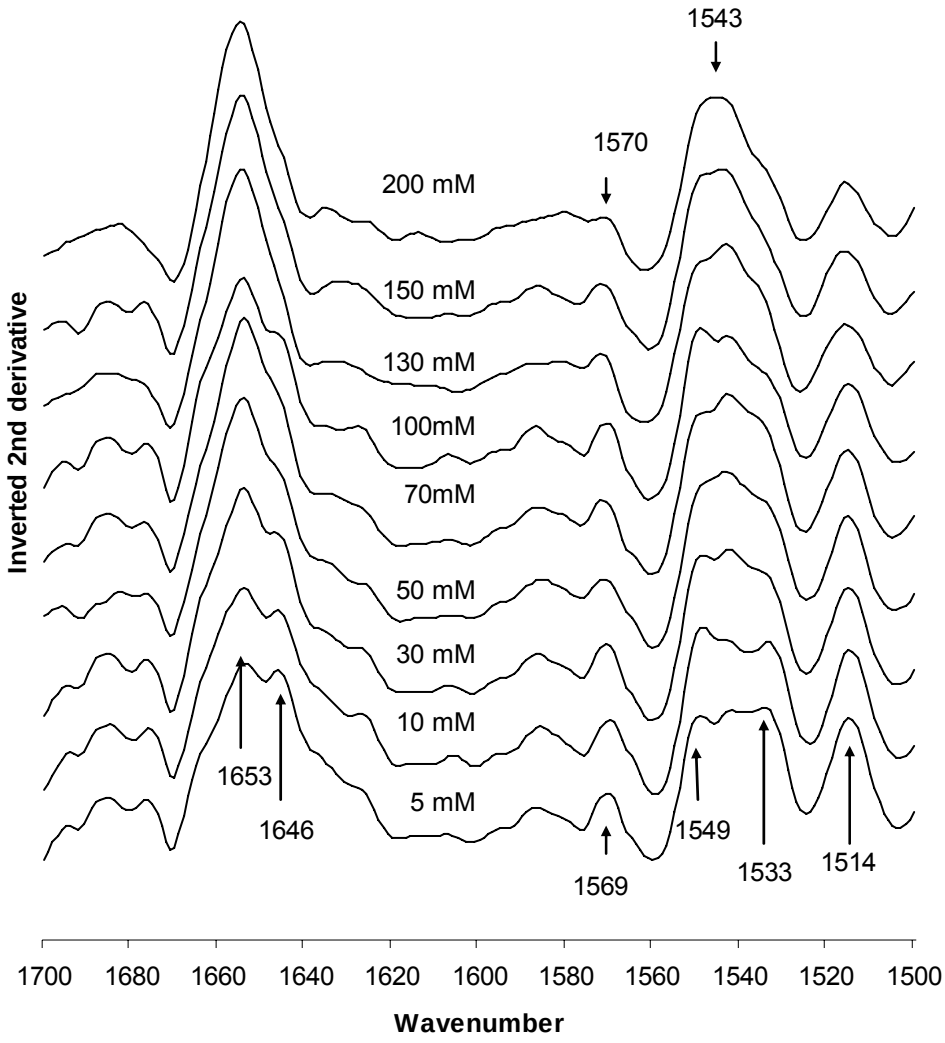

Fig. 3.10 Inverted 2nd derivative spectra of released BSA in amide I and amide II region: adsorbed protein has been released using pH 7.4 PBS at different concentrations (from 5 mM to 200 mM) for 40 min respectively. The spectra are recorded on the complex of protein and aluminium hydroxide.

The inverted 2nd derivative FTIR spectra of free BLG, adsorbed BLG, and released BLG are given in Fig. 3.11. In the amide I region, β-sheet band shifts from 1636 cm^{-1} to 1631 cm^{-1} for released BLG as compared to adsorbed BLG, and thus the spectrum of released BLG more closely resembles that of free BLG. In the amide II range, bands at 1569, 1551, 1533, and 1514 cm^{-1} for released BLG are similar to free one. These indicate released BLG regain its native structure. However, it is not as

complete as BSA. Fig. 3.12 shows the inverted 2nd derivative spectra of BLG which are released using different PBS concentrations, from 5 mM to 200 mM. The spectra were also measured on the complex of protein and aluminium hydroxide. It is seen that β-sheet band at 1636 cm^{-1} shifts to 1631 cm^{-1}, and band at 1541 cm^{-1} becomes stronger. A few bands 1665, 1644, 1569, 1551, 1533 and 1514 cm^{-1} decrease intensity as a function of PBS concentration. These changes make the spectrum become more native-like since there is more released protein in the sample.

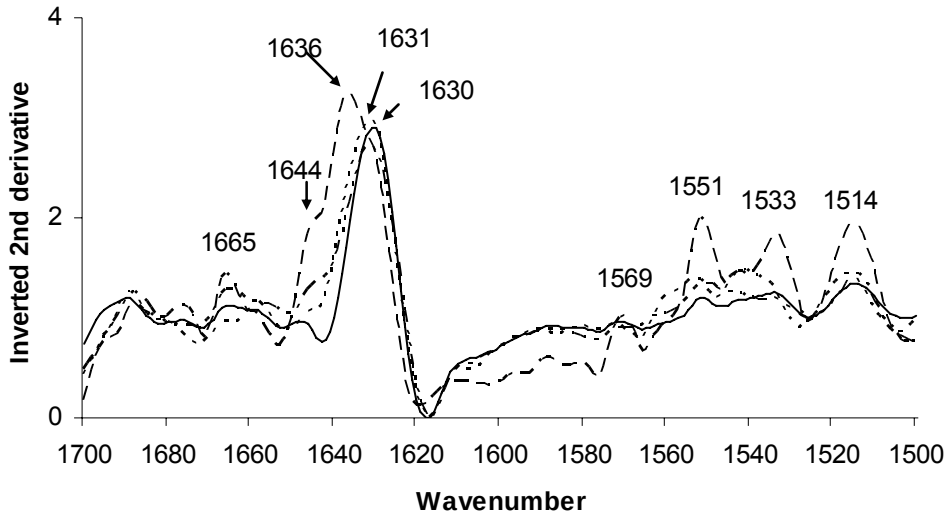

Fig. 3.11 Inverted 2nd derivative spectra of BLG in amide I and amide II region: free BLG (solid line), adsorbed BLG (dashed line), released BLG which measured on the complex of protein and aluminium hydroxide (dotted line), and released BLG which measured on protein alone after centrifugation (dash-dotted line).

The structural information from CD spectra are in agreement with the FTIR results. The CD spectra of released BSA and free BSA as well as released BLG and free BLG are given in Fig. 3.13 A and B, respectively. The almost identical spectra illustrate that released BSA refold to its native state. The spectra of released BLG and free BLG are similar except lower ellipticity between 194-206 nm for released BLG. This is an indication that released BLG may not totally refold to its native state. In addition, this confirms the results obtained by FTIR. To confirm that the free proteins remain the native state before CD measurement, free BSA and BLG were at different temperatures. The spectra are presented in Fig. 3.13 C and D, respectively.

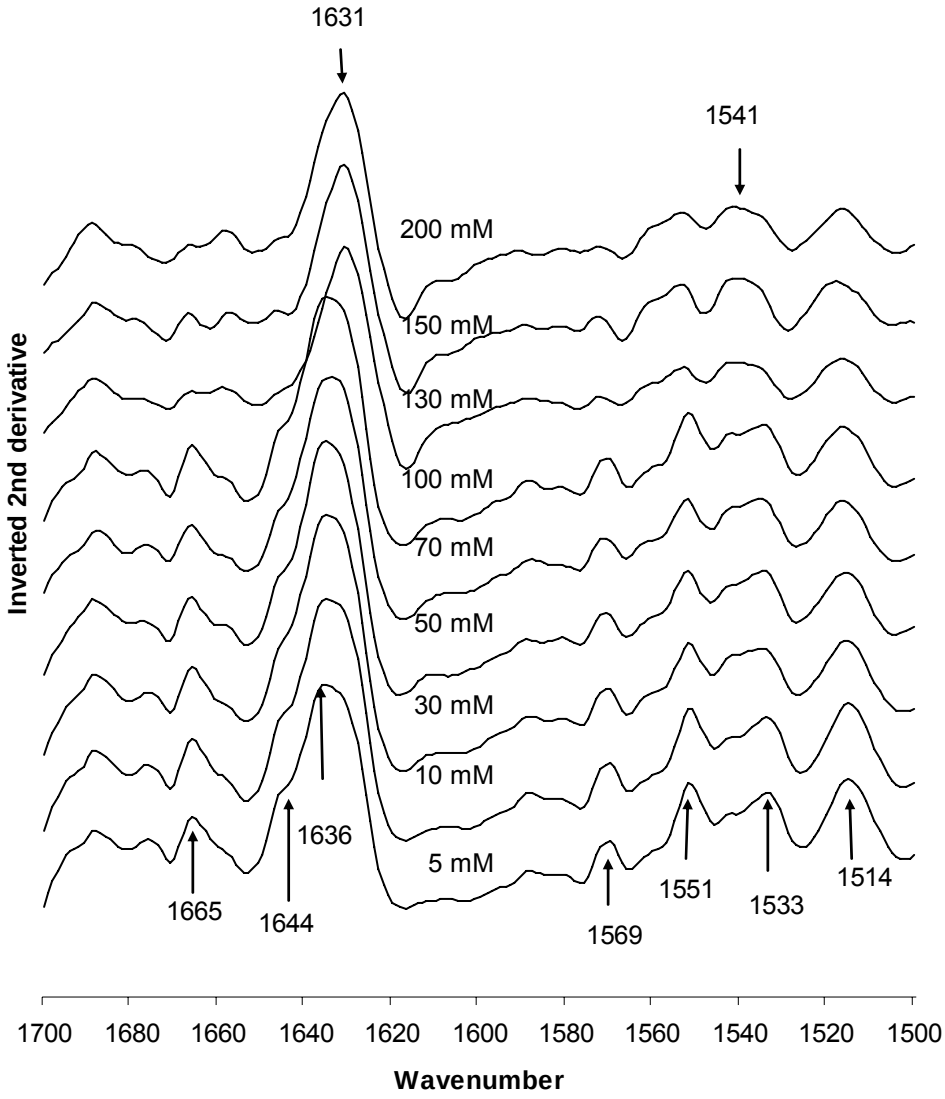

Fig. 3.12 Inverted 2nd derivative spectra of released BLG in amide I and amide II region: adsorbed protein has been released using pH 7.4 PBS at different concentrations (from 5 mM to 200 mM) for 40 min respectively. The spectra are recorded on the complex of protein and aluminium hydroxide.

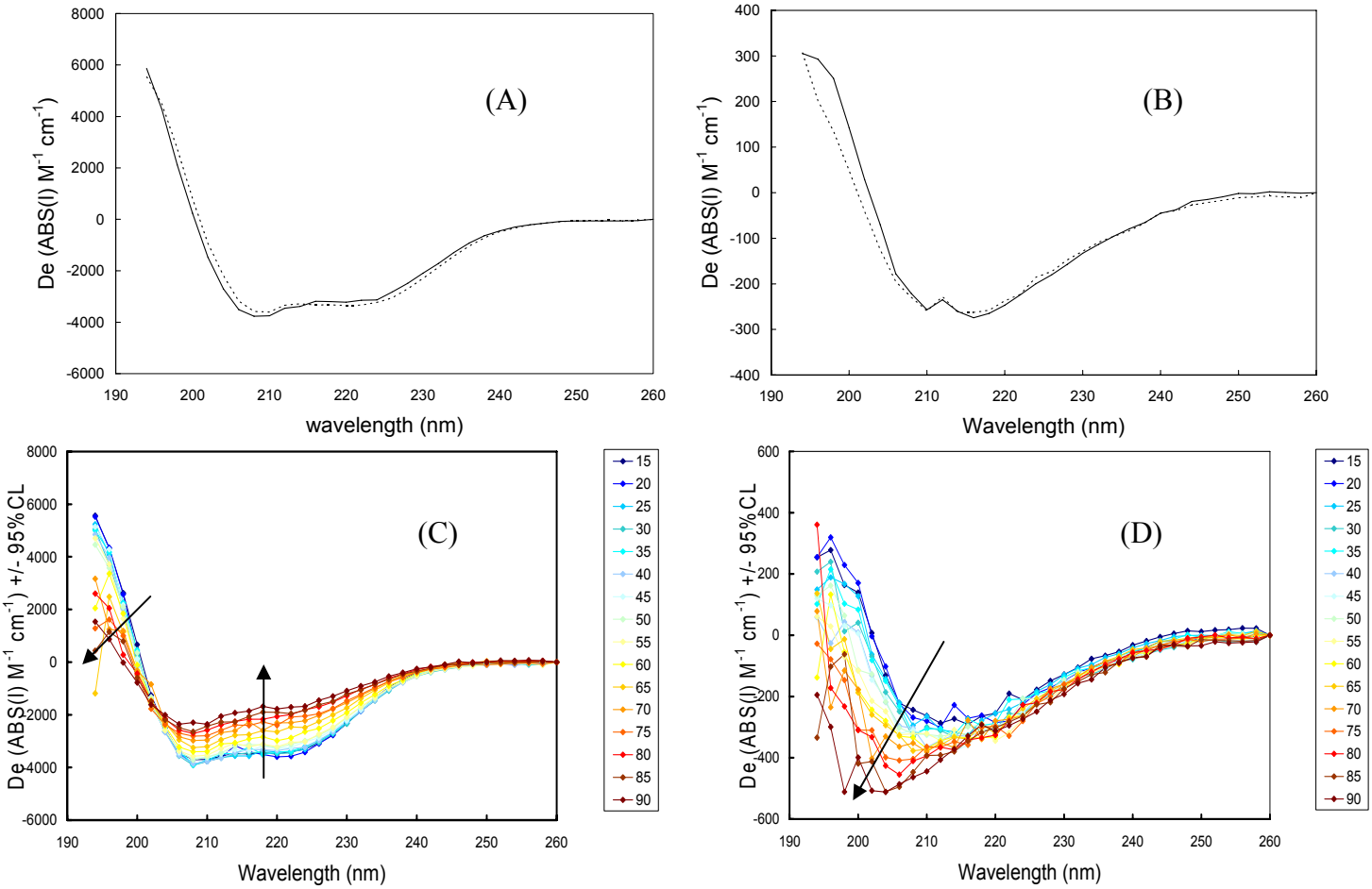

Fig. 3.13 CD spectra BSA (A, C) and BLG (C, D): free protein (solid line) and released protein (dotted line); C and D represent CD spectra of BSA and BLG at different temperatures respectively. The arrows indicate the direction of increasing temperature.

4 Conclusion

FTIR-ATR spectroscopy provides direct information on the secondary structural changes of the model antigens when adsorbed to aluminium hydroxide, and following release. It is shown that the secondary structure of BSA and BLG change when adsorbed by aluminium hydroxide. The adsorption-induced structural changes depend on how much protein is adsorbed by the aluminium hydroxide. Maximal adsorption gives a more native-like structure than low protein adsorption.

PBS replace pre-adsorbed antigen from aluminium hydroxide. The recovery of released protein is approximate 80% after 40 min in the presence of PBS. The released antigens generally refold to their native state. However, released BSA regains its native structure more completely than does BLG.

References

1. Goldsby RA., Kindt T, Osborne BA, Immunology, 4th edition. New York: W.H. Freeman and Company, 2001, p 63-65.
2. Schoneich C, Hageman MJ, Borchardt RT. Stability of peptides and proteins. In: Controlled Drug Delivery. Challenges and strategies (Park K, Ed.). Washington DC: ASC professional reference books, p. 205-228.
3. Manning MC, Patel K, Borchardt RT. Stability of protein pharmaceuticals. Pharmaceutical Research 1989; 6: 903-918.
4. Fu K, Greibenow K, Hsieh L, Klibanov AM, Langer R. Use of FTIR spectroscopy to characterize the secondary structure of proteins encapsulated with PLGA microspheres. Journal of Controlled Release 1999; 58: 357-366.
5. Yang TH, Dong A, Meyer J, Johnson OL, Cleland J, Carpenter JF. Use of infrared spectroscopy to assess secondary structure of human growth hormone within biocegradable microspheres. Journal of Pharmaceutical Sciences-Columbus 1999; 88: 161-165.
6. Castelain C, Genot C, Conformational changes of bovine serum albumin upon its adsorption in dodecane-in-water emulsions as revealed by front-face steady-state fluorescence. Biochimica et Biophysica Acta 1994; 1199: 59-64.
7. Kowalczyk D, Slomkowski S, Wang FW. Changes in conformation of human serum albumin and gamma globulins upon adsorption to polystyrene and poly latexes: Studies by fluorescence spectroscopy. Journal of Bioactive and Compatible Polymers 1994; 9: 282-309.
8. Maste MCL, Norde W, Visser AJWG. Adsorption-induced conformational changes in the serine proteinase sannase: A tryptophan fluorescence and circular dichroism study. Journal of Colloid and Interface Science 1997; 196: 224-230.
9. Hem SL, White JL. Characterization of aluminum hydroxide for use as an adjuvant in parenteral vaccines. Journal of Parenteral Science and Technology 1984; 38: 2-10.
10. Jones LS, Peek LJ, Power J, Marham A, Yazzie B, Middaugh CR. Effects of adsorption to aluminum salt adjuvants on the structure and stability of model protein antigens. The Journal of Biological Chemistry 2005; 280: 13406-13414.
11. Barth A, Zscherp C. What vibrations tell us about proteins, Quarterly reviews of biophysics 2002; 35: 369-430.
12. Haris PI. Theory and basic principles- 3. Fourier transform infrared spectroscopic studies of

peptides: potentials and pitfalls. ACS Symposium Series 2000; 750: 54-95.

13. Sharp JS, Forrest JA, Jones RAL. Surface denaturaration and amyloid fibril formation of insulin at model lipid-water interface. Biochemistry 2002; 41: 15810-15819.
14. Giacomelli CE, Bremer MGEG, Norde W, ATR-FTIR study of IgG adsorbed on different silica surface. Journal of Colloid and interface Science 1999; 220: 13-23.
15. Tarasevich YI, Monakhova LI. Interaction between globular proteins and silica surfaces. Colloid Journal 2002; 64: 482-487.
16. Bummer PM. An FTIR study of the structure of human serum albumin adsorbed to polysulfone. International Journal of Pharmaceutics 1996; 132:143-151.
17. Chittur KK. FTIR/ATR for protein adsorption to biomaterial surfaces. Biomaterials 1998; 19: 357-369.
18. Itri R, Caetano W, Barbosa LRS, Baptista MS. Effect of urea on bovine serum albumin in aqueous and reverse micelle environments investigated by small angle X-ray scattering, fluoresecence and circular dichroism. Brazilian Journal of Physics 2004; 34: 58-63.
19. Kossovsky N, Nguyen A, Sukiassians K, Festekjian A, Gelman A, Sponesler E. Secondary structure of albumin acquired rapidly by modified conventional ATR-FTIR is comparable to CD spectral data. Journal of Colloid and Interface Science, 1994; 166: 350-355.
20. Liu J, Feldkamp JL, White JL, Hem SL. Adsorption of phosphate by aluminium hydroxycarbonate. Journal of Pharmaceutical Science 1984; 10: 1355-1358.
21. Robert P, Devaux MF, Mouhous N, Dufour E. Monitoring the secondary structure of proteins by near infrared spectroscopy. Applied Spectroscopy, 1999; 53: 226-232.
22. Servagent NS, Revault M, Quiquampoix H, Baron MH. Conformational changes of bovine serum albumin induced by adsorption on different clay surfaces: FTIR analysis. Journal of Colloid and Interface Science 2000; 221: 272-283.
23. Sawyer L, Kontopidis G, Wu SY.β-lactoglobuli - A three-dimensional perspective. International Journal of Food Science and Technology 1999; 34: 409-418.
24. Lefevre T, Subirade M. Interaction of β-lactoglobulin with phospholipids bilayers: a molecular level elucidation as revealed by infrared spectroscopy. International Journal of Biological Macromolecules, 2000; 28: 59-67.
25. Lenk TJ. Infrared studies of protein adsorption and transitions on polyurethanes. PhD dissertation, University of Washington Chemical Engineering. 1994
26. Noinville SS, Revault M, Quiquamoix H, Baron MH. Conformational changes of bovine

serum albumin induced by adsorption on different clay surfaces: FTIR analysis. Journal of Colloid and Interface Science, 2000; 221: 273-283.

27. Schladitz C, Vieira EP, Hermel H, Mohrwald H. Amyloid-β-sheet formation at the air-water interface. Biophysics 1999; 77: 3305-3310.
28. Kendrick BS, Cleland JL, Lam X, Nguyen T, Randolph TW, Manning MC, Carpenter JF. Aggregation of recombinant human interferon gamma: kinetics and structural transitions. Journal of Pharmaceutical Science 1998; 87: 1069-1076.
29. Dong A, Prestrelski SJ, Allison SD, Carpenter JF. Infrared spectroscopy studies of lyophilization- and temperature-induced protein aggregation. Journal of Pharmaceutical Science 1995; 84:415-424.
30. Lefevre T, Subirade M. Conformational rearrangement of β-lactoglobulin upon interaction with an anionic membrance. Biochimica et Biophysica Acta, 2001; 1549: 37-50.
31. Urano H, Fukuzaki S. Conformation of adsorbed bovine serum albumin governing its desorption behavior at alumina-water interfaces. Journal of Bioscience and Bioengineering 2000; 90: 105-111.
32. Hajra S, Chattoraj DK. Protein adsorption at solid-liquid interfaces: part II- adsorption from binary protein mixture, Indian Journal of Biochemistry and Biophysics 1991; 2: 124-132.
33. Xie J, Riley C, Kumar M, Chittur K. FTIR/ATR study of protein adsorption and brushite transformation to hydroxyappatite. Biomaterials, 2002; 23: 3609-3616.
34. Norde W. Behavior of proteins at interfaces, with special attention to the role of the structure stability of the protein molecule. Clinical Material, 1992; 11: 85-90.
35. Oberg KA, Fink AL. A new attenuated total reflectance Fourier transform infrared spectroscopy method for the study of proteins in solution. Analytical Biochemistry, 1988; 256: 92-106.
36. Weet MVD, Hennink W, Jiskoot W. Protein instability in poly (lactic-co-glycolic acid) microparticles. Pharmaceutical Research, 2000; 17: 1159-1167.
37. Cleland JL, Powell MF, Shire SJ. The development of stable protein formulations: a close look at protein aggregation, deamidation, and oxidation. Critical Reviews in Therapeutic Drug Carrier System, 1993; 10: 307-377.
38. Rinella JV, Workman RF, White JL, Hem SL. Elutabilility of proteins from aluminum-containing vaccine adjuvants by treatment with surfactants. Journal of Colloid and Interface Science 1998; 197: 48-56.

39. Engel MFM, Visser AJWG, Mierlo CPM. Refolding of adsorbed bovine α-lactalbumin during surfactant induced displacement from a hydrophobic interface. Langmuir 2003; 7: 2929-2937.

Chapter IV: The structural stability of model antigens adsorbed by aluminium hydroxide in heating and aging processes in comparison to the antigens in solutions

Abstract

The structural stability of two model antigens adsorbed to aluminium-containing adjuvant was studied. The two model antigens were bovine serum albumin (BSA) and β-lactoglobulin (BLG), and the method used was Fourier transform infrared – attenuated total reflection (FTIR-ATR) spectroscopy. The stability was studied during heating and storage. The results showed that the structure of proteins when adsorbed onto the surface of aluminium hydroxide was more stable than proteins in solution at high temperature and/or after a period of storage. This indicated that adsorption by aluminium-containing adjuvants protected antigens against degrading. This phenomenon was more pronounced for BSA than BLG. The reason might be that there are more free BLG in the sample system compared to BSA. Reduced adsorption of proteins to the adjuvant in a vaccine may facilitate the degradation of the antigen in the vaccine.

1 Introduction

Aluminium-containing adjuvants are used in vaccines to adsorb the antigens and enhance the immune response upon injection. Although the mechanism by which aluminium-containing adjuvants potentiate the immune response is not fully understood, it is generally accepted that the antigens should be adsorbed by the adjuvants [1]. The World Health Organization recommends that at least 80% of tetanus and diphtheria toxoids should be adsorbed onto aluminium-containing adjuvants [2]. Therefore, vaccines are produced by selecting adjuvants, pH, buffer, and/or ionic strength to achieve maximal adsorption of the antigens [1].

The study of Jones *et al.* [3] and our previous work [4] have shown changes in secondary structure when protein antigens are adsorbed by an aluminium hydroxide adjuvant. The stability of this modified structure is of major importance, since it may affect degradation of the antigens during the storage and/or due to high temperature, and this could potentially pose a risk to patients. The term stability, when it relates to proteins, is often used in a variety of ways [5]. It includes chemical and/or physical degradation. Chemical degradation refers to modifications involving covalent bonds, such as deamidation, oxidation, and disulphide bond shuffling. Physical degradation includes protein unfolding, undesirable adsorption to surfaces, and aggregation [6, 7]. However, the definition in this paper is the stability of the secondary structure of protein.

In this study the secondary structures of two model antigens were investigated during heating and storage in comparison to the antigens in solutions using Fourier transform infrared-attenuated total reflection (FTIR-ATR) spectroscopy. For the storage experiments, apart from normal storage temperature (4ºC), an accelerated degradation test (ADT) was also employed, which subjected the samples to elevated temperature (37ºC) at which denaturation should occur more rapidly than at the normal storage temperature. It is well known that some vaccines are temperature sensitive [8]. Both high and low (freezing) temperatures can cause inactivation of vaccines. The structural stabilities of the model antigens were investigated at different heating temperatures in this work, since the temperature alterations are an important problem during the transportation and storage of vaccines, especially in developing countries where the quality of the cold chain is not always optimal [9].

2 Materials and methods

2.1 Materials

Clinical reagent grade bovine serum albumin (BSA, reference L84960) and approximate 90% β-lactoglobulin (BLG, reference L3908) were purchased from ICN biomedical Inc and Sigma

respectively. Both proteins were used directly without further purification. Aluminium hydroxide adjuvant was purchased from Superfos Biosector A/S (Denmark). A stock aluminium hydroxide adjuvant was prepared by adjusting pH to 8 by the addition of 1 M NaOH. All other chemicals were analytical grade and obtained from commercial sources without further treatment.

2.2 Sample preparation

A stock protein solution (20 mg/ml) was prepared by dissolving a certain amount protein in Milli-Q water. Model vaccines were prepared by mixing the appropriate amount of protein stock solution and aluminium hydroxide. The final calculated aluminium concentration was 3.4 mg/ml and the final protein concentrations 4 mg/ml. The final pH value for BSA and BLG model vaccines were 7.41 and 7.60, respectively. Samples were mixed gently by end-over-end rotation for 30 min to obtain the maximal protein adsorption. Protein water solutions were prepared by diluting the stock solution to 4 mg/ml using Milli-Q water. Blank samples containing 3.4 mg/ml aluminium hydroxide without proteins, were prepared by diluting the stock aluminium adjuvants using Milli-Q water.

2.3 FTIR-ATR measurement

Spectra were collected using a FTIR spectrometer (PerkinElmer Spectrum One), which was mounted with a three bounces ZnSe ATR crystal (PerkinElmer). For the storage process, samples were stored at 4 ºC and 37 ºC between experiments, respectively. All samples were measured at room temperature. For the heating process, the samples were divided into different vials and were heated at different temperature (25, 37, 50, 60, 70, 80, 90 ºC) for 30 min, respectively; and cooled to room temperature before FTIR spectra were recorded.

A sample film was obtained by depositing an 8 μl sample onto the ATR crystal and evaporating the solvent. The calculated amount of aluminium hydroxide for each film was 27.2 μg; and the calculated amount of protein was 32 μg. Spectra were directly recorded on the film by co-adding 128 scans with a resolution of 4 cm^{-1} at a scan speed 0.2 cm/s. Control spectra were recorded by measuring the blank samples which contained the same components except protein under the same experiment conditions. All samples were analyzed at least in duplicate.

2.4 Data analysis

All FTIR spectra were analyzed using the Unscrambler ver. 9.2 software (Camo process AS). Replicated spectra of the same sample were averaged first. For the adsorbed proteins, the spectra of a corresponding blank sample were subtracted from the spectra of the adsorbed proteins. A flat baseline from 1900 to 1740 cm^{-1} was obtained for each spectrum after subtraction. A 23-point

Savitsky-Golay smoothing function was applied to each spectrum from 1800 cm^{-1} to 1200 cm^{-1}. The second derivative spectra were calculated using an 11-point Savitsky-Golay function from 1750 to 1220 cm^{-1}. The inverted second derivative spectra were obtained by multiplying by -1 for convenient interpretation. Finally, the spectra were baseline corrected and mean normalized.

3 Results and discussion

3.1 Structural stability during the heating process

FTIR-ATR spectroscopy was applied to monitor the secondary structure of the model antigens in solution and adsorbed onto aluminium hydroxide as a function of temperature. The potential changes of the secondary structure were detected in the amide I (1700-1600 cm^{-1}) and amide II (1600-1500 cm^{-1}) regions of the inverted secondary derivative spectra.

For BSA adsorbed by aluminium hydroxide, the distinguishable spectral changes occur at or above 70 ºC (Fig.4.1). Results showed that the α-helix band around 1653 cm^{-1}decreases, but increases in β-sheet structure at 1636 cm^{-1}. Another spectral difference in the amide I region observed is the intensity of the band at high wavenumbers 1693 cm^{-1}. This band increases as a function of temperature, especially above 70 ºC. In the amide II region, the intensity of bands around 1549 cm^{-1} and 1533 cm^{-1} decreases when the temperature increases. However, compared to the spectra of BSA in solution (Fig.4.2), the above mentioned heating-induced spectral changes are less pronounced. BSA in solution has significantly low thermal stability. A band resulting from intermolecular aggregation is induced around 1626 to 1622 cm^{-1}, even at very low temperature, i.e. 25 ºC. This band increases as a result of increasing temperature. Two other bands increase around 1695 cm^{-1} and 1680 cm^{-1} as function of temperature. These three bands relate to intermolecular anti-parallel β-sheet formation [10-12]. A molecule of BSA contains 17 disulphide bonds and one free thiol of a cysteine residue [13]. Thus it is reasonable to assume that a new S-S bond results from intermolecular reaction of thiol-groups. Liu *et al.* [14] showed that no aggregation was observed if the free sulfhydryl group was alkylated. These aggregation-induced bands were also observed in other heat-denatured protein aggregates [15-17]. In the amide I region, the main α-helix absorption at 1653 cm^{-1} shifts to 1652 cm^{-1} and the intensity decreases dramatically with increasing temperature. Therefore, BSA in solution loses α-helix but gains intermolecular β-sheet structure. In the Amide II region, spectra at high temperature lose the band at 1548 cm^{-1}, but a few bands increases around 1533 cm^{-1} and 1532 cm^{-1}.

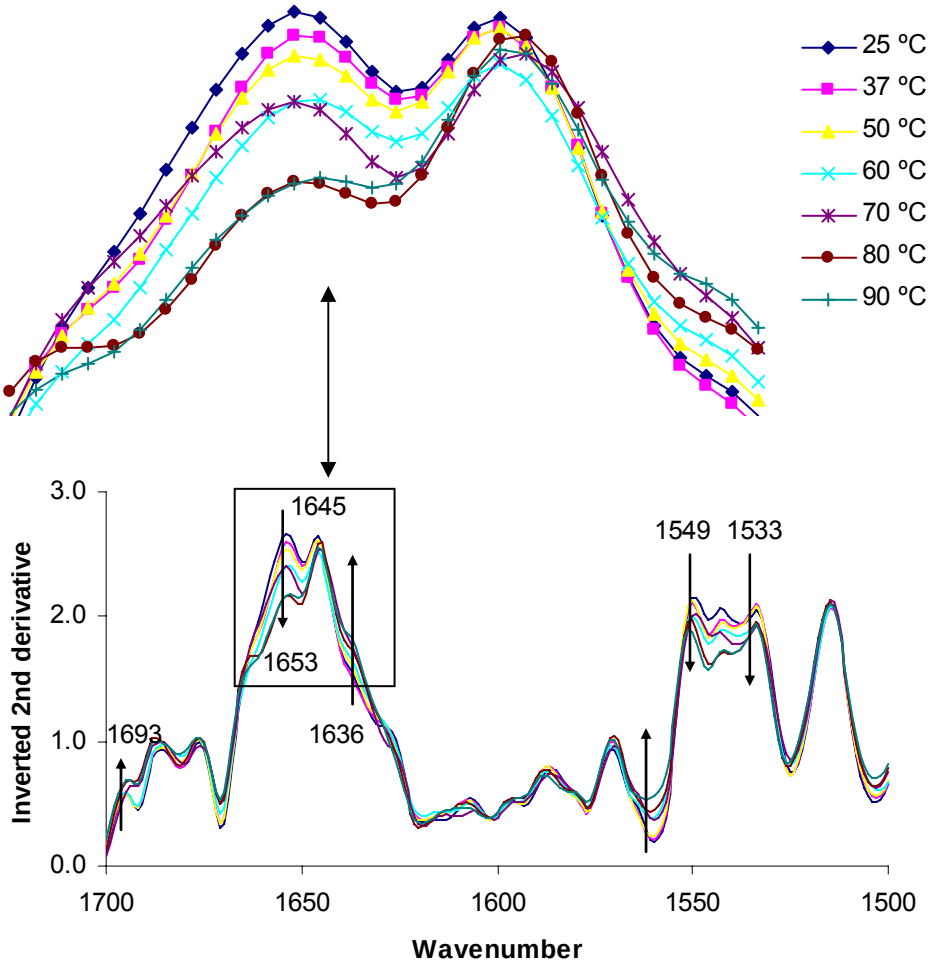

Fig.4.1 Inverted 2nd derivative spectra of adsorbed BSA in amide I and amide II regions. BSA was adsorbed by aluminium hydroxide and incubated for 30 min before heated at different temperatures for 30 min. The arrows represent increasing temperatures.

The spectral stability of adsorbed BSA (Fig.4.1) differs dramatically from that of BSA in solution (Fig.4.2), revealing that a modified structure of BSA is induced by adsorption onto aluminium hydroxide. It confirms the conclusion in our previous study [4]. It also indicates that the modified adsorbed structure increases the thermal stability of BSA, which prevents intermolecular aggregating of protein during the heating process.

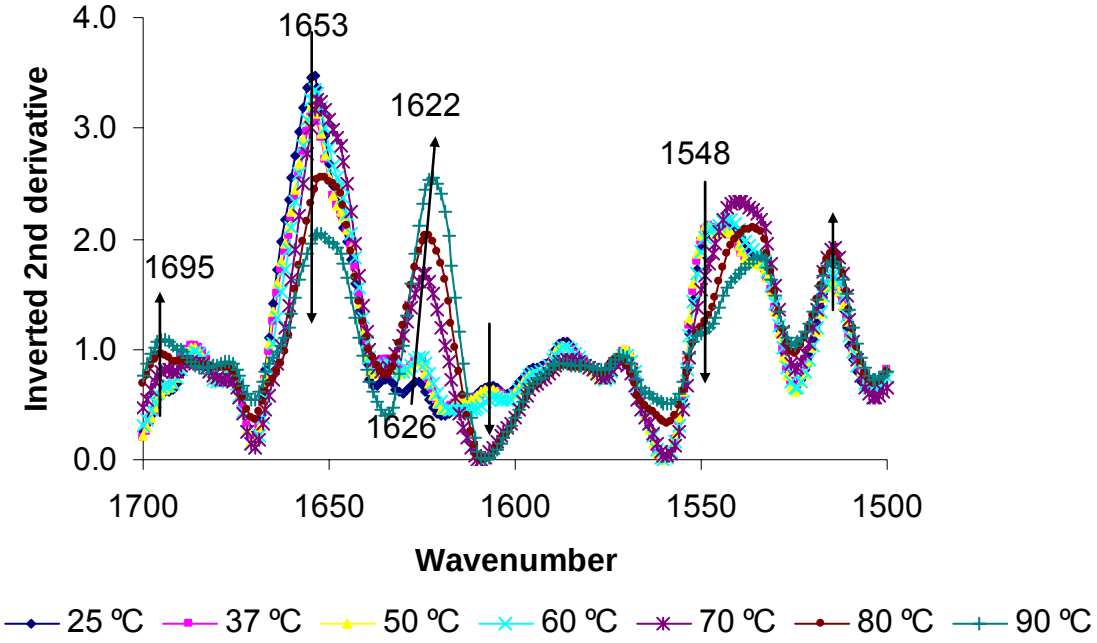

Fig.4.2 Inverted 2nd derivative spectra of BSA solution was in amide I and amide II regions. BSA solution was heated at different temperatures for 30 min. The arrows represent increasing temperatures

In the case of BLG, the spectra of adsorbed protein (Fig.4.3) are also significantly different from that of the protein in solution (Fig.4. 4). The bands of adsorbed protein are located at wavenumbers that are similar to the corresponding components of the free BLG, which indicates that the secondary structure of adsorbed BLG dramatically changes as compared to the protein in solution. As the temperature is increasing, the band of the adsorbed BLG around 1630 cm^{-1} loses intensity, but there is a gain in the random structure as seen at 1644 cm^{-1}. The main broad β-sheet band shifts from1636 cm^{-1} to 1638 cm^{-1}.

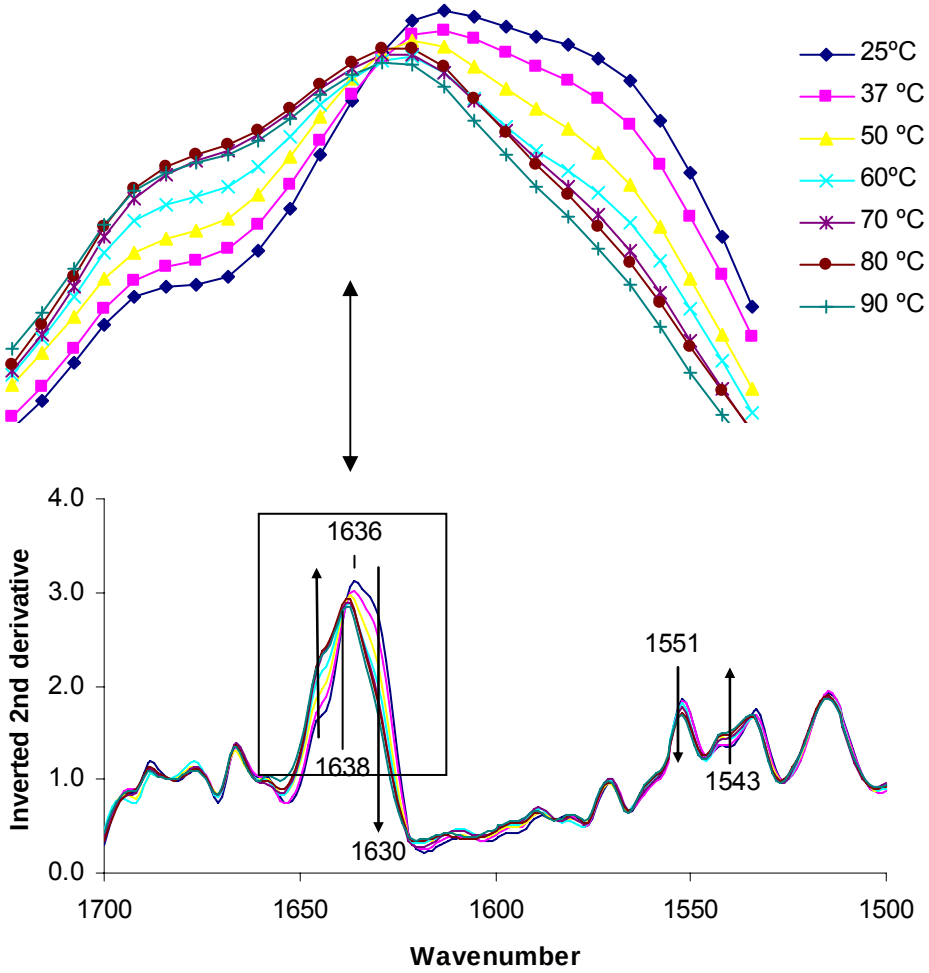

Fig.4.3 Inverted 2nd derivative spectra of adsorbed BLG in amide I and amide II regions. BLG was adsorbed by aluminium hydroxide and incubated for 30 min before heated at different temperatures for 30 min. The arrows represent increasing temperatures.

For BLG in solution, the spectra at different temperatures are presented in Fig.4.4. The main β-sheet band appears at 1628 cm^{-1} and the band broadens with increasing temperature. It can be seen that the band at 1694 cm^{-1} increases at high temperatures (80, 90 ºC), but no peak is induced around 1623 cm^{-1}. The aggregation of BLG should be similar to BSA due to intermolecular thiol-disulphide interchanges, since BLG also contains one free thiol group and two disulphide bridges [18, 19]. However, the association state of BLG results from equilibrium between its monomeric and dimeric forms. Dimeric BLG is characterized by having two components around 1632 cm^{-1} and 1623 cm^{-1}, while monomeric BLG reveals only one component near 1630 cm^{-1} [20]. Therefore, in the current

experimental conditions, BLG seems to be primarily in the monomeric form. This probably results from low protein concentration [21, 22]. Infrared spectra of BLG vary significantly in the low concentration range (0.25-10% w/v) [19]. The spectra are characterized by one band between 1640 and 1623 cm^{-1} at low concentrations, whereas two bands around 1634 and 1623 cm^{-1} are present at high concentrations. High temperatures [19] and low ionic strength [23] may also result in the BLG spectrum having one FTIR band between 1640 and 1623 cm^{-1} instead of two bands around 1634 and 1623 cm^{-1}.

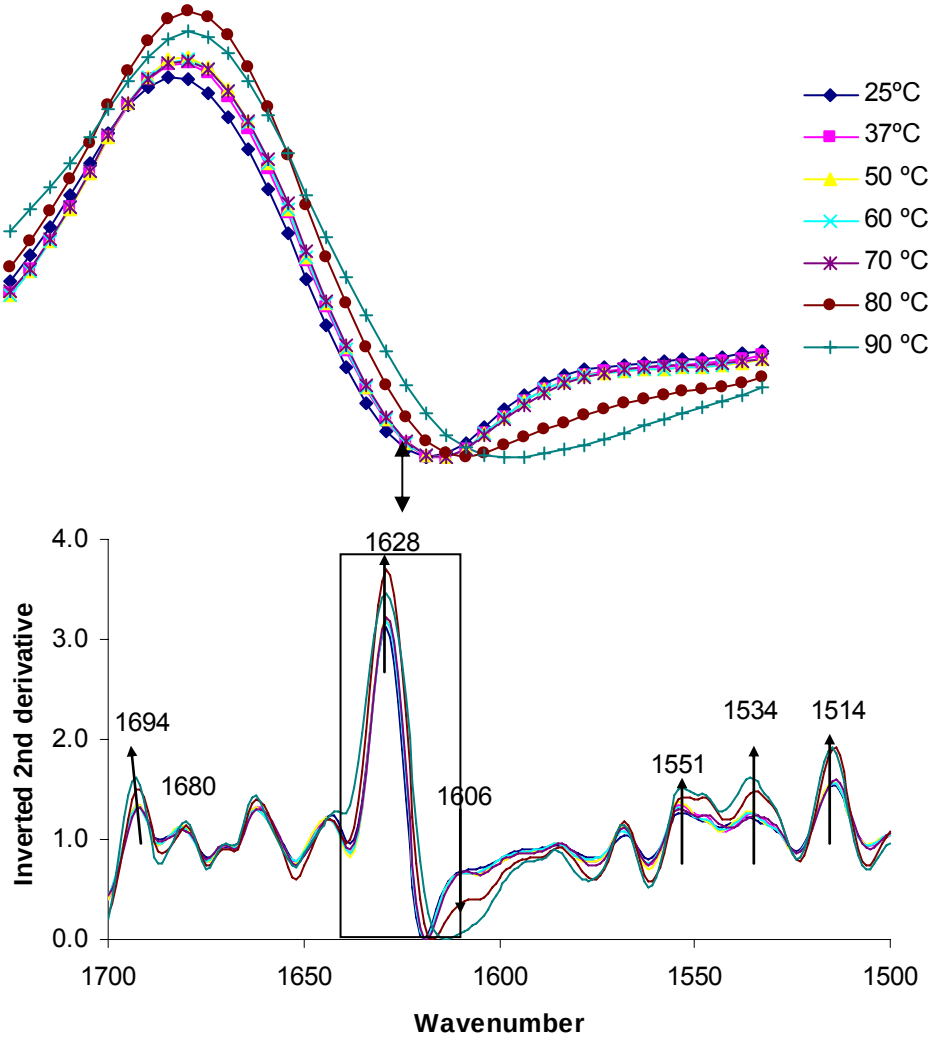

Fig.4.4 Inverted 2nd derivative spectra of BLG solution in amide I and amide II regions. BLG solution was heated at different temperatures for 30 min. The arrow represents increasing temperatures.

A small band around 1680 cm^{-1} is induced for free BLG at high temperature (80, 90 ºC). It can also

be attributed to the formation of intermolecular β-sheets that result from the self-aggregation of the proteins [24]. The intensity of this band is weak probably because the spectra are recorded at room temperature. The decreased temperature may facilitate refolding of the BLG structure. In the amide II region, the intensities of bands around 1551, 1534, and 1514 cm^{-1} increase significantly.

In this study, no intermolecular aggregation occurred for adsorbed protein at high temperature (above 70 ºC), while free protein aggregates under same conditions. The results suggest that the adsorption onto aluminium hydroxide can prevent intermolecular aggregating of the antigen when it is exposed to high temperature. However, the structure of adsorbed protein also changes at very low temperature (37 ºC). Jones and co-workers [3] demonstrated that the transition of aluminium hydroxide adsorbed BSA started at approximately 35 ºC using differential scanning calorimetry. This temperature was lower than the temperature which caused transition of BSA in solution. Thus, it was concluded that proteins adsorbed to aluminium-containing adjuvant show significantly reduced thermal stability compared to the protein in solution. However, they only observed the temperatures at which the protein started to destabilize, but made no conclusion concerning the high temperature effects. The difference of the FTIR measurements in these two studies is that Jones *et al.* [3] measured the slurry after centrifugation compared to evaporated films which were analyzed in this work. When measuring slurry, the sample has to be smeared onto the ATR surface, which may increase the variability because the sample may not be uniform. Furthermore, the water content in the slurry sample may also affect the measurement of the protein spectra, although most of the water absorbance can be subtracted. Jones *et al.* [3] measured the sample at the denaturing temperature in comparison to room temperature in this work. Another source of variability is the different buffers, which were used for model vaccine preparation. A previous study illustrated that the influence of the buffer plays an important role in the structural stability of BSA [25].

The thermal effect on the stability of absorbed BSA and BLG is not the same. This result agrees with the study of Jones *at al*. [3] showing that the stability of ovalbumin was less affected by adsorption than BSA.

3.2 Structural stability during the storage process

The structural stability of adsorbed antigen is important especially when the vaccine is stored for long periods prior to use. It is well known that vaccines lose their potency during storage, especially at high temperature [26]. The mechanism by which vaccine loses potency is not clear. The structural stability may influence the immunogenicity of the vaccine. FTIR-ATR spectroscopy was applied here to monitor the structural changes of protein antigens during the storage in the amide I

and the amide II region of the inverted secondary derivative spectra.

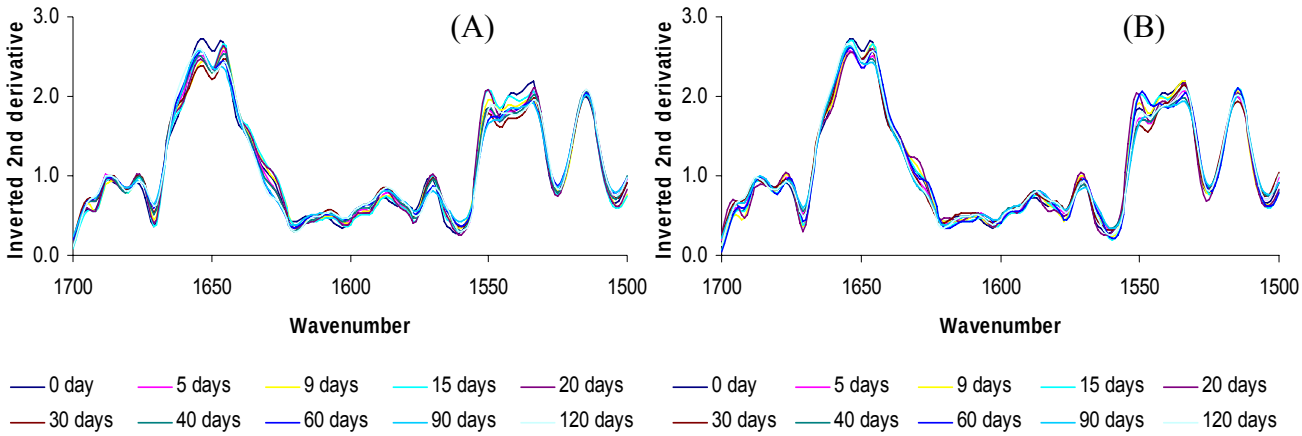

Fig.4.5 Inverted 2nd derivative spectra of adsorbed BSA during 120 days storage in amide I and amide II regions. BSA was adsorbed by aluminium hydroxide and stored at 37 ºC (A) and 4 ºC (B) respectively.

The alteration of the secondary structure of two model antigens during 4 months storage is studied in this work. Fig.4.5 shows the second derivative FTIR spectra of adsorbed BSA which was stored at 37 ºC and 4 ºC, respectively. Similar spectra indicate that the structure of adsorbed BSA by aluminium hydroxide is stable. Slight spectral differences occur, but the changes are irregular. The spectral variability may be caused by experiment-to-experiment variation and inconsistent measurement of the temperature. FT-NIR spectroscopy shows the same irregular alteration of spectra (Chapter V).

The stability of BSA in solution stored at 37 ºC and 4 ºC were also investigated. The secondary structure of BSA in solution changes dramatically in 44 days (Fig.4.6), and white sedimentation is observed within 65 days when stored at 37 ºC. A new peak is induced at 1625 cm^{-1} after 16 days storage. The intensity of the peak increases as a function of time. The band is due to the intermolecular anti-parallel β-sheet formation. On other hand, α-helix band around 1653 cm^{-1} decrease with increasing storage time (Fig.4.6). Thus, for BSA in solution, α-helix is reduced accompanied by an increase in anti-parallel β-sheet explained by intermolecular aggregation. BSA in solution is quite stable when it is stored at 4 ºC. The spectrum changes after 65 days of storage by shifting to low wavenumber (Fig.4.7).

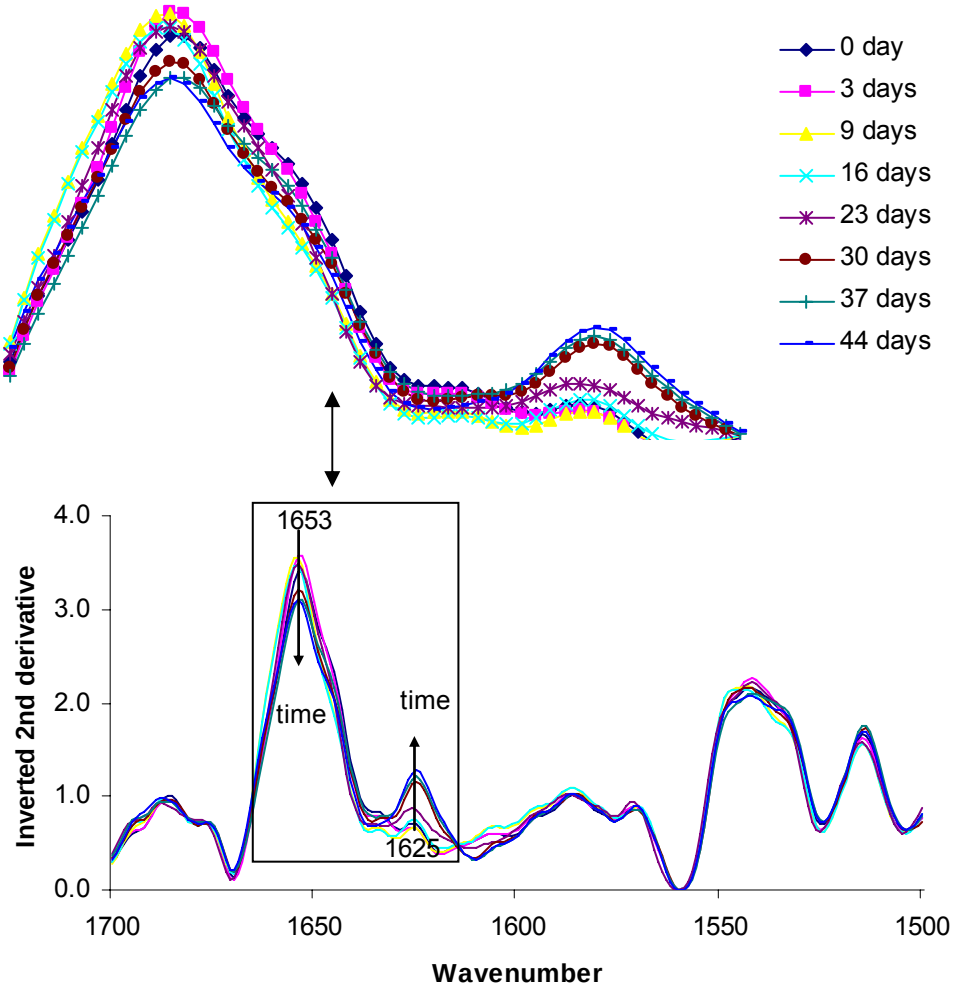

Fig.4.6 Inverted 2nd derivative spectra of BSA solution during 44 days storage in amide I and amide II regions. BSA solution was stored at 37 ºC.

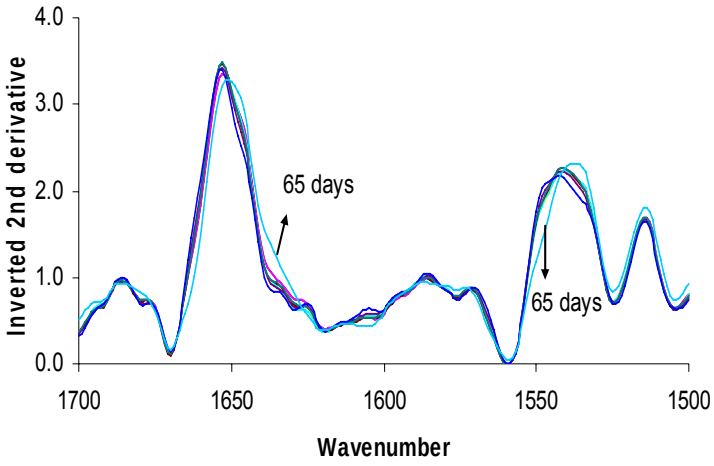

Fig.4.7 Inverted 2nd derivative spectra of BSA solution during 65 days storage in amide I and amide II regions. BSA solution was stored at 4 ºC.

In the case of BLG, the secondary derivative FTIR spectra of adsorbed BLG stored at 37 ºC and 4 ºC are given in Fig.4.8 and Fig.4.9, respectively. The β-sheet band around 1636 cm^{-1} shift to higher wavenumbers, and the intensity decreases as a function of time. The change is more pronounced in the early stage (first three weeks) of storage. On the other hand, the bands from 1606 to 1587 cm^{-1} increase with storage. In the amide II region, bands around 1551 and 1534 cm^{-1} increase. The results agree with another study [27], in which it was demonstrated that adsorption of BLG to an oil-water interface lead to time-dependent changes in the protein structure. The dramatic changes of adsorbed BLG may result from free protein in the samples. BLG (4 mg/ml) cannot be totally adsorbed by 3.4 mg/ml aluminium hydroxide. Adsorbed BLG desorbs from aluminium hydroxide during storage, while the amount of adsorbed BSA remains constant (Chapter V). Moreover, if 8 mg/ml BSA is added to 3.4 mg/ml aluminium hydroxide it will lead to more free BSA in the system and the sample aggregates rapidly. The data do not allow for an accurate estimation of structural analysis due to the aggregation after 4 weeks at 37 ºC. Therefore, free antigens in vaccine may facilitate the degradation of the system. FT-NIR analysis of BLG model vaccine also showed a time-dependent decrease of the spectral intensity (Chapter V). Furthermore, the alteration of pH during storage may also affect the structural stability of adsorbed BLG.

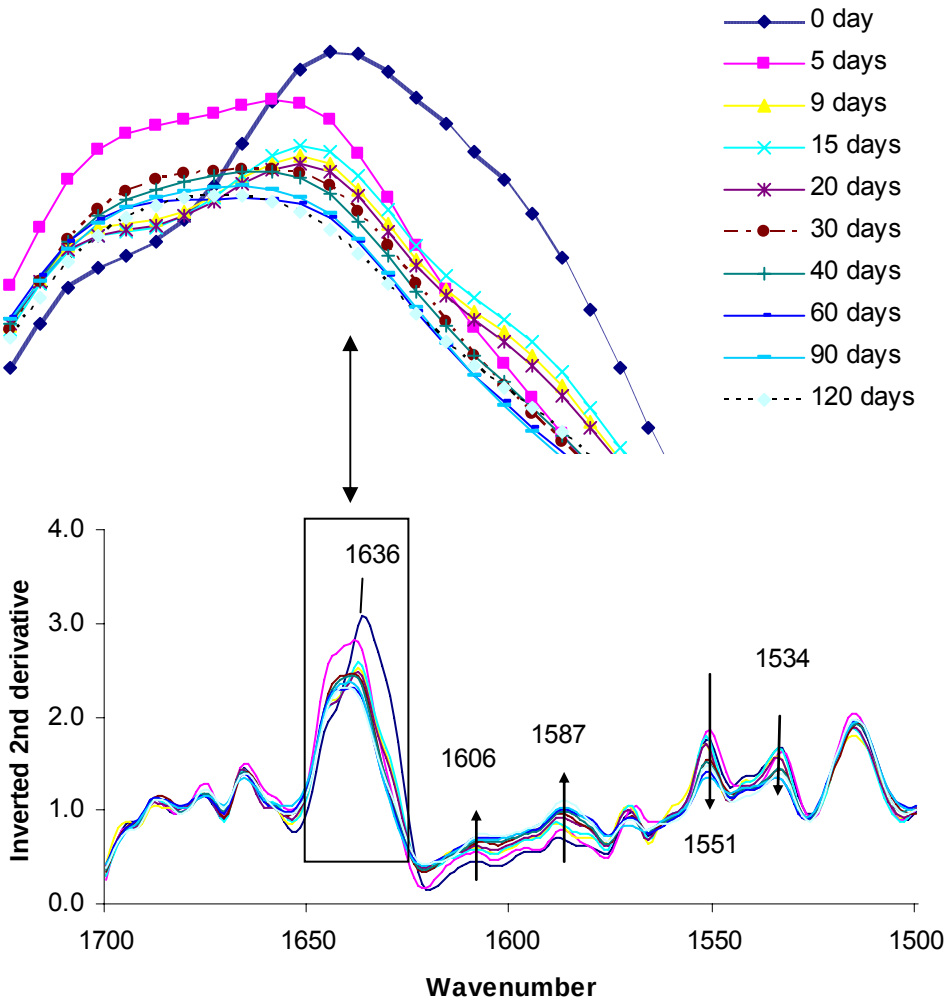

Fig.4.8 Inverted 2nd derivative spectra of adsorbed BLG during 120 days storage in amide I and amide II regions. BLG was adsorbed by aluminium hydroxide and stored at 37 ºC.

For BLG in solution, the changes of FTIR spectra differ when comparing storage at 37 ºC and 4 ºC (Fig.4.10 and Fig.4.11). The β-sheet band at 1630 cm^{-1} increases and it shifts to lower wavenumbers 1628 cm^{-1} for BLG solution with increasing storage time at 37 ºC. It indicates that the molecules of BLG aggregate due to intermolecular interaction. No new band is induced around 1623 cm^{-1} because of the low protein concentration [21, 22]. If BLG solution is stored at 4 ºC, the β-sheet band at 1630 cm^{-1} loses intensity as function of storage time. However, a band around 1545 cm^{-1} increases, which can be described as random structure. In other words, BLG loses β-sheet but gains random structure when the solution is stored at low temperature. When BLG is stored at 37 ºC, the variability of the spectra around 1586 cm^{-1} is evident. The intensity of this band increases as

function of time. The band around 1608 cm^{-1}, however, decreases with time.

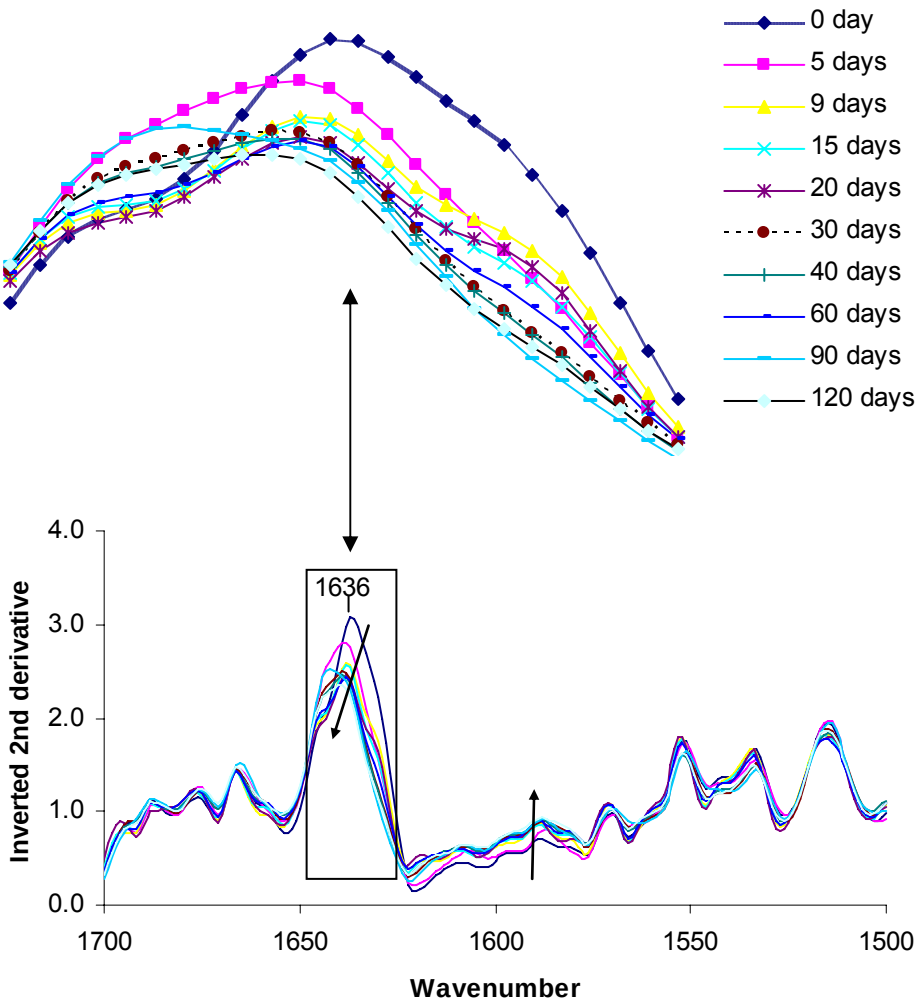

Fig.4.9 Inverted 2nd derivative spectra of adsorbed BLG during 120 days storage in amide I and amide II regions. BLG was adsorbed by aluminium hydroxide and stored at 4 ºC.

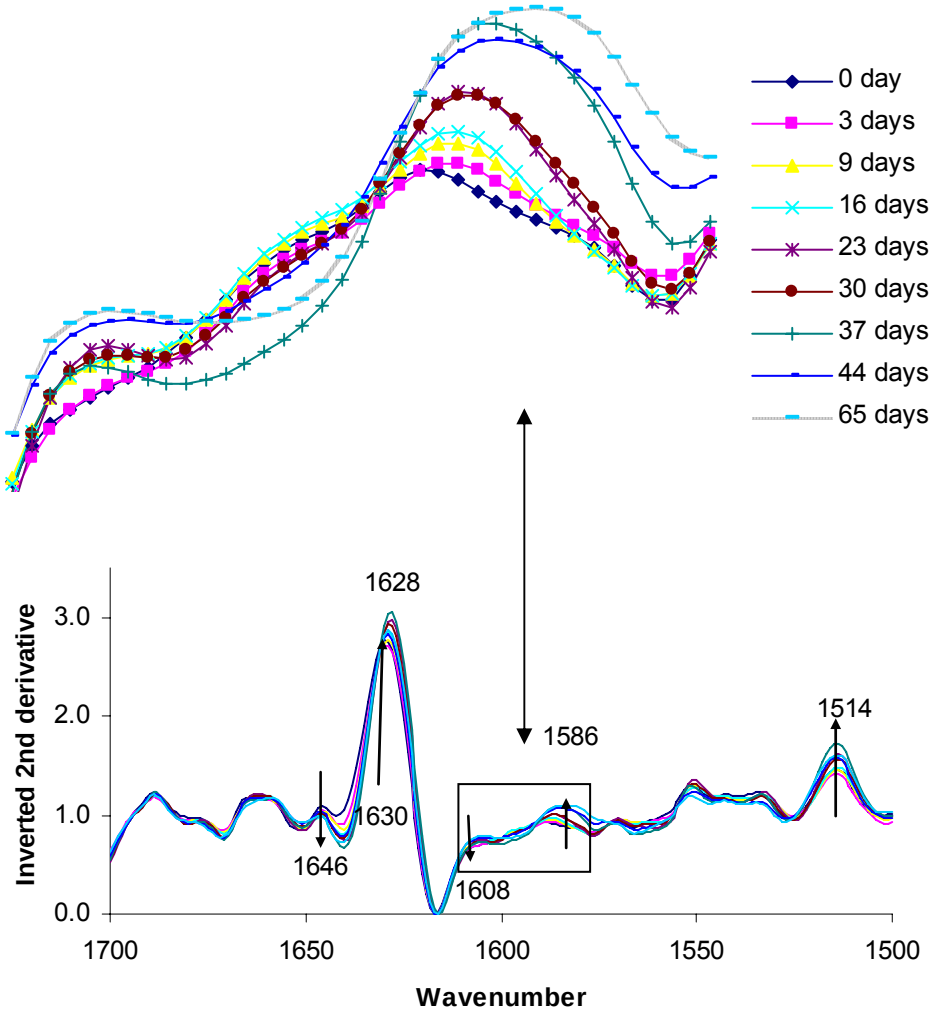

Fig.4.10 Inverted 2nd derivative spectra of BLG solution during 65 days storage in amide I and amide II regions. BLG solution was stored at 37 ºC.

.

Based on these observations the adsorption by aluminium hydroxide prevents aggregating compared to the proteins in solution. Aggregation is obvious for BSA when it is stored at 37 ºC. In the case of BLG model vaccine, due to the low protein concentration, this phenomenon is not observed. As expected, at elevated temperature (37 ºC), both for adsorbed protein and free protein and both for BSA and BLG, the proteins denature or degrade more rapidly than at the normal storage temperature (4 ºC). The degradation of BLG solution differs when it is stored at 4 ºC and 37 ºC.

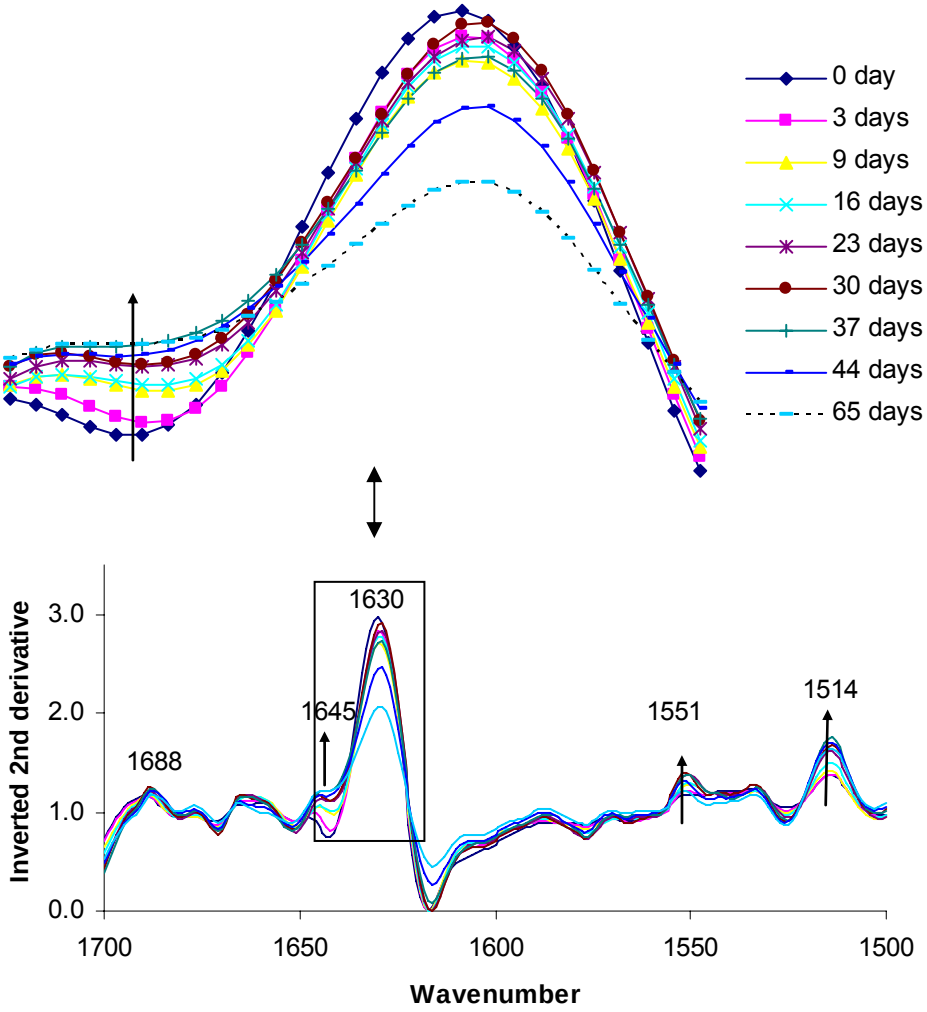

Fig.4.11 Inverted 2nd derivative spectra of BLG solution during 65 days storage in amide I and amide II regions. BLG solution was stored at 4 ºC.

4 Conclusion

FTIR-ATR spectroscopy can be used to monitor the changes of the secondary structure of protein antigens during vaccine storage and temperature variation. This study has shown that the structure of an antigen can be stabilized by adsorption onto aluminium hydroxide during exposure to high temperature and/or during storage. It may be one of reasons why adjuvant can enhance the immune response and/or exert its activities [28]. This phenomenon of structural stabilization is more obvious for BSA than BLG, which may be ascribed to the low protein concentration of BLG. Another explanation is that it may be that there is more free protein which is not adsorbed onto aluminium hydroxide in the BLG model vaccines. In any case the structural stabilisation seems to be protein

specific. Free protein antigens present in vaccines may facilitate degradation of the vaccine, but further experiments are required to confirm this hypothesis.

References

1. Chang MF, Shi Y, Nail SL, HogenEsch H, Adams SB, White JL, Hem SL. Degree of antigen adsorption in the vaccine or interstitial fluid and its effect on the antibody response in rabbits. Vaccine, 2001, 19: 2884-2889.
2. World Health Organization. Immunological adjuvants. World Health Organization Technical Report Series No. 595. Geneva: World Health Organization, 1976: 6-8.
3. Jones LS, Peek LJ, Power J, Markham A, Yazzie B. Effects of adsorption to aluminum salt adjuvants on the structure and stability of model protein antigens. The Journal of Biological Chemistry, 2005; 280: 13406-13414.
4. Zheng Y, Lai X, Ipsen H, Larsen JN , Løwenstein H, Søndergaard I, Jacobsen S. Characterization of the structural changes of model antigens using FTIR-ATR. submitted to Vaccine, 2006.
5. Manning MC, Patella L, Borchardt RY. Stability of protein pharmaceuticals. Pharmaceutical Research, 1989; 6: 903-917.
6. Chi EY, Krishnan S, Randolph TW, Carpenter JF. Physical stability of proteins in aqueous solution: mechanism and driving faces in nonnative protein aggregation. Pharmaceutical Research, 2003; 20: 1325-1336.
7. Randolph TW, Jones LS. Surfactant-protein interactions. In: Carpenter JF, Mannings MC (Eds.). Rational design of stable protein formulations, theory and practice. Kluwer Academic/Plenum Publishers, New York, 2002, p198.
8. Frank KJ. Monitoring temperature-sensitive vaccines and immunologic drugs, including anthrax vaccine. American Journal of Health-System Pharmacy, 1999; 56: 2052-2055.
9. Coenen F, Tolboom JTBM, Frijlink HW. Stability of influenza sub-unit vaccine: does a couple of days outside the refrigerator matter. Vaccine, 2006; 24: 525-531.
10. Militello V, Casarino C, Emanuele A, Giostra A, Pullara F, Leone M. Aggregation kinetics of bovine serum albumin studied by FTIR spectroscopy and light scattering. Biophysical Chemistry, 2004; 107:175-187.
11. Meersman F, Smeller L, Heremans K. Comparative Fourier transform infrared spectroscopy study of cold-, pressure- and heat-induced unfolding and aggregation of myoglobin. Biophysical Journal. 2002; 82: 2635-2644.

12. Stokkum JHM, Linsdell HL, Hadden JM, Haris PI, Chapman D, Bloemenda L. Temperature-induced changes in protein structures studied by Fourier transform infrared spectroscopy and globe analysis. Biochemistry, 1995; 34: 10508-10518.
13. Foster JF. Some aspects of the structure and conformational properties of serum alumin. In: Roseoer VM, Oratz M, Rothschild MA (Eds.). Albumin structure, function, and uses. Pergamon Press, Oxford, England. 1977. p53-84.
14. Liu WR, Langer R, Klibanov AM. Moisture-induced aggregation of lyophilized proteins in the solid state. Biotechnology and Bioengineering, 1991; 37: 177-184.
15. Schladitz C, Vieira EP, Hermel H, Mohrwald H. Amyloid-β-sheet formation at the air-water interface. Biophysics 1999; 77: 3305-3310.
16. Kendrick BS, Cleland JL, Lam X, Nguyen T, Randolph TW, Manning MC, Carpenter JF. Aggregation of recombinant human interferon gamma: kinetics and structural transitions. Journal of Pharmaceutical Science 1998; 87: 1069-1076.
17. Dong A, Prestrelski SJ, Allison SD, Carpenter JF. Infrared spectroscopy studies of lyophilization- and temperature-induced protein aggregation. Journal of Pharmaceutical Science, 1995; 84: 415-424.
18. McKenzie HA, Ralston GB, Shaw DC. Location of sulfhydryl and disulfide groups in bovine-lactoglobulins and effect of urea. Biochemistry, 1972; 21: 4539-4546.
19. Lefevre T, Subirade M. Interaction of β-lactoglobulin with phospholipids bilayers: a molecular level elucidation as revealed by infrared spectroscopy. International Journal of Biological Macromolecules, 2000; 28: 59-67.
20. Lefevre T, Subirade M. Conformational rearrangement of β-lactoglobulin upon interaction with an anionic membrance. Biochimica et Biophysica Acta, 2001; 1549: 37-50.
21. Lefevre T, Subirade M. Structural and interaction properties of β-lactoglobulin as studied by FTIR spectroscopy. International Journal of Food Science and Technology, 1999; 34: 419-428.
22. Czarnik MB, Murayama K, Wu Y, Ozaki Y. Two-dimensional attenuated total reflection/infrared correlation spectroscopy of adsorption-induced and concentration-dependent spectral variations of β-lactoglobulin in aqueous solutions. Journal of Physical Chemistry, 2000; 104: 7803-7811.

23. Aymard P, Durand D, Nicolai T. The effect of temperature and ionic strength on the dimerisation of β-lactoglobulin. International Journal of Biological Macromolecules, 1996; 19: 213-221.
24. Clark AH, Saunderson DHP, Suggett A. Infrared and laser-Raman spectroscopic studies of thermally-induced globular protein gels. International Journal of Peptide and Protein Research, 1981; 17: 353-364.
25. Larsericsdotter H, Oscarsson S, Buijs J. Structure, stability, and orientation of BSA adsorbed to silica. Journal of Colloid and Interface Science, 2005; 289: 26-35.
26. Arya SC, Agarwal N. Efficacy of measles vaccine interlinked with potency and storage. Acta Tropica, 2004; 90: 223-225.
27. Fang Y, Dalgleish DG. Conformation of β-lactoglobulin studied by FTIR: effect of pH, temperature, and adsorption to the oil-water interface. Journal of Colloid and Interface Science, 1997; 196: 292-298.
28. Guideline on adjuvants in vaccines for human use. The European Medicines Agency. http://www.emea.eu.int Feb, 2006.

Chapter V: Stability of model vaccines during storage analysed by NIR spectroscopy

Abstract

Two model vaccines were monitored during storage at normal and elevated temperatures. The results showed that the release of pre-adsorbed protein antigen decreases drastically. It may indicate why vaccine loses or decreases potency during storage. The protein adsorption by aluminium hydroxide and pH of vaccine also change during storage, and these two parameters are protein specific. NIR spectroscopy is for the first time used to monitor the aging of vaccine. The results suggest that it may be possible to detect the changes of adsorption/desorption of protein antigens, but difficult to determine the alteration of particle size during vaccine storage, even though analyzing the particle size of aluminium hydroxide may be practical. The rotation effects on both model vaccines and aluminium hydroxide are also investigated. Drastically rotation increases the particle size of aluminium hydroxide and may denature protein antigens. Thus, it should be minimised in vaccine productions.

1 Introduction

It is well known that vaccines may lose potency prior to vaccination after long period storage, especially at high temperatures [1]. To ensure the optimal potency of vaccines, storage and handling need careful attention. However, the 'cold chain' system required during storage and shipment is not always optimal in developing countries [2]. The stability of vaccine especially the rate at which vaccine may lose its potency is of great importance to decide whether the vaccine should be destroyed, retesting or used [3]. It is also valuable to ensure reproducible efficacy of the vaccination. The loss of potency has been studied for some specific vaccines during storage at different conditions [4, 5], but the reason that vaccine loses potency is not clear. Previous investigators hypothesised that it might be due to the reversal of protein adsorption from aluminium adjuvant or because of the secondary, tertiary or quaternary structure or even fragmentation of the protein antigens [6, 7].

To well understand the stability of vaccine and the potential reasons that vaccines lose the potency during storage, a few parameters such as pH, adsorption capacity onto aluminium adjuvant, in vitro release of the adsorbed antigen and near infrared (NIR) absorbance of two model vaccines were investigated in this study. To our knowledge, NIR spectroscopy (more details are available in Chapter I and Chapter VI) was for the first time reported here for monitoring the aging process during vaccine storage. Apart from stored at the normal storage temperature (4 ºC), an elevated temperature (37 ºC) was also applied in this study, at which the degradation of vaccine should occur more rapidly than at 4 ºC.

2 Materials and methods

2.1 Materials

Clinical reagent grade BSA (reference L84960) and approximate 90% BLG (reference L3908) were purchased from ICN biomedical Inc and Sigma respectively. Both proteins were used directly without further purification. Aluminium hydroxide adjuvant was purchased from Superfos Biosector A/S (Denmark). A stock aluminium hydroxide adjuvant was prepared by adjusting pH to 8 by the addition of 1 M NaOH. Other chemicals were all of analytical grade and obtained from commercial sources.

2.2 Model vaccine preparation

Model vaccines were prepared by mixing the appropriate amount of protein stock solution and

aluminium hydroxide. The final calculated aluminium concentration was 1.14 mg/ml and the final protein concentration was 2.5 mg/ml. Samples were mixed gently by end-over-end rotation. The protein adsorption capacity onto aluminium hydroxide was investigated as the function of time at room temperature. To study the influence of the rotation time on the aluminium hydroxide, two concentrations in two different tubes were studied. The samples were measured using FT-NIR spectroscopy and the slopes of the NIR absorption curves were probed.

The model vaccines for storage experiments were produced at the identical conditions with 30 min rotation. Thereafter, all samples were stored at 4 ºC and 37 ºC, respectively.

2.3 Experimental procedures

Model vaccine preparation

Protein adsorption capacity was determined by measuring the light absorbance at 280 and 320 nm using a UV/VIS spectrophotometer (Lamda 800, PerkenElmer instruments) with a 1 cm pathlength after centrifugation at 9000 × g for 10 min. Protein adsorption capacity was calculated by following equation (Eq. 5.1):

$$AC = \frac{C_{pro} - \frac{A_{280} - A_{320}}{\varepsilon}}{C_{Alum}} \qquad \text{Eq. 5.1}$$

where AC is adsorption capacity, ε is extinction coefficient, C_{pro} is total added protein and C_{Alum} is total added aluminium hydroxide, A_{280} and A_{320} are the UV absorbance of protein at 280 nm and 320 nm, respectively.

The data of rotation effects on protein adsorption capacity and aluminium hydroxide were analyzed using the Prism software, version 4.03 (GraphPad Software, USA).

Stability of model vaccine during storage

One randomly selected vial for each sample was withdrawn every week. After the sample had reached room temperature, pH was determined using a pH meter (Meterlab PHM220, Radiometer Analytical SAS).

The same sample was gently mixed for 10 min before Fourier transform near infrared spectroscopy (FT-NIR) analysis using a FT-NIR spectrometer (PerkinElmer Spectrum One, PerkinElmer) with an InGaAs detector. Each spectrum was the average of 80 scans at 16 cm^{-1} resolution over the range of 780-2500 nm. The raw NIR spectra were investigated and subsequently analysed by a partial least squared regression (PLS) modelling using the Unscrambler software, version 9.2 (Camo process AS, Oslo, Norway).

Protein release from aluminium hydroxide was estimated by addition of pH 7.4 phosphate buffer (PBS) to a final concentration of 150 mM. The samples were equilibrated at room temperature under continuous orbital rotation for 30 min. Then, the samples were centrifuged for 10 min at 9000 × g. The protein in the supernatant was determined using the procedure mentioned above. The protein recovery from aluminium hydroxide was calculated using Eq. 3.1.

3 Results and discussion

3.1 The production of model vaccines

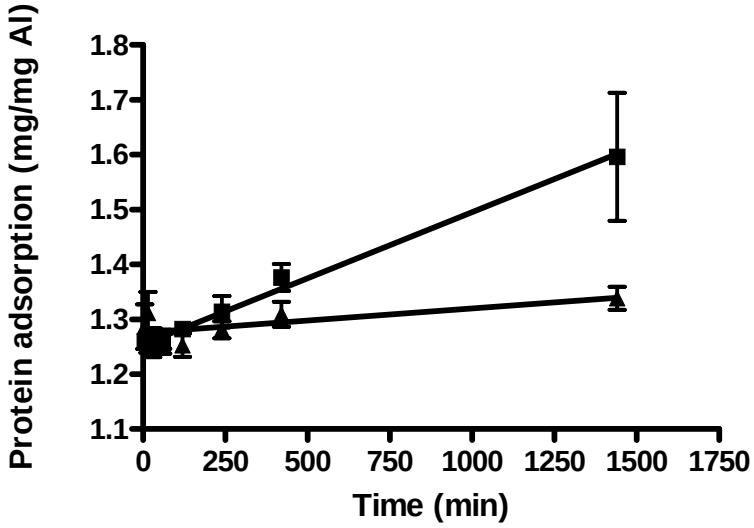

Fig. 5.1 Protein adsorption capacity as a function of rotation time: (■): BSA; and (▲): BLG.

Vaccines are produced by mixing antigens and aluminium-containing adjuvants, and rotating the mixture to obtain maximal adsorption. The rotation time may affect the final protein adsorption capacity. In this work, we investigated the changes of adsorption capacity of two model vaccines. It is observed that the adsorption capacities significantly increase as a function of rotation time for both BSA ($p < 0.0001$) and BLG ($p = 0.04$) model vaccines, see Fig. 5.1. This result may be explained by different mechanisms. For example the proteins aggregate and precipitate and therefore contribute to an overestimation of the protein adsorbed. Another reason could be an increase in particle size of the aluminium hydroxide. The larger particles might adsorb more protein. However, antigens may not easily be released from the adjuvant in this case. Therefore, prolonged rotation of vaccines is not recommended.

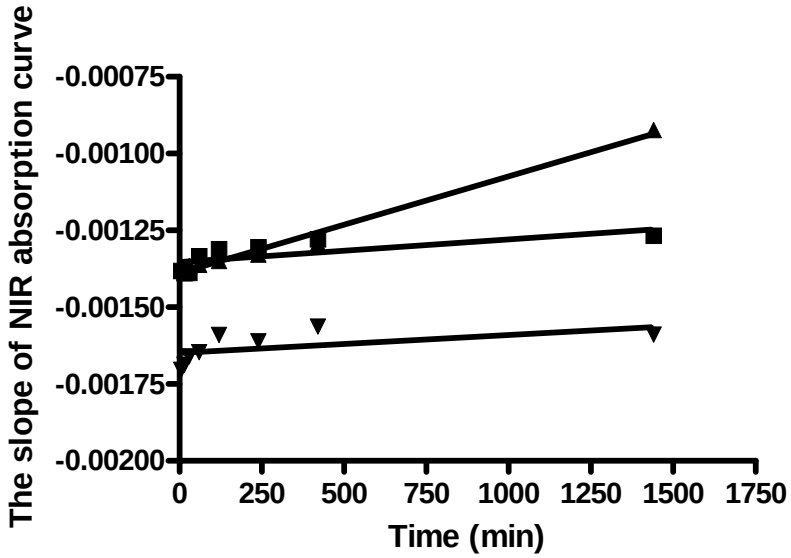

Fig. 5.2 Stability of aluminium hydroxide as a function of rotation time: (■): 1.14 mg/ml aluminium hydroxide 1.5 ml in a 2 ml tube ($p = 0.04$); (▲): 1.14 mg/ml aluminium hydroxide 18 ml in a 50 ml tube ($p < 0.0001$); and (▼): 2.28 mg/ml aluminium hydroxide 1.5 ml in 2 ml tube ($p = 0.15$).

Previous studies indicated that the slope of the NIR absorption spectrum can reflect the particle size of suspension samples [8]. An increasing slope reflects an expanding particle size. The rotation effects on particle size of aluminium hydroxide are shown in Fig. 5.2. The sample with a low concentration aluminium hydroxide is more pronouncedly influenced by rotation time than high concentrations. The free space in the sample container also seems affect the results; a large free space leads to a more drastic change. Thus, vigorous rotation also should also be avoided for aluminium hydroxide.

The model vaccines for the storage experiments are produced by gentle rotation for 30 min. The aluminium hydroxide is used without further treatment after pH adjustment.

3.2 Changes in protein adsorption capacity during model vaccines storage

Vaccines are produced by maximal adsorption of antigens onto aluminium-containing adjuvants in order to enhance the immune response following vaccination. Even though the mechanism by which aluminium-containing adjuvants potentiate the immune response is not fully understood, it is generally accepted that the antigens should be adsorbed to the adjuvants [9]. The World Health Organization recommends that at least 80% of tetanus and diphtheria toxoids should be adsorbed

onto aluminium-containing adjuvants [10].

Adsorption capacity is a measure of the maximal mass unit of protein adsorbed per mass unit of aluminium. It is an important parameter for physicochemical characterization of the adsorption of an antigen.

The changes in adsorption capacity of two model vaccines were investigated in this work. The data are shown in Fig. 5.3. The mechanism of protein adsorption onto adjuvants is not clear, but electrostatic force and hydrophobic interactions play an important role in this process [11]. Aluminium hydroxide is a crystalline aluminium oxyhydroxide, which has an isoelectric point (pI) of approximately 11, thus, it is a good adsorbent for acidic proteins at neutral pH [12]. The adsorption capacities of BSA and BLG are 1.91 and 1.95 mg / mg aluminium respectively for the freshly prepared vaccines as measured in the present study. The adsorption capacity of BSA remains constant during 7 weeks of storage. It can be observed that aluminium hydroxide can adsorb more protein at 37 ºC than at 4 ºC. This may result from aggregation of protein at high temperature. In contrast, the adsorption capacity of BLG is reduced as a function of storage time both at room temperature and at elevated temperatures. The reduction is more pronounced within the first two weeks. The elevated temperature accelerates this decline. Therefore, the alteration of adsorption capacity during storage may be a protein specific parameter. López *et al.* [13] demonstrated that the adsorption of synthetic SPf(66)n malaria vaccine occurred with small variations during storage at three different temperatures. Accelerated reduction was also observed when vaccine was stored at a higher temperature in their study. Adsorption of antigens onto aluminium hydroxide is an important parameter for inducing an adequate humoral immune response [14]. Reduced adsorption may result in loss of potency during vaccine storage.

The change in antigen adsorption during vaccine storage may be caused by changes in the protein antigens and/or the aluminium adjuvant, as well as the changes in their interactions. In a previous study a continuous decline in the capacity of aluminium hydroxide to adsorb Congo red dye was observed during storage at temperature of 4 to 10 ºC for 5.5 years [1]. In the present study, however, the aging of aluminium hydroxide may not be the dominating reason, since both BSA and BLG model vaccines were prepared using same batch of aluminium hydroxide and stored and under the same experimental conditions, and yet produced different results. Degradation of protein or changes in the interaction between protein and adsorbent may have greater influences.

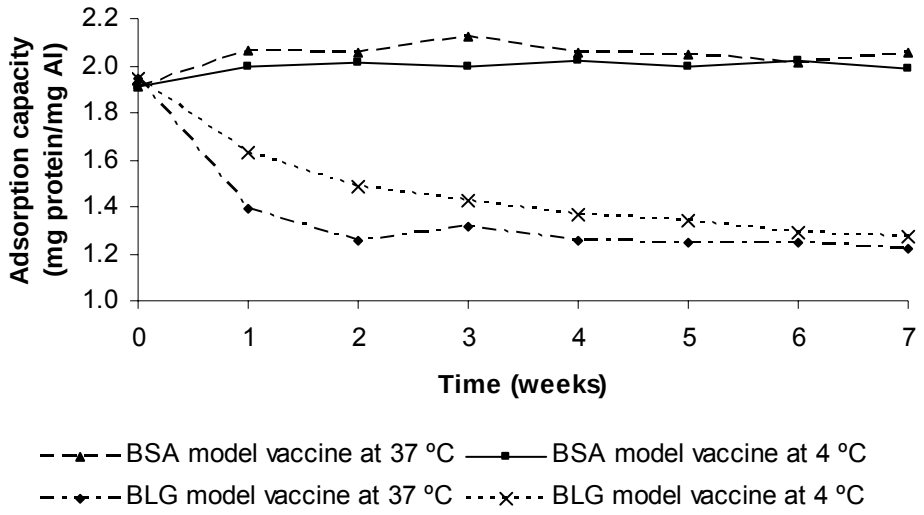

Fig. 5.3 Changes in protein adsorption capacity during model vaccines storage at two different temperatures.

3.3 Protein antigen recovery from model vaccines during storage

One hypothesis for the enhancement of immune responses by aluminium containing adjuvants is formation of a depot at the site of injection allowing the antigen to be gradually released [15, 16]. In addition to the term 'release', terms such as 'displacement' [17] and 'elution' [18-20] are also used to indicate the detachment of molecules from an interface. Release can be defined as a process in which other molecules displace pre-adsorbed protein molecules by competing for adsorption onto the surface.

Surfactants have been well studied in the release of pre-adsorbed protein from surfaces [17-20]. Rinella and co-workers [20] have shown that nonionic and zwitterionic surfactants caused no or small degree of release of ovalbumin from aluminium hydroxide, while ionic surfactants were much more effective. They proposed that the effectiveness of surfactants in displacing pre-adsorbed proteins was directly related to their ability to denature the protein.

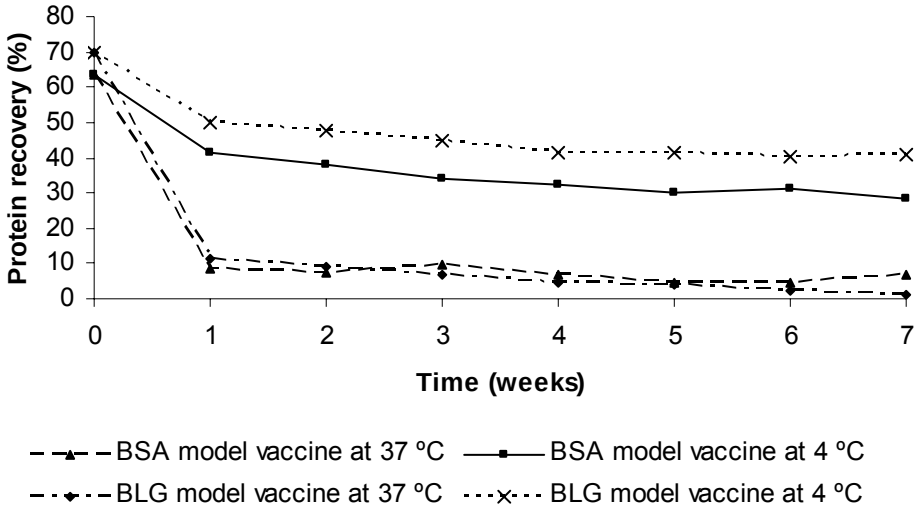

Fig. 5.4 Protein recovery from aluminium hydroxide in model vaccines during storage at two different temperatures.

In the previous study (Chapter III), It was shown that 150 mM PBS at pH7.4 is a good candidate to release model antigens from aluminium hydroxide, because the phosphate anion can easily be adsorbed onto aluminium hydroxide by ligand exchange [21]. Protein recoveries from freshly prepared BSA and BLG model vaccines were 63.74% and 69.91% respectively at the present experimental conditions. Protein recoveries as a function of storage for the two model vaccines at two storage temperatures are illustrated in Fig. 5.4. The amount of released protein decreases dramatically in the first week, especially when the vaccines are stored at 37 ºC. The BSA recovery declines from 63.74% to 8.34% after one week, and the BLG recovery changes from 69.91% to 11.23% in the same period. After 7 weeks of storage, the recoveries are 6.73% and 0.98% for BSA and BLG respectively. For vaccines stored at 4 ºC, the protein recoveries decrease to 28.75% and 40.76% for BSA and BLG, respectively, after 7 weeks. The loss of protein recovery has also been observed for other proteins, releasing agents, and a variety of surfaces [19, 22]. An aging effect was noted as less fibrinogen was released from polyurethane surfaces using 3% sodium dodecyl sulfate (SDS) with increasing storage [23]. In another study [24], there was no protein recovery from the Montanide® ISA 720 adjuvant after 8 weeks storage at 37 ºC. The potency was tested and showed that the vaccine had lost all immunogenicity. In contrast, no aging effect was observed in the previous studies [25]. Aging at 4 ºC did not affect the release of lysozyme in interstitial fluid, but decreased the release of ovalbumin within 11 weeks storage. Furthermore, by adding SDS within 10 days after the vaccine was prepared, Rinella *et al.* [20] demonstrated that there was no change of

protein release of the model vaccine composed of ovalbumin-aluminium hydroxide by adding SDS within 10 days after the vaccine was prepared. Therefore, the release of adsorbed protein is not only dependent on the specific protein, but also depends on the releasing agents and the absorbents.

The loss of protein recovery may result from conformational changes of adsorbed protein molecules due to intra- and intermolecular aggregation which leads to a more tightly bound complex. However, FTIR analysis (chapter IV) showed that the secondary structure of adsorbed BSA did not change during four months of storage; while the structure of adsorbed BLG changed dramatically. The release of both BSA and BLG are reduced during storage in the present work. Therefore, the conformational change of the adsorbed protein is not the only reason leading to loss of protein release. Degradation of the aluminium adjuvant, changes in the interaction between the protein and the adjuvant, and changes in protein-water bonding may also play an important role.

Another hypothesis described that the loss of protein release was due to a change in the adsorption mechanism from principally electrostatic attraction to the much stronger ligand exchange [25].

3.4 Changes in pH of model vaccines during storage

The pH was measured weekly in the two model vaccines stored at two temperatures for 7 weeks, see Fig. 5.5. It can be observed that changes in pH are accelerated at elevated temperature. For the BSA model vaccine, pH decreased during the 7 weeks of storage at 37 ºC, while it remained constant at 4 ºC. In the case of the BLG model vaccine, pH decreased at 4 ºC; but when stored at 37 ºC, the pH decreased during the first two weeks and then increased. In a previous study, pH changes were also observed in the storage of outer membrane vesicles vaccines at 56 ºC [26]. Furthermore, the pH of milk samples first decreased and then increased during 100 days of storage [27].

The pH changes may be explained by chemical degradation of the proteins, such as oxidation, deamidation, and fragmentation. In this connection it was noticed that the BLG model vaccine smelled like sulphide during the later stage of storage when opening the vial. However, this was not further investigated in this study. The degradation of aluminium hydroxide may also play a role in the pH change, since the pH of a diluted aluminium hydroxide (1.14 mg/ml) declines as a function of time at room temperature (Fig. 5.6). Other investigators also demonstrated that the pH changed in diluted aluminium-containing adjuvants [28]. The alteration of pH may affect the structural stability of the proteins. In chapter IV, it is shown that the structure of adsorbed BSA remained constant, while adsorbed BLG changed dramatically. Moreover, the structural changes of adsorbed BLG were different when stored at 4 ºC as compared to 37 ºC. Further experiments are required to ascertain whether the slight change in pH can lead structural changes.

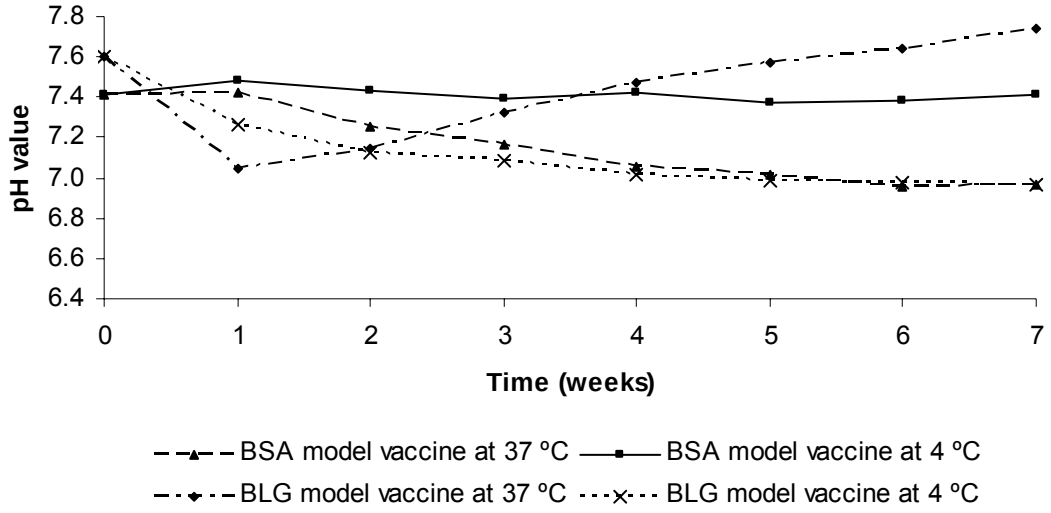

Fig. 5.5 Changes in pH the model vaccines during storage at two different temperatures.

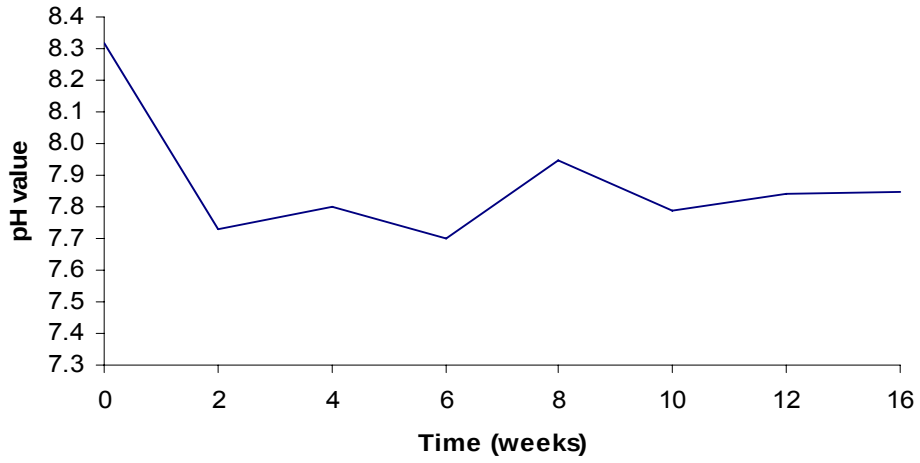

Fig. 5.6 Changes in pH of aluminium hydroxide (1.14 mg/ml) during storage at room temperature.

3.5 Changes in NIR spectra of model vaccines during storage

NIR can be used to monitor the amount of protein adsorbed by aluminium-containing adjuvant [29] as well as the particle size [29-33]. To our knowledge, this study represents the first study to use NIR spectroscopy to monitor the aging process during vaccine storage. The NIR spectra of BSA and BLG model vaccines at both 4 ºC and 37 ºC during the storage are presented in Fig. 5.7.

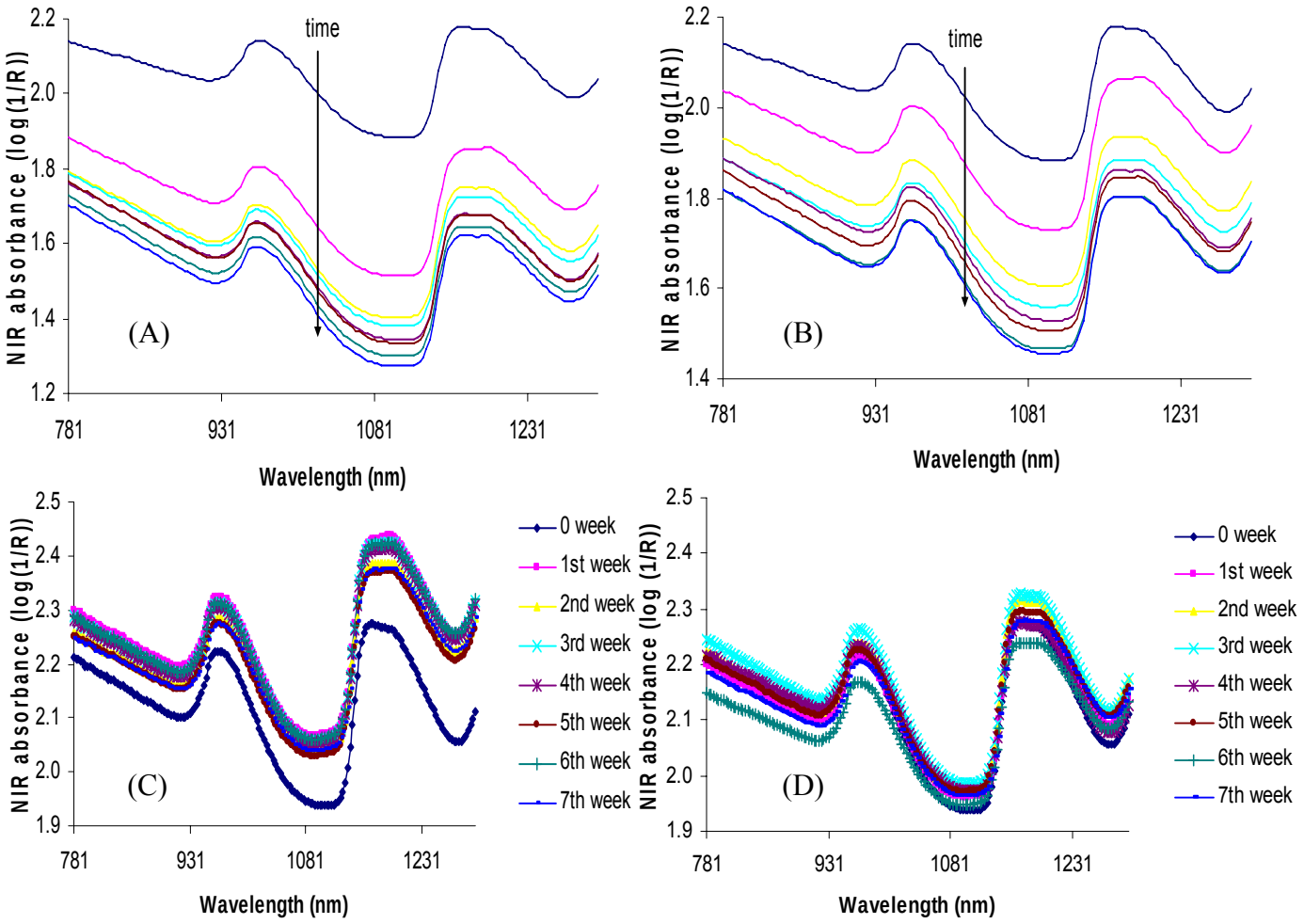

Fig. 5.7 NIR spectra of BLG (A, B) and BSA (C, D) model vaccines: stored at 37 ºC (A, C) and 4 ºC (B, D) for 7 weeks. The arrows indicate the direction of change with time.

The intensity of the NIR spectra for BLG model vaccine dramatically decreased at both 4 ºC and 37 ºC during the storage. The decrease was more pronounced during the first two weeks. In the case of BSA model vaccine, the NIR spectra also changed during the storage, but not nearly as dramatic and furthermore, the spectral changes were not a regular function of time. In both cases, however, the NIR spectra underwent rapid modification with time of storage at 37 ºC. Similar changes were seen with samples stored at 4 ºC, although at a slower rate compared to storage at 37 ºC. The regular spectral change of the BLG model vaccine and the irregular spectral change of the BSA model vaccine during the storage agree well with FTIR-ATR studies [34].

To investigate the mechanism behind the changes in the NIR spectra during the storage of model vaccines, PLS regression was performed in order to construct a calibration model correlating NIR

absorption (780-1300 nm) to protein adsorption (reference data of protein adsorption, see section 3.2). The model was assessed by full cross validation and showed a correlation of 0.98 and RMSEP of 0.06 mg protein / mg Al, see Fig. 5.8. The model indicates that the decrease of NIR absorbance is due to a reduction in the amount of protein adsorbed onto aluminium hydroxide during the storage. The results suggest that NIR spectroscopy can be used as a fast method to monitor adsorbed protein in vaccine samples.

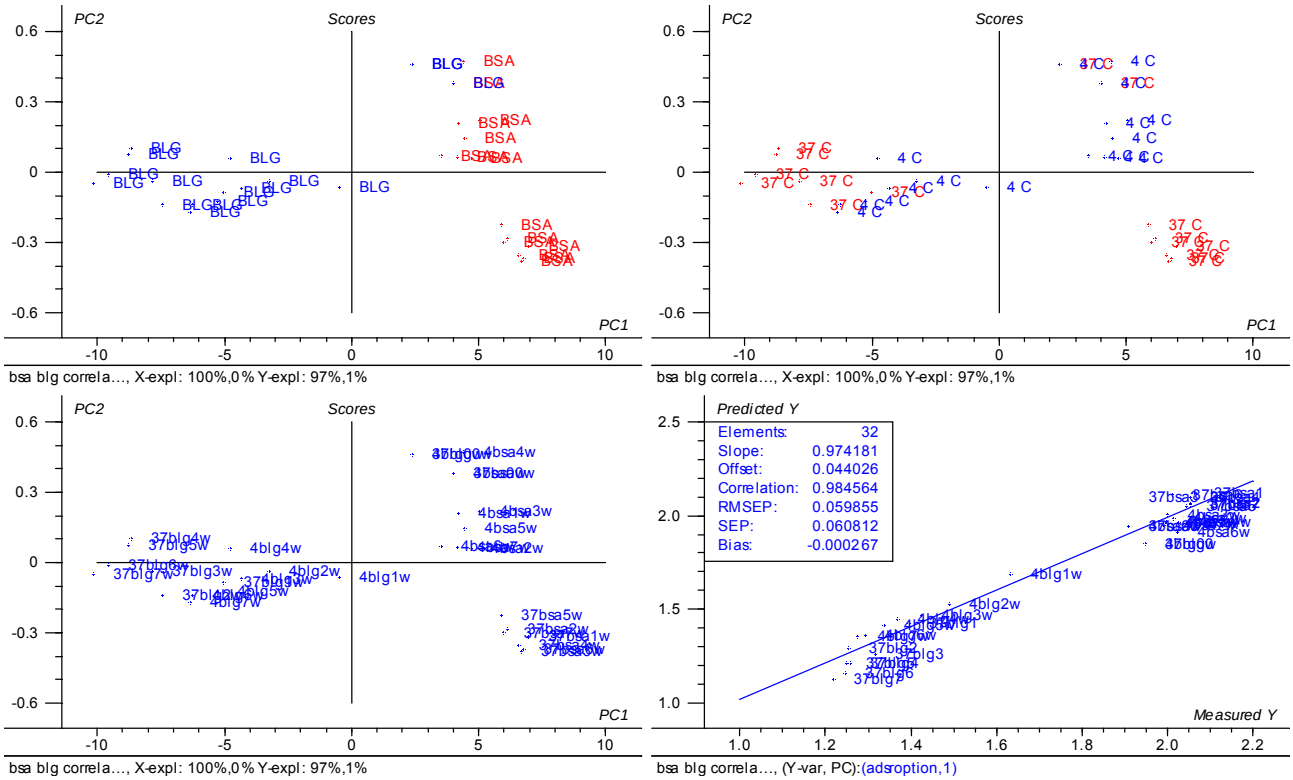

Fig. 5.8 PLS model: the correlation between NIR absorbance and protein adsorption, R^2 = 0.98 and RMSEP = 0.06 mg protein/ mg Al.

By inspecting the scores plots, the first principle component (PC1) describes the amount of adsorbed protein onto aluminium hydroxide: BSA vaccine stored at 37ºC > BSA stored at 4 º C > BLG vaccine stored at 4 º C > BLG stored at 37 ºC. BSA model vaccine stored at 37 ºC and 4 ºC are separated by PC2. This may be due to a change in particle size resulting from aggregation of protein antigen, aluminium hydroxide or the interaction between them. To confirm the influence of aluminium hydroxide, the aging of aluminium hydroxide alone is also studied by NIR spectroscopy in this work. The same concentration aluminium hydroxide (1.14 mg/ ml) without protein is stored at room temperature and measured as a function of time. The spectra are given in Fig. 5.9. The NIR

absorbance of aluminium hydroxide increases as a function of storage time. The change was caused by increasing light scattering resulting from morphological and structural changes. It indicates that the particle size of aluminium hydroxide change during storage. However, for the model vaccines the change in particle size is concealed by the changes of protein adsorption/desorption. Therefore, it may be difficult to determine the alteration of particle size of a vaccine during the storage using NIR spectroscopy.

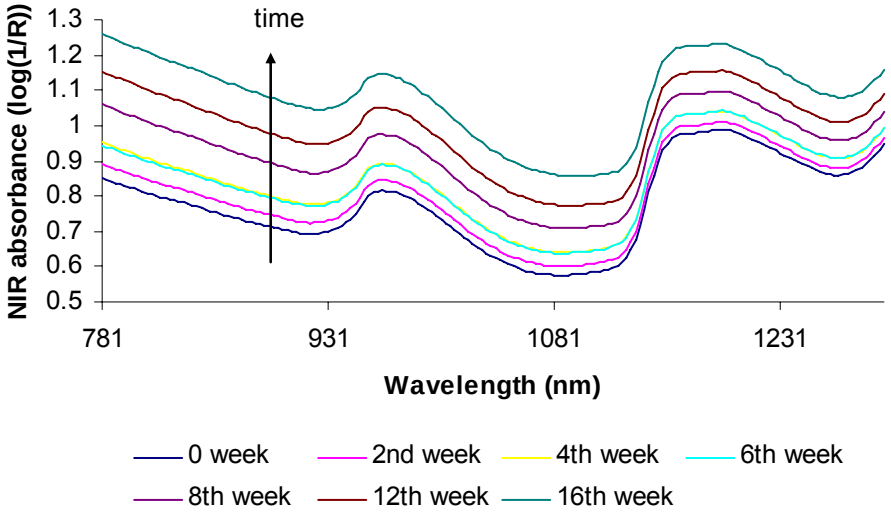

Fig. 5.9 NIR spectra of aluminium hydroxide: stored at room temperature over 16 weeks. The arrow presents the

4 Conclusion

This study systematically monitored changes of model vaccines during storage at normal vaccine storage temperature and at an elevated temperature. The data presented here show that the release of pre-adsorbed protein antigen decreases during storage. This may indicate why vaccine may change potency during storage. The protein adsorption by aluminium hydroxide and the pH of the vaccine also change during storage, and these two parameters are protein specific. Model vaccines generally undergo rapid modification with the time when stored at 37 ºC. Similar changes are observed upon storage at 4 ºC, although at a slower rate. NIR spectroscopy is for the first time used to monitor the aging of vaccine. The results suggest that it may be possible to detect changes in adsorption/desorption of protein antigens, but impossible to determine the alteration of particle size during vaccine storage, even though analyzing the particle size of aluminium hydroxide alone may be practical. Both BSA and BLG model vaccines as well as aluminium hydroxide are profoundly

affected by rotation. Vigorous rotation increases the particle size of aluminium hydroxide and may denature protein antigens. Thus, it should be minimised in vaccine production.

References

1. Galazka A, Milstien J, Zaffran M. Thermostability of vaccines. World Health Organization, 1998; Geneva. http://wwwlive.who.ch/vaccines-documents/ DocsPDF/www9661.pdf
2. Jeremijenko A, Kelly H, Sibthorpe B, Attewell R. Improving vaccine storage in general practice refrigerators. British Medical Journal, 1996; 312: 1651-1652.
3. Labuza TP, Fu B. Vaccine stability and the use of time-temperature integrators for monitoring the cold chain in distribution. http://courses .che.umn.edu/oofscn8334-1f-folder/vaccine.
4. Arya S, Agarwal N. Efficacy measles vaccine interlinked with potency and storage. Acta Tropica, 2004; 90: 223-225.
5. Miles AP, McClellan HA, Rausch KM, Zhu D, Whitemore MD, Singh S, Martin LB, Wu Y, Giersing BK, Stowers AW. Montanide ISA 720 vaccines: quality control of emulsions, stability of formulated antigens, and comparative immunogenicity of vaccine formulations. Vaccine, 2005; 23: 2528-2537.
6. Dimayuga R, Scheifele D. Effects of freezing in DPT and DPT-IPV vaccine adsorbed. Canada Communicable Disease Report, 1995; 21: 101-103.
7. Boros CA, Hanlon M, Gold MS, Roberton DM. Storage at -3 ºC for 24 h alters the immunogenicity of pertussis vaccine. Vaccine, 2001; 19: 3537-3542.
8. Lai X, Zheng Y, Ipsen H, Jacobsen S, Larsen JN, Løwenstein H, Søndergaard I. Particle size determination in suspensions using near-infrared transmittance spectroscopy. Submitted to Applied Spectroscopy, 2006.
9. Chang MF, Shi Y, Nail SL, HogenEsch H, Admas SB, White JL, Hem SL. Degree of antigen adsorption in the vaccine or interstitial fluid and its effect on the antibody response in rabbits. Vaccine, 2001; 19: 2884-2889.
10. World Health Organization. Immunological adjuvants. World Health Organization Technical Report Series No. 595. Geneva: World Health Organization, 1976: 6-8.
11. Al-Shakhshir RH, Regnier F, White JL, Hem SL. Contribution of electrostatic and hydrophobic interaction to the adsorption of proteins by aluminium adjuvants. Vaccine, 1995; 13: 41-44.
12. Seeber SJ, White JL, Hem SL, Predicting the adsorption of proteins by aluminium-containing adjuvants. Vaccine, 1991; 9: 201-203.

13. López MC, Thomas MC, Olivares M, Alonso P, Alonso C. The effect of temperature on the stability of the synthetic SPf(66)n malaria vaccine. Vaccine, 1995; 13: 1180-1182.
14. Amador R, Moreno A, Valero V, Murillo L, Mora AL, Rojas M, Rocha C, Salcedo M, Guzman F, Espejo F, Nunez F, Patarroyo ME. The first field trials of the chemically synthesized malaria vaccine SPf66: safety, immunogenicity and protectivity. Vaccine, 1992; 10: 179-184.
15. Jones LS, Peek LJ, Power J, Markham A, Yazzie B, Middaugh R. Effects of adsorption to aluminium salt adjuvants on the structure and stability of model protein antigens. The Journal of Biological Chemistry, 2005; 280: 13406-13414.
16. Rogan D, Babiuk LA. Animal health: biologics/biopharmaceutics – novel vaccines from biotechnology. Revue Scientifique et Technique – Office International des Epizooties, 2005; 24: 159-174.
17. Engel MFM, Visser AJWG, Mierlo CPMV. Refolding of adsorbed bovine α-lactalbumin during surfactant induced displacement from a hydrophobic interface. Langmuir, 2003; 19: 2929-2937.
18. Rapoza RJ, Horbett TA. Effects of concentration and adsorption time on the elutability of adsorbed proteins in surfactant solutions of varying structures and concentrations. Journal of Colloid interface Science, 1990; 136: 480-493.
19. Bohnert JL, Horbett TA. Changes in adsorbed fibrinogen and albumin interactions with polymers indicated by decreases in detergent elutability. Journal of Colloid Interface Science, 1985; 111: 363-377.
20. Rinella JV, Workman RF, Hermodson MA, White JL, Hem SL. Elutability of proteins from aluminum-containing vaccine adjuvants by treatment with surfactants. Journal of Colloid and Interface Science, 1998; 197: 48-56.
21. Bleam WF, Pfeffer PE, Goldberg S, Taylor RW, Dudley RA. ^{31}P solid-state nuclear magnetic resonance study of phosphate adsorption at the boehmite/aqueous solution interface. Langmuir, 1991; 7: 1702-1712.
22. Slack SM, Horbett TA. Changes in the strength of fibrinogen attachment to solid surfaces: an explanation of the influence of surface chemistry on the vorman effect. Journal of Colloid Interface Science, 1989; 133: 148-165.

23. Chinn JA, Posso SE, Horbett TA, Ratner BD. Postadsorption transitions in fibrinogen adsorbed to polyurethanes: changes in antibody binding and sodium dodecyl sulfate elutability. Journal of Biomedical Materials Research, 1992; 26: 757-778.
24. Miles AP, McClellan HA, Rausch KM, Zhu D, Whitemore MD, Singh S, Martin LB, Wu Y, Giersing BK, Stowers AW. Montanide ISA 720 vaccines: quality control of emulsions, stability of formulated antigens, and comparative immunogenicity of vaccine formulations. Vaccine, 2005; 23: 2528-2537.
25. Shi Y, HogenEsch H, Hem SL. Change in the degree of adsorption of proteins by aluminium-containing adjuvants following exposure to interstitial fluid: freshly prepared and aged model vaccines. Vaccine, 2002, 20: 80-85.
26. Arigita C, Jiskoot W, Westdijk J, Ingen CV, Hennink WE, Crommelin DJA, Kersten GFA. Stability of mono- and trivalent meningococcal outer membrane vesicle vaccines. Vaccine, 2004; 22: 629-642.
27. Kelly AL, Foley J. Proteolysis and storage stability of UHT milk as influenced by milk plasmin activity, plasmin/β-lactoglobulin complexation, plasminogen activation and somatic cell count. International Dairy Journal, 1997; 7: 411-420.
28. Burrell LS, White JL, Hem SL. Stability of aluminium-containing adjuvants during aging at room temperature. Vaccine, 2000; 18: 2188-2192.
29. Lai X. PhD thesis. The Technical University of Denmark, 2006.
30. Otsuka M. Comparative particle size determination of phenacetin bulk powder by using Kubelka-Muck theory and principle componenet regression analysis based on near infrared spectroscopy. Powder Technology, 2004; 141: 244-250.
31. O'Neil AJ, Jee RD, Moffat AC. Measurement of the percentage volume particle size distribution of powdered microcrystalline cellulose using reflectance near infrared spectroscopy. The Analyst, 2003; 128: 1326-1330.
32. Pasikatan MC, Steele JL, Spillman CK, Haque E. Near infrared reflectance spectroscopy for online particle size analysis of powders and ground materials. Journal of Near Infrared Spectroscopy, 2001; 9: 153-164.
33. Santos AF, Lima EL, Pinto JC. In-line evaluation of average particle size in styrene suspension polymeriztions using near-infrared spectroscopy. Journal of Applied Polymer Science, 1998; 70: 1737-1745.

34. Zheng Y, Lai X, Ipsen H, Larsen JN , Løwenstein H, Søndergaard I, Jacobsen S. The structural stability of the adsorbed model antigens by aluminium hydroxide in heating and aging processes in comparison to the antigens in solutions. Submitted to Vaccine, 2006.

Chapter VI: Determination of residual moisture content of lyophilized allergen vaccines by NIR spectroscopy

Abstract

Residual moisture content is an important parameter for lyophilized vaccines. Currently, Karl Fischer (KF) titration is widely used for moisture determination in routine analysis. However, this method is time-consuming, sample destructive and requires environment polluting reagents, as well as the results rely on the random samplings. Near infrared spectroscopy (NIR) was used as a fast, non-invasive and non-destructive method to determinate the residual moisture content in lyophilized allergy vaccines in this study. Five different vaccine products were investigated, which contained water from 0.168 to 1.51 % (w/w) analyzed by KF titration as reference measure. Different data pre-treatments, wavelength selection and partial least squares regression were applied to construct calibration models. Acceptable multi-products model (with RMSEP 10.20 µg H_2O/vial, 2 PLS factors) and product-specific models were obtained. The results summarized in this work suggest that NIR is an optimal alternative for determination moisture content in lyophilized vaccines.

1 Introduction

Lyophilization (freeze-drying) is widely applied for the preservation and storage of many vaccines. Lyophilized vaccines always contain some water, known as residual moisture, which is usually constitutes between 1% and 5% of the final product after the bulk of the aqueous solvent has been removed during the freeze-drying process. Residual moisture content (RMC) is a critical quality parameter influencing not only the vaccine appearance and quality but also its shelf life [1-3]. Therefore, RMC should be sufficiently low so that immunological potency and integrity of the product are not compromised over time. However, RMC of the vaccine should not be so low that the properties of the product are deteriorated due to over-drying. Over-drying results in broken product cake. It may also cause the structure of the antigen to change, which may induce aggregation of the protein complex, and lead to increased difficulty predicting the release profile of the antigens. Furthermore, RMC is also an important parameter for manufacturers to control their lyophilizing cycle.

Pharmaceutical companies have to verify that the RMC in their products is consistently within specifications. Currently, KF titration is widely used for RMC determination in lyophilized products [4]. This method is time-consuming, sample destructive and requires environment polluting reagents. Thermogravimetry and gas chromatography are also applied for RMC analysis [5, 6]. However, the methods are also expensive, time-consuming and destructive. Ambient moisture may affect the results for low moisture level samples since the vials have to be opened before analysis. IN addition, many random samples have to be analysed for each batch in the production line, which is a resource consuming procedure, and random sampling has inherent disadvantages. Clusters of products deviating in water content caused by momentary production problems may not always be monitored and entire batches of the product may have to be rejected due to the results from the outliers that have been sampled. It would therefore be advantageous to replace these procedures with an automated online method.

Near infrared spectroscopy (NIR) offers many advantages over traditional methods for moisture determination. It is a physical, non-invasive, non-destructive method. Thus, the analysis can be performed through sealed glass vials, directly on the final product without opening the vials. It is suitable for online analysis because NIR radiation can penetrate the glass vial making sample preparation redundant. NIR analyses are typically rapid and the spectra provide information on both physical and chemical properties of the product analysed, such as sample identity and concentration, particle size, hardness, and even taste. NIR is easy and safe to use, since there is no

sample preparation, no reagents are used, and no wastes are produced. Lastly, the use of NIR spectroscopy avoids random sampling in the control of RMC.

Water is the strongest absorbing compound in the NIR region, exhibiting four absorption maxima around 970, 1190, 1450, and 1940 nm. The NIR absorption of water has been well investigated because of its importance in all applications of the technique. Strong absorption bands of water appear around 1400-1450 nm and 1900-1950 nm, which are due to the first overtone of OH stretching and combination of the OH stretching band and OH bending [7]. Variations in the water band around the 1400 nm region are dependent on the state of water in the sample. In samples with a water content reaching 70-90% the adsorption band appears at similar wavelengths to those of pure water, around 1400-1410 nm. In dry samples the band associated with free water seems to disappear except for a trace of absorption near 1430 nm [8]. These two bands have often been used to quantify water content in various samples. Other water bands in the NIR region are located at 970 nm and 1190 nm. The intensities of these bands are not strong, since they arise from the second overtone of the OH stretching band, as well as the combination of the first overtone of the OH stretching and the OH bending [7].

The determination of moisture content by NIR spectroscopy in both transmittance and reflectance modes have been described extensively in the literature, covering applications in agriculture, forestry, textiles, chemicals, and pharmaceutical areas. NIR has been used for lyophilized products and for tablet analyses. NIR is also applied to measure the amount of moisture during granulation, drying, and purification stages of solids and liquids, and the monitoring of moisture during process optimization [9-16]. Most of the early studies using NIR for water determination have been summarized and discussed by Blanco *et al.* [13], and recent applications have been reviewed by Reich [9].

NIR applications for protein pharmaceuticals, however, have not been widely adopted [9, 11]. Lyophilized pharmaceutical products typically contain 1% to 2% residual water, which is a narrow range for the construction of a calibration model. In order to compensate for the narrow range previous studies have extended the range by adding artificial samples, which were obtained by adsorbing and/or further secondary drying [11, 17]. The artificial calibration samples, however, were damaged before NIR measurements, and the model did not improve the prediction results significantly.

To our knowledge, NIR has never been used to determine RMC in vaccine products. The objective of this study was to develop a non-invasive, non-destructive and rapid method for RMC

determination for lyophilized allergen vaccines. All samples were directly measured using a Fourier transform NIR (FT-NIR) spectrometer without sample preparation, i.e. through the bottom of the intact glass vials by diffuse reflectance. A general calibration model was constructed for five vaccine products using KF titration as reference method. Calibration models for each vaccine product were also built for comparison. The models were validated by cross validation.

2 Materials and methods

2.1 Samples

Five different lyophilized allergy vaccine products, a total of 95 vials were collected by random sampling. Detailed information is given in Tab. 6.1.

2.2 NIR measurement

All NIR measurements were carried out using a FT-NIR spectrometer (PerkinElmer Spectrum One, PerkinElmer) with an InGaAs detector. NIR spectra were collected in the reflectance mode at ambient temperature, although products were stored refrigerated. Each spectrum was the average of 80 scans at 16 cm^{-1} resolution over the range 700-2500 nm. For each sample, four spectra were collected by rotating the vial in different angles. Therefore, a total of 380 spectra were obtained.

2.3 KF titration analysis

After NIR measurement, the same vials were analyzed for RMC using a 737 KF Coulometer (Metrohm, Switzerland). A well-defined amount of dry methanol (1 ml) was added to each test vial. The vial was mixed thoroughly using a Vortex mixer until the sample was uniform. The vial was incubated at room temperature for two hours, and centrifuged at 2000 rpm. The RMC was detected immediately after centrifugation. A plastic syringe was rinsed first using dry methanol. Approximately 400 µl sample was drawn into the syringe. Pointing the needle upwards, air bobbles and excess materials was removed until 350 µl samples remained in the syringe. Sample was added under the surface of the fluid. The needle was pulled away from the surface of the fluid, and simultaneously the plunger was drawn back to avoid leaving sample drops inside the membrane. Then the equipment was started.

Tab. 6.1 The detailed information of calibration samples

Vaccine products	Concentration of allergy (SQ-U)	Vials of each concentration	Batches of each concentration	Total bottles	RM (µg/vial, KF)
Api mel	45	3	3	16	22.9-70.7
	450	3	3		
	4500	3	3		
	45000	2	3		
	450000	5	3		
Cat	45	6	2	33	16.8-122.7
	450	7	2		
	4500	6	2		
	45000	6	2		
	450000	8	2		
Der	45	1	1	7	24.9-74.4
	450	1	1		
	4500	1	1		
	45000	1	1		
	450000	3	1		
Grass	45	2	2	16	22.4-66.1
	450	2	2		
	4500	2	2		
	45000	4	2		
	450000	6	2		
Ves	45	3	3	23	24.6-151.0
	450	3	3		
	4500	3	3		
	45000	3	3		
	450000	11	3		

The final RMC for each sample was calculated from the following formula (Eq. 6.1):

$$RMC = \frac{(A - B) * C}{D} \qquad \text{Eq. 6.1}$$

A= measured water content

B= blank (average of 3 measurements of 350 ml dry methanol)

C= volume of methanol added (ml)

D= volume of methanol injected (ml)

The RMC was given in µg for each vial (µg H_2O/vial).

2.4 Calibration model construction

The KF data were assigned to their corresponding NIR spectra. Partial least squares (PLS) regression was performed to build calibration models using the Unscrambler software, version 9.2

(Camo process AS). Different data pre-treatments were applied to remove baseline offset and other physical information before PLS regression. The number of PLS components or factors (PLS factors), correlation (R^2) and root mean square error of prediction were used to describe the calibration models.

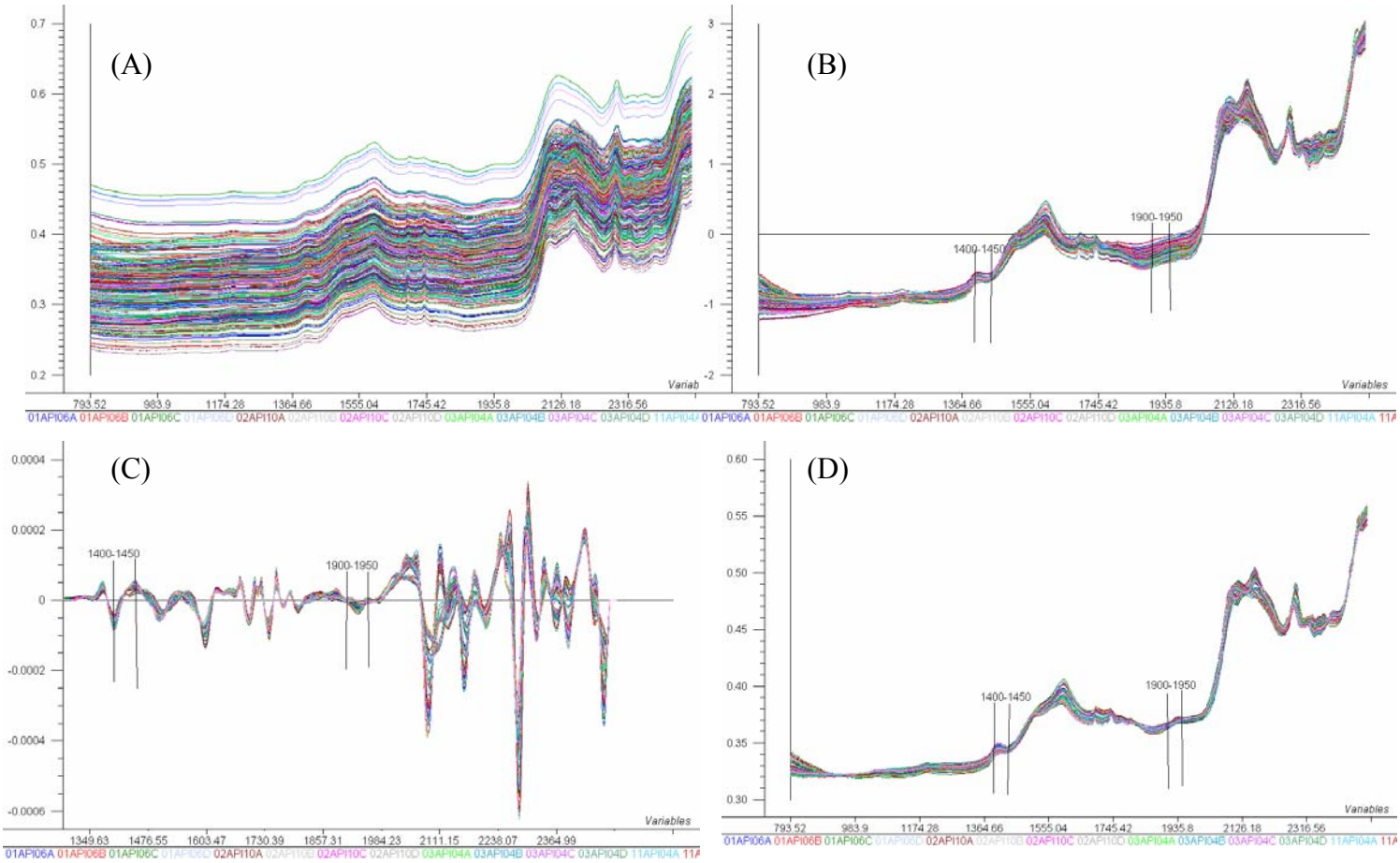

Fig. 6.1 380 NIR spectra of 95 calibration samples: raw spectra (A), EMSC spectra (B), EMSC + 2nd derivative (C), SNV (D). X axis represents wavelength (nm) and Y axis represents NIR absorbance (log (1/R)).

3 Results and discussion

3.1 Relationship between RMC and NIR data

The major challenges in this work are the small amount of sample, low RMC, and variances of sample cakes and bottles. The sample amount is approximately 10 mg/vial. The overall range of RMC in these lyophilized samples (as analyzed by KF titration and given in Tab. 6.1) is in the range from 16.8 to 151.0 µg/vial, which correspond to 0.17 – 1.51% (w/w). The detailed information of RMC in each vial is presented in Appendix I. Raw NIR spectra of the 95 calibration samples are

shown in Fig. 6.1.A. Because of the small amount of sample a part of the NIR radiation passes through the sample cake and cannot be reflected back to the detector, which results in low NIR absorbance and baseline offsets. Light scattering due to the physical conditions of the sample such as particle size, density and bottle variation affect the raw spectra as well. Due to these reasons and the very low water content, the two water bands at 1400-1450 nm and 1900-1950 nm are almost missing, especially for the latter peak.

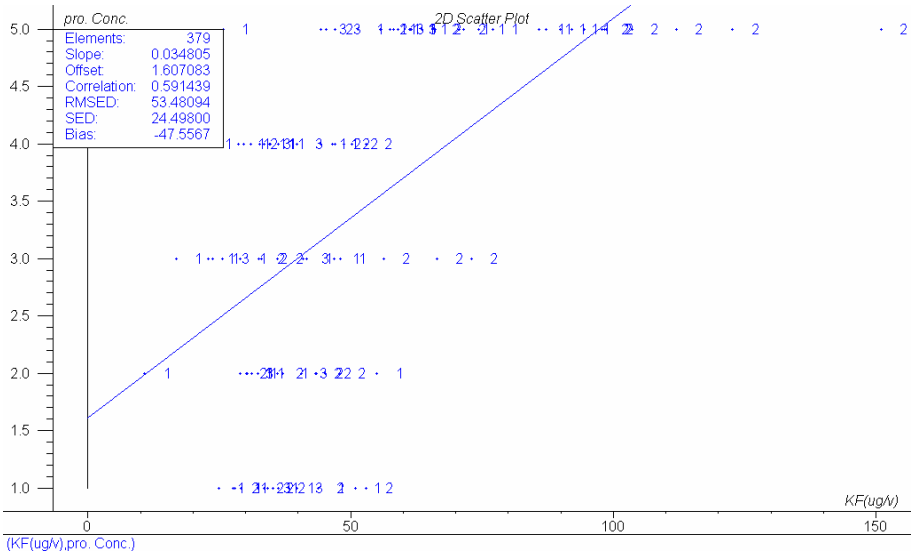

Fig. 6.2 The correlation between RMC and protein content

Different methods of data pre-treatments were tested to remove the effect of light scattering, see Fig. 6.1. In Fig. 6.1.B the spectra are shown after pre-treatment using extended multiplicative scatter correction (EMSC). EMSC is a method suited for removal of physical effects from the chemical information [18]. By visual inspection of the EMSC spectra, there is no clear quantitative relationship between the NIR adsorption and the RMC levels, although most light scattering interferences in the raw spectra are drastically reduced. However, these lyophilized samples contain not only residual moisture, but also other components, such as antigens, adjuvants, inorganic salts, and other chemicals to facilitate the lyophilizing process and cake formation. All these compounds may interact with water, which results in spectral variation in other regions. Water information can also be derived from these spectral alterations indirectly. For example, there is 60% correlation between RMC and the protein contents in the data set, see Fig. 6.2.

3.2 Multi-products calibration model for RMC

Since no clear correlation between differences in the NIR spectra and RMC at 1400-1450 nm and

1900-1950 nm were detected, all significant X variables (wavelength) after Jack-knifing were taken into account in the calibration model. For comparison, one NIR water band (1900-1960 nm) was also investigated to construct models. First, we attempted to make build one model w involving all five vaccine products using PLS regression. The sample size in this study was not large enough, even though it covered 5 products, 3 batches and 5 different antigen concentrations. To solve this problem all NIR spectra were used as calibration data set instead of dividing them into calibration and prediction data sets. Calibration models were built after different data pre-treatment procedures and assessed by segment cross validation (numbers of each segment is four, since there are four spectra for each sample). The models that considered the whole wavelength were rebuilt using significant X variables from Jack-knifing. Each pre-treatment performed differently and the corresponding results for the prediction are listed in Tab. 6.2.

Acceptable correlations (from 0.88 to 0.93, Tab.2) were obtained for each PLS model. This is an indication that PLS is a good tool that can extract spectral variations related to varying moisture levels. Spectral pre-treatments are preformed to remove the spectral noise and improve the performance of the calibration models. In this study, most pre-treatment methods applied (Tab. 6.2) improved the performance of the calibration models. NIR region 1900-1960 nm is still a good wavelength window for quantitative water analysis; even though there were no clear water band alterations in the spectra by visual inspection. The model based on this region was better than the model with the significant X variables from Jack-knifing, since less PLS factors were used. This is due to less noise in region 1900-1960 nm. Spectra should contain more information when spanning the entire NIR window, but also contain more noise. Thus, it requires more PLS factors to explain the data set.

Tab. 6.2 Calibration models built by PLS regression with different data pre-treatment methods based on the entire data set: MSC- multiplicative scatter correction; SNV- standard normal variate; EMSC- Extended multiplicative scatter correction; PLS factors- PLS components or factors; RMSEP- root mean square error of prediction

Wavelength window	Data Pre-treatment	Jack-knifing	Optimum PLS factors	Correlation	RMSEP (μg H_2O/vial)
Whole region	None	Yes	8	0.88	12.02
	Baseline correction	Yes	8	0.88	10.91
	MSC	Yes	10	0.89	11.73
	2^{nd} derivative	Yes	7	0.89	11.38
	SNV	Yes	8	0.88	12.00
	EMSC	Yes	6	0.93	8.83
	EMSC + 2^{nd} derivative	Yes	5	0.92	8.85
1900-1960	None	No	4	0.90	10.37
	EMSC	No	3	0.91	9.09
	2^{nd} derivative	No	2	0.90	10.20
	SNV	No	3	0.89	10.82
	Baseline	No	2	0.90	10.37
	Baseline + 2^{nd} derivative	No	5	0.88	11.31
	EMSC + 2^{nd} derivative	No	2	0.90	10.23

The best calibration model was obtained with second derivative data over region 1900-1960nm after removal of 4 outliers. The model has a RMSEP of 10.20 μg H_2O/vial with 2 PLS factors. The RMC correlation plot of the data set for the best EMSC model is given in Fig. 6.3. For this plot, a slope of 1 and an offset of 0 should be ideal. In this case, a slope of 1 and an offset of -3.83×10^{-7} were achieved. Correlation was 0.90 and the root mean square error of deviation (RMSED) was 9.94.

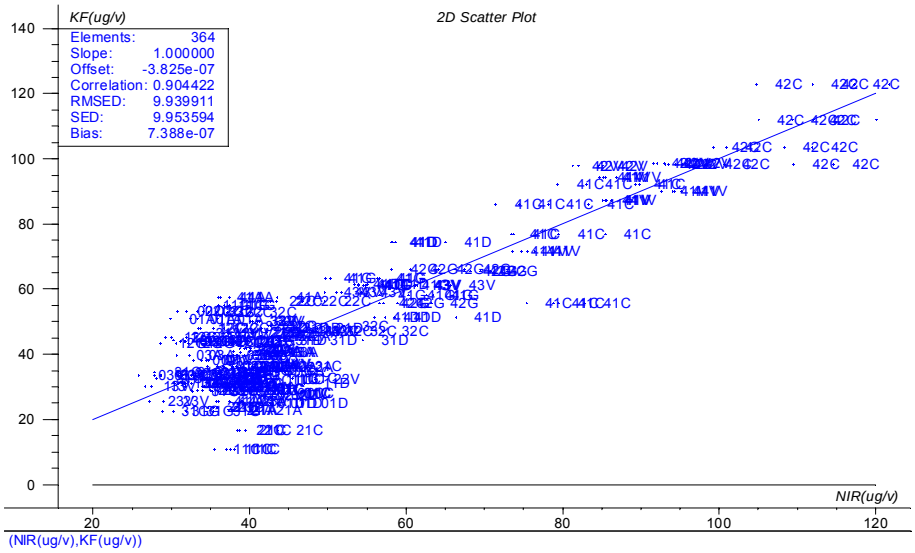

Fig. 6.3 The RMC correlation plot between NIR prediction and KF measurement: slope is 1; offset is -3.85×10^{-7}; correlation is 0.90; and RMSED is 9.94 µg/vial.

Tab. 6.3 Calibration models built by PLS regression with different data pre-treatment methods based on the reduced data set

Wavelength	Data pre-treatment	Jack-knifing	Optimum PLS factors	Correlation	RMSEP (µg H_2O/vial)
whole region	None	Yes	8	0.89	10.90
	EMSC	Yes	3	0.90	9.96
	2nd derivative	Yes	7	0.92	8.90
	EMSC + 2nd derivative	Yes	5	0.93	8.75
1990-1960	None	No	4	0.89	10.59
	EMSC	No	2	0.92	8.99
	2nd derivative	No	2	0.90	9.23
	EMSC + 2nd derivative	No	2	0.90	9.75

Four NIR spectra were recorded for each sample at different angles. These four spectra should yield same information, e. g. RMC, if the angle effect can be completely excluded. In this case the four spectra can be regarded as four replicates. Therefore, the four NIR spectra can be averaged to one spectrum for each sample. A total of 95 spectra for 95 samples were obtained in this case.

Calibration models were built on this reduced data set using different pre-treatments and assessed by full cross validation. The results are shown in Tab. 6.3. The best calibration model was obtained with EMSC data over 1900-1960 nm after removing 5 outliers. The model had a RMSEP of 8.99 µg H_2O/vial with 2 PLS factors. The RMC correlation plot of the reduced data set for this calibration model is presented in Fig. 6.4. This plot is slightly better than the one based on the entire data set because of the higher correlation (0.93) and lower RMESD (8.65).

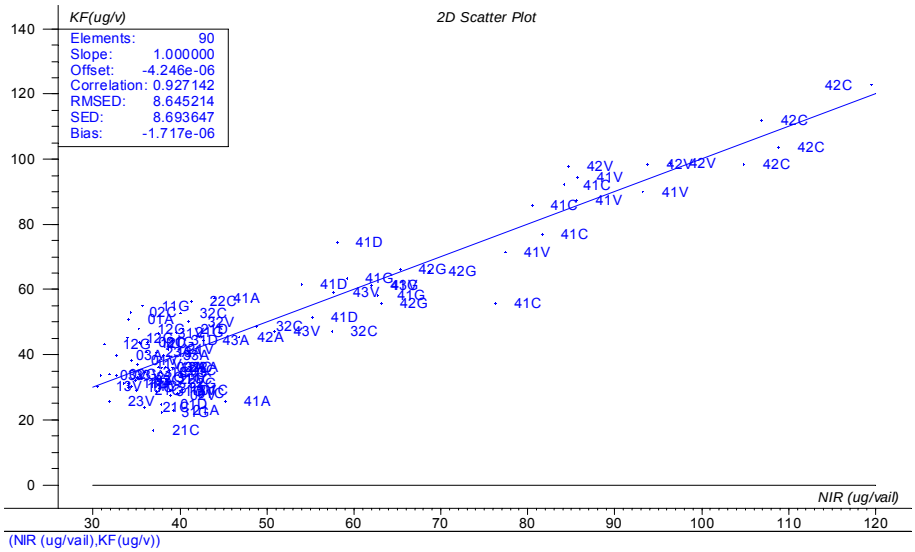

Fig. 6.4 The RMC correlation plot between NIR prediction and KF measurement base on reduced data set: slope is 1; offset is -4.25×10^{-6}; correlation is 0.92; and RMSED is 8.64 µg/vial.

The best model, which was based on the reduced data, did not differ significantly compared to the model with the original data set. This shows that the angle effect cannot be excluded, and these four spectra resulting from 4 different angles may therefore not represent the real information of the sample. This interference may, however, be removed with a sample spinner. A spinner rotates the sample during detection resulting in a truly average spectrum.

3.3 Product-specific calibration model for RMC

The multi-calibration model set included five different products; however, different protein antigens may interact with water in different ways affecting the final calibration model. To investigate the product-specific effect, calibration models were built for each product except Der, because the samples size (n=7) was too small. Calibration models were constructed on the reduced data set (the average spectrum of the four spectra resulting from four different angles for each sample) and assessed by full cross validation using different data pre-treatment methods in two wavelength

windows: whole wavelength and 1900-1960 nm. The results are shown in Appendix II.

Tab. 6.4 Comparison of multi-product models and product-specific models

Models	Optimum PLS factors	Correlation	RMSEP (μg H_2O/vial)	RMSEP (% w/w)
Multi-products model (all data set)	2	0.90	10.20	0.10
Multi- products model (reduced data set)	2	0.92	8.99	0.09
model for Cat (reduced data set)	2	0.95	8.66	0.09
model for Grass (reduced data set)	1	0.92	5.54	0.06
model for Ves (reduced data set)	2	0.97	6.66	0.07

Both EMSC and second derivative pre-treatment improved the performance of the calibration models for each product. Wavelength selection e.g. 1900-1960 nm, also benefits the models for Cat and Ves. The best calibration model for Cat is obtained with 2nd derivative data over the significant X variables in region of 1900-1960 nm. The model has a RMSEP of 8.86 μg H_2O/vial with 2 PLS factors. For Grass, the best calibration model is achieved with EMSC data over the significant X variables in the whole NIR region. The model possesses a RMSEP of 5.54 μg H_2O/vial with one PLS factor. The best model for Ves is gained with 2nd derivative data using the significant X variables in region of 1900-1960 nm. The model has a RMSEP of 6.66 μg H_2O/vial with 2 PLS factors. The RMC correlation plots of the calibration data sets for the best models are shown in Fig. 6.5.

For the Api mel product it was not possible to build an acceptable calibration model for the determination of RMC. This may be caused by the small sample size (n=16) and large batch effect (3 batches). Further investigations are acquired for this product.

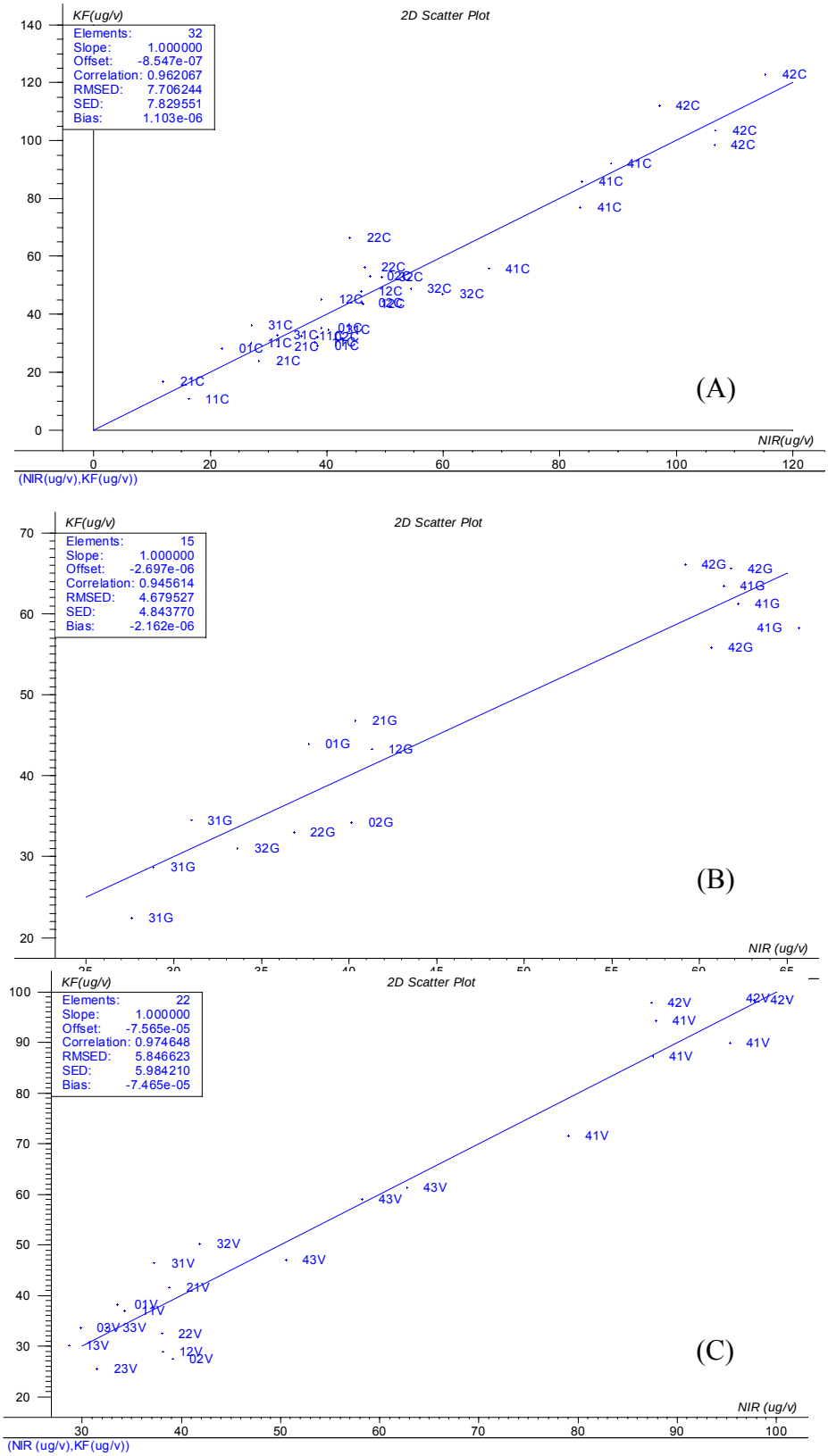

Fig. 6.5 The RMC correlation plot between NIR prediction and KF measurement based on reduced data set: (A) Cat: slope is 1; offset is -8.55×10^{-7}; correlation is 0.96; and RMSED is 7.70 µg/vial; (B) Grass: slope is 1; offset is -2.70×10^{-7}; correlation is 0.95; and RMSED is 4.68 µg/vial; (C) Ves: slope is 1; offset is -7.47×10^{-5}; correlation is 0.97; and RMSED is 5.85 µg/vial

For comparison, in Tab. 6.4, both the product-specific calibrations models and the multi-product models are outlined. The product-specific models are slightly better than the multi-product models;

however, the sample sizes in the current product-specific models are not large enough, because 100 samples is ideal in a training data set [19]. Thus, further investigations are required for the product-specific models. Nevertheless, a multi-product calibration model is more useful for routine analysis because of easy use.

4 Conclusion

This study for the first time demonstrates that NIR spectroscopy is reliable method for RMC prediction in lyophilized allergy vaccines. RMC results obtained from NIR spectroscopy show good agreement with results obtained by KF titration. The acceptable product-specific models and multi-product models indicate that NIR spectroscopy can be used as a quantitative method to determine RMC in lyophilized allergy vaccines. The models based on product-specific data are slightly better than models based on multi-product data; however, a general multi-product model is more useful, since one model can predict all samples in a pharmaceutical production of allergy vaccines.

Reference

1. Klibanov AM, Schefiliti JA. On the relationship between conformation and stability in solid pharmaceutical protein formulations. Biotechnology Letters, 2004; 26: 1103-1106.
2. Costantino HR, Griebenow K, Mishra P, Langer R, Klibanov AM. Fourier-transform infrared spectroscopic investigation of protein stability in the lyophilized form. Biochimica et Biophsica Acta, 1995; 1253: 69-74.
3. Schwendeman SP, Costantino HR, Gupta RK, Siber GR, Klibanov AM, Langer R. Stabilization of tetanus and diphtheria toxoids against moisture-induced aggregation. Applied Biological Sciences, 1995; 92: 11234-11238.
4. Food and Drug Administration. Guideline for the determination of residual moisture of residual moisture in dried biological products. Docket No. 89D-0140.
5. May JC, Del Grosso A, Etz N, Wheeler R, Rey L. Thermogravimetry and vapour pressure moisture. Application to determination of residual moisture in BCG vaccine. Journal of Thermal Analysis and Calorimetry, 2006; 83 (1): 31-33.
6. May JC, Del Grosso AV, Wheeler RM, Etz NM. TG/MS capillary interface. Applications to determination of residual moisture in BCG vaccine and other freeze-dried biological products. Journal of Thermal analysis, 1997; 49: 929-936.
7. Luck WAP. Structure of water and aqueous solution. Verlag Chemie-Physik, Weinheim, Germany, 1974: p248-284.
8. Büning-Pfaue H. Analysis of water in food by near infrared spectroscopy. Food Chemistry 2003; 82: 107-115.
9. Reich G. Near-infrared spectroscopy and imaging: Basic principle and pharmaceutical application. Advanced Drug Delivery Reviews, 2005: 1109-1143.
10. Bakeev KA. Near-infrared spectroscopy as a process analytical tool; Part II: at-line and on-line applications and implementation strategies. Spectroscopy 2004; 19: 39-42.
11. Lin TP, Hsu CC. Determination of residual moisture in lyophilized protein pharmaceuticals using a rapid and non-invasive method: near infrared spectroscopy. PDA Journal of Pharmaceuticals Science and Technology, 2001; 56:196-205.
12. Dziki X, Bauer JF, Szpylman JJ, Quick JE, Nichols BC. The use of near-infrared spectroscopy to monitor the mobility of water within the sarafloxacin crystal lattice, Journal of Pharmaceutical and Biomedical Analysis, 2000; 22: 829-848.

13. Blanco M, Coello J, Itirriaga H, Maspoch S, de la Pezuela C. Near-infrared spectroscopy in the pharmaceutical industry. Analyst 1998; 123: 135R-150R.
14. Zhou X, Hines P, Borer ME. Moisture determination in hygroscopic drug substances by near infrared spectroscopy, Journal of Pharmaceutical and Biomedical Analysis 1998; 17: 219-225.
15. Kamat MS, Lodder RA, DeLuca PP. Near-infrared spectroscopic determination of residual moisture in lyophilised sucrose through intact glass vials. Pharmaceutical Research, 1989; 6: 961-965.
16. Ciurczak EW, Torlini RP, Demkowicz MP. Determination of particle size of pharmaceutical raw materials using near-infrared reflectance spectroscopy. Spectroscopy, 1986; 1: 36-39.
17. Sukowski L. NIR based process analytical technology: In-line residual moisture determination for a complete batch inspection of lyophilized end-products. PhD thesis, University of Basel, Deutschland, 2003
18. Martens H, Nielsen JP, Engelsen SB. Light scattering and light absorbance separated by extended multiplicative signal correction application to near-infrared transmission analysis of powder mixtures. Analytical Chemistry, 2003; 75: 394-404.
19. Williams PC, Norris K. Variables affecting near-infrared spectroscopic analysis. In: Williams P, Norris K (Eds.), Near-infrared technology in the agricultural and food industries. American Association of Cereal Chemists, Inc. St. Paul, Minnesota, USA. 2001, p171-185.

Chapter VII: Classification and identification of lyophilized allergen vaccines by NIR spectroscopy

Abstract

In pharmaceutical production scenario quality control is essential to guarantee safety, efficacy and reproducibility of the products. However, there is no method which can meet all requirements in routine analysis. Near infrared spectroscopy combined with SIMCA as a rapid non-destructive tool to classify and identify allergy vaccines at different concentrations, different species and different batches has been demonstrated in this work. The results indicate that the highest concentration vaccines are successfully classified from low concentrations (100% at the level of 95% confidence) without the bee venom (api). Five different vaccine products at highest concentration are discriminated from each other by a SIMCA model. The classification of different batches may be possible for the highest concentrations vaccines. However, more experiments are required for low concentration samples and if many batches involved data. The results indicate that NIR spectroscopy can be applied as a rapid and non-destructive tool to classify and identify allergen vaccines.

1 Introduction

In a pharmaceutical production scenario, quality control is essential to guarantee safety, efficacy and reproducibility of products, as well as to document identity, potency, and quality. Quality control involves analysis of raw materials, intermediate productions, and final products [1], and thus, quality control is performed in different ways, and at different steps in the production as well as in careful analysis of final products [2]. In every case, a lot of random samples have to be withdrawn and analysed in order to control the production process in an optimal way [3]. Conventional quality control methods involve time-consuming, laborious, and costly procedures, and often also require reagents [4], which also needs to be controlled. It would be desirable to overcome these disadvantages by the introduction of new methods. The new technique should be sufficiently accurate and precise and without sample preparation, preferentially with simultaneous determination of several parameters in a single experiment; and it should be fast, efficient, and suitable for online or inline analysis [1]. Near infrared spectroscopy (NIR) is such a method.

NIR spectroscopy has many advantages over other analytical techniques. It offers many interesting applications in pharmaceutical research, production, and quality control, such as identification and qualification of raw materials, product quality control and process monitoring. Reich [5] recently reviewed the application of NIR in the pharmaceutical industry. NIR spectroscopy has played a significant role in quality control analysis to identify and classify the material [6-8]. NIR users have called this application ‘qualitative analysis’, ‘discriminant analysis’, ‘product identification’, ‘pattern recognition’, or other terms [6].

In our previous study, NIR was demonstrated to be an as a fast, non-invasive, and non-destructive method to determine the residual moisture content in lyophilized vaccines in Chapter VI. The advantages of NIR spectroscopy has been discussed as well. One great advantage of NIR is that a variety of information can be extracted from a same spectrum. Besides moisture content, the same spectrum contains information capable of classifying and identifying different vaccine products. Moreover, it is an easy way to provide information of the reproducibility from batch to batch. In the present work, we describe a simultaneous and rapid identification and classification assay for the determination of different species of allergy vaccines at different concentrations and different batches.

2 Materials and methods

2.1 Samples

Commercially available allergen vaccines (ALK-Abelló A/S, Denmark) used in this study

comprised the following species: bee venom (api), cat hair and dander (cat), house dust mite (der), grass pollen (grass), and wasp venom (vespula). A total of 665 random samples representing different concentrations and different batches were sued. Detailed information is given in Appendix C.

2.2 NIR measurement

All NIR measurements were carried out using a FT-NIR spectrometer (PerkinElmer Spectrum One, PerkinElmer) with an InGaAs detector. NIR spectra were recorded in the reflectance mode through the bottom of the intact glass vials at ambient temperature. Each spectrum was the average of 80 successive scans at 16 cm^{-1} resolution. The spectral region used for the data analyses was from 700 to 2500 nm, the data were measured in 1.67 nm intervals, which resulted in 1078 data points per spectrum. For each sample, four spectra were collected by rotating the vial at different angles. Therefore, a total of 2660 spectra were obtained.

2.3 Data analysis

Spectra were exported in ASCII format into The Unscrambler software, version 9.2 (CAMO, Oslo, Norway) for further analysis.

3 Results and discussion

3.1 Data pre-treatment

Since multivariate NIR spectral data contain huge numbers of X variables and because of the large sample set (665 samples), there is a need to reduce the number of X variables for relatively rapid analyses. An increase of the data interval to 8.35 nm result in each spectrum having 216 data points after reduction. The entire data set is randomly divided into a calibration set (training set) and a test set, with the calibration set being sufficiently large (532 samples) to detect unknown variation. The test data set (665 samples) is composed of the calibration set (532 samples) and other new samples (123 samples).

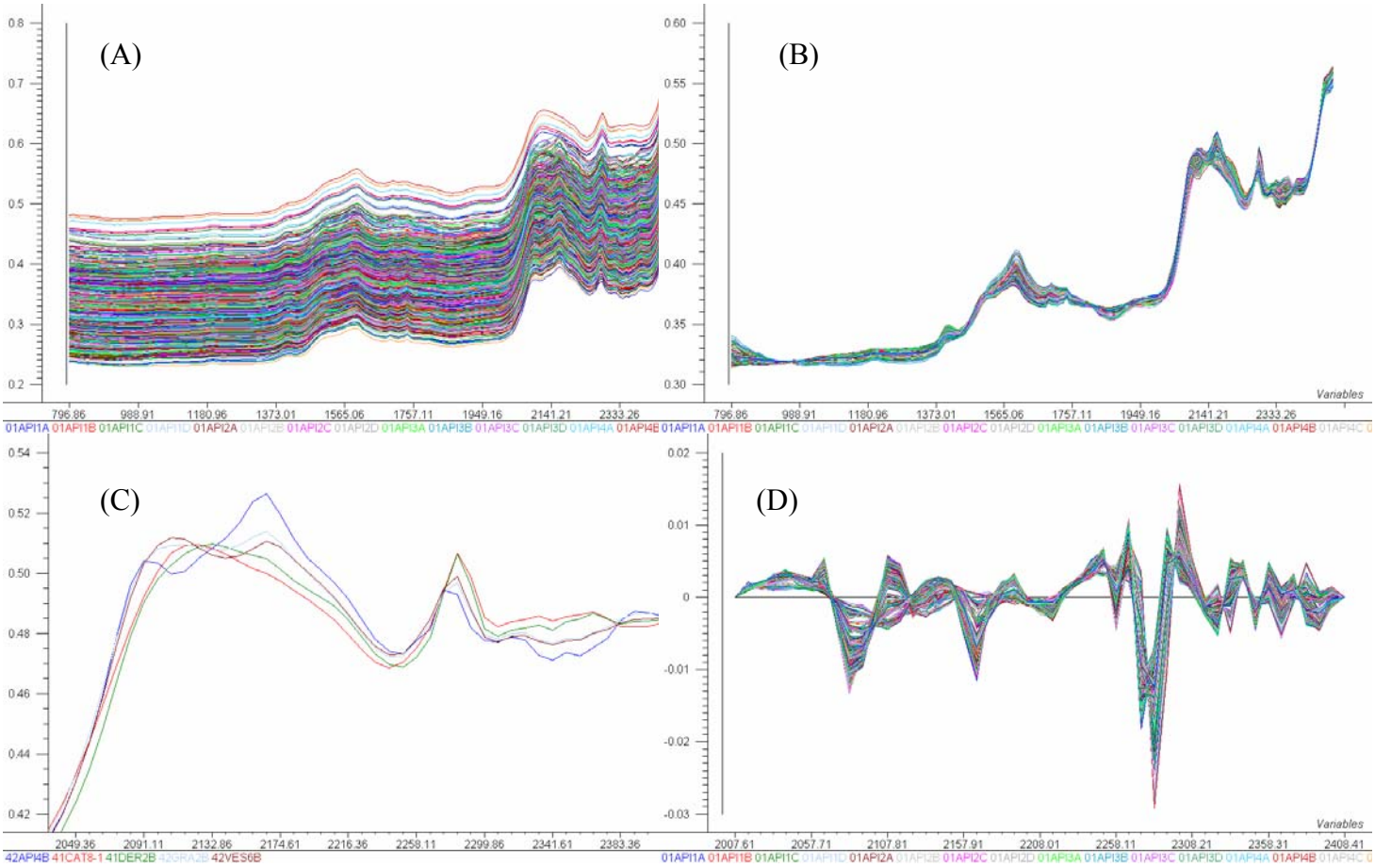

Fig 7.1 NIR spectra of five allergen vaccines: raw spectra (A); EMSC spectra (B); the mean EMSC spectra for each vaccine product at region 2000-2400 nm (C); EMSC 2nd derivative spectra at region 2000-2400 nm (D). X indicates wavelength (nm) and Y represents absorbance: $A = \log(1/R)$.

Raw NIR spectra often exhibit a baseline shift due to variation in the sample presentation and properties of the samples. Due to the small amount of sample (10 mg/vial), part of the NIR radiation passes through the sample cake and cannot be reflected back to the detector, which results in low NIR absorbance and baseline offsets (Fig. 7.1A). Other parameters can affect the spectra as well, such as particle size, density, vial variances, temperature, humidity, and the stability of the instrument. Different data pre-treatment methods are applied to remove the influence of light scattering. Among these methods, EMSC is effective to remove physical effects from the chemical information [9].

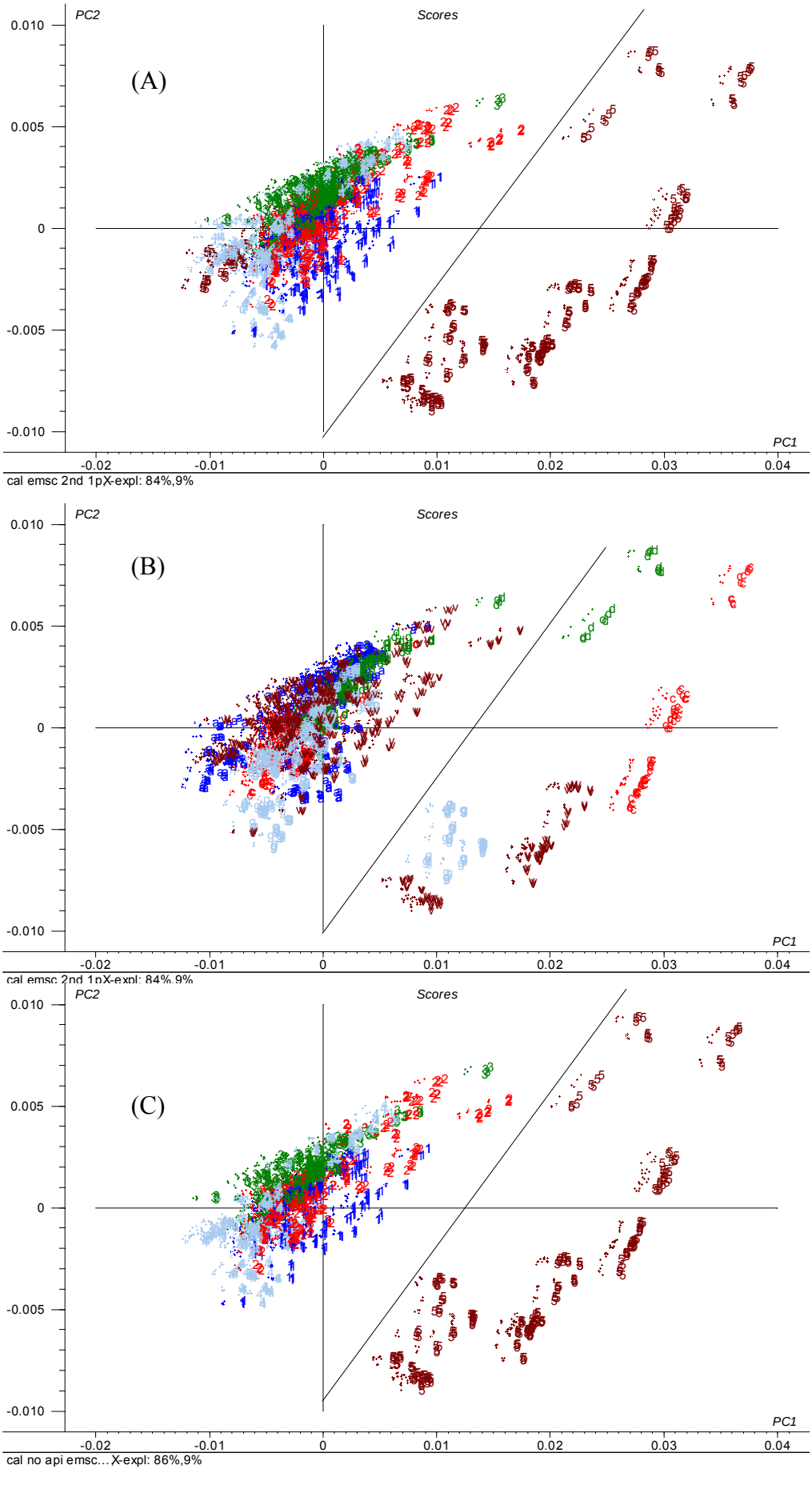

Fig. 7.2 PC1 and PC 2 score plots for the vaccine products: (A) Five products are grouped by different concentrations. 1—45 SQ; 2—450 SQ; 3—4,500 SQ; 4—45,000 SQ; and 5—450,000 ; (B) grouped by different species. a—api; c—cat; d—der; g—grass; and v—vespula; (C) Four products after removing api are grouped by different concentrations.

The spectra after EMSC pre-treatment are shown in Fig. 7.1B. Most light scattering interferences in the raw data are removed by the EMSC function. In Fig. 7.1C, the mean EMSC spectra of five different vaccines at the highest concentration are shown in the region from 2000 nm to 2400 nm. By inspection of these spectra, the shapes of the spectra are slight different from each other. It indicates that the classification of different vaccine products may be possible. The second derivative spectra are calculated using a segment of 3 points Savitsky-Golay function from 2000 nm to 2400 nm on the EMSC data, and are shown in Fig. 7.1D. After EMSC and second derivative correction, the spectral differences are more distinguishable.

3.2 Classification of different concentrations for vaccine products

Each vaccine product is represented in five different concentrations in this work, from 45 to 450,000 SQ with a 10 fold interval. A single principal component analysis (PCA) model for five products is constructed using the EMSC + 2^{nd} derivative data at wavelength region from 2007 to 2408 nm. This wavelength window contains much protein information. The PC1 and PC2 score plots are shown in Fig. 7.2. Samples are grouped by different concentrations in Fig. 7.2A, and the same plot is also showing grouping by different products in Fig. 7.2B. It is easily observed that the highest concentration (i.e. 450,000 SQ) is separated from the other four low concentrations, except for the api samples, where only two PCs are used. The first and second PC can explain 84% and 9% data variance, respectively. From the analysis of the score plots, it is evident that the PC1 promotes the separation of different concentrations. However, the api samples at 450,000 SQ are overlapping with low concentrations even though more PCs are used. Thus, the discrimination of api at 450,000 SQ from other products concentrations may be impossible when using one single PCA model. After excluding the api samples, a new PCA model was built for other four products. The score plot is given in Fig. 7.2C. All samples containing the highest concentrations are discriminated from the low concentrations by the PC1. The SIMCA model is constructed on two PCA models of highest concentration and low concentrations.

To verify the prediction ability of the SIMCA model, a test data set consisting of the calibration data and 73 new samples were predicted. The results showed almost 100% correct predication at a confidence level of 95% except a few outliers which were removed during the building of the PCA models. The predicting results in details are available in Appendix D.

Due to the complicated nature and heterogeneity of the data set (different species, concentrations and batches), the other low concentrations (e.g. < 450,000 SQ) cannot be distinguished with the use of one single PCA model. The classification of low concentrations may be possible if a PCA model

is built for each specified product. However, the classification using too many PCA models is troublesome in routine quality control.

3.3 Classification of different vaccines at the highest concentration

A single PCA model was constructed for five different kinds of vaccines at the highest concentration (i.e. 450,000 SQ) based on EMSC data at wavelength from 2007 to 2408 nm. The three dimensional score plot is shown in Fig. 7.3. The different vaccines were distinguished from each other. The PC1, PC2 and PC3 explain 79%, 12% and 5% data variance, respectively. It is observed that the api and vespula vaccines are not related in the score plot, even though both belong to the venom group of vaccines. This may indicate that the protein antigens in these two vaccines are not similar. The influence of excipients may also play a role. The batch to batch difference for vespula vaccine is quite clear: one batch is totally separated from the other two batches.

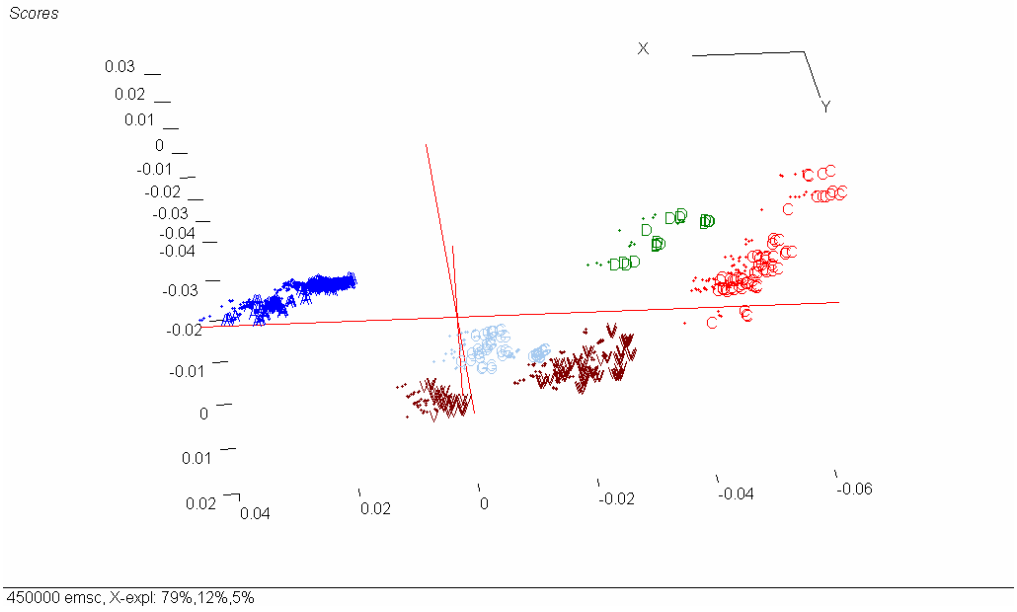

Fig. 7.3 The score plot of five different kinds of vaccines at concentration of 450,000 SQ. A—api; C—cat; D—der; G—grass; and V—vespula.

The SIMCA model was built on PCA models from each product. The predictions of the SIMCA model was verified by using a test data set containing the calibration data and the other new 18 samples. A hundred percent correct prediction results at a confidence level of 95% was obtained. Detailed information about the prediction is available in Appendix E.

3.4 Classification of different batches of the same vaccine product at different concentrations

One single model, which can predict different batch samples for all products, is not possible because the variables of concentration and species are more distinguishable in the data set. Therefore, the model for classifying different batches has to be built on specific products and specific concentrations. In the following section, PCA and SIMCA models are constructed for each product at each concentration except der vaccine since it only contains one batch samples.

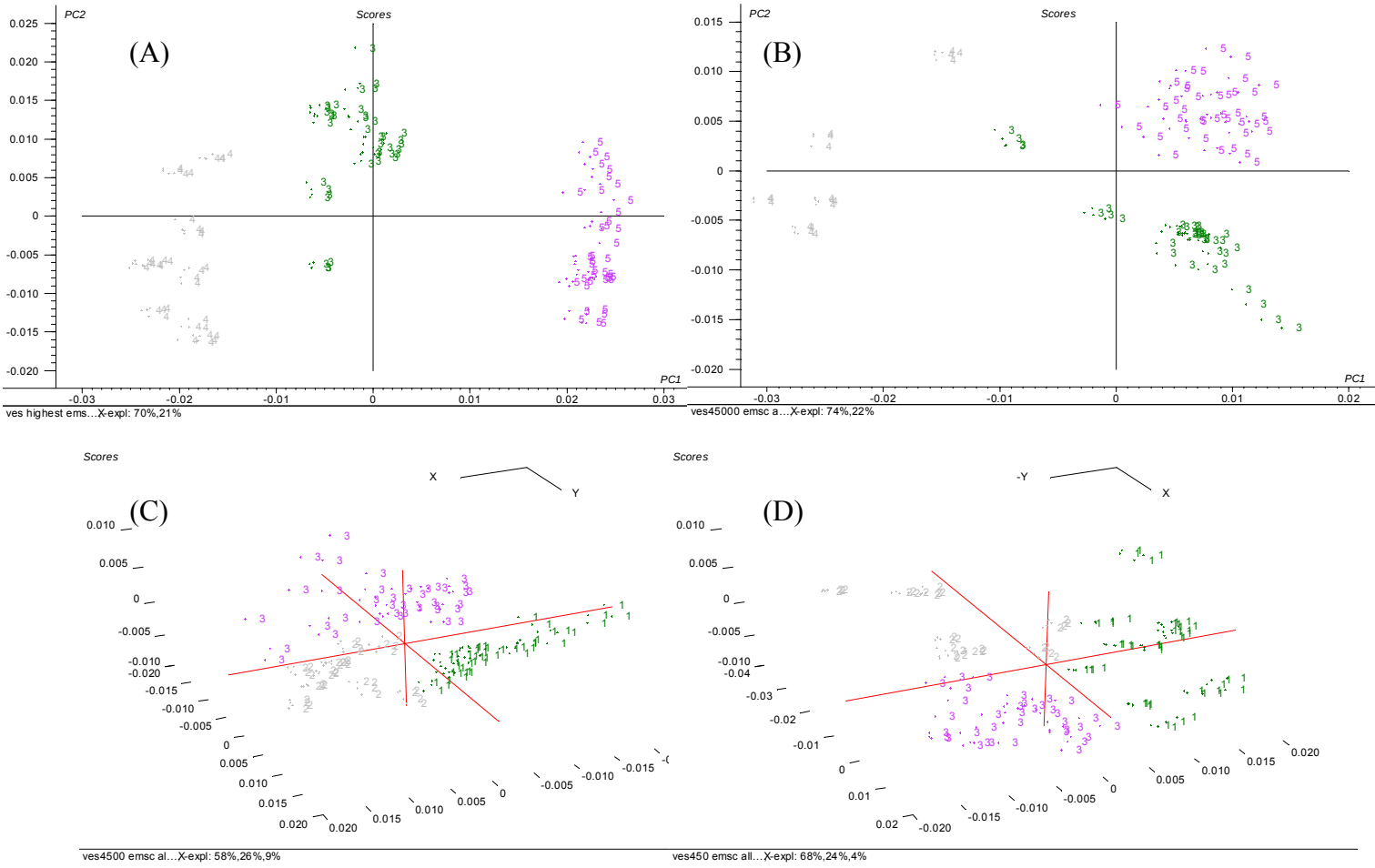

Fig. 7.4 The score plots of three batches of vespula vaccines. (A) 450,000 SQ; (B) 45,000 SQ: 3—0000031223-7; 4—0000040986-16; 5—0000052716-20 (C) 4,500 SQ; (D) 450 SQ: 1—0000031223-7; 2—0000040986-16; 3—0000052716-20

Classification of different batches for vespula vaccines

A PCA model was constructed for the vespula vaccine at concentration of 450,000 SQ using EMSC data after one outlier had been removed. The whole wavelength region was applied in this case,

since batch to batch difference not only results from the differences in the antigens, but the excipients play a more important role. Thus, wavelength selection (e.g. 2000-2400 nm) may not give a good calibration model. Fig. 7.4A shows the PC1 and PC2 score plot. It is observed that three different batch samples are separated from each other using two PCs. Since there are no influences from different species and concentrations, the batch variable has the largest data variance, and PC1 explains 70% data variance. PCA models for low concentrations (e.g. 45000, 4500 and 450 SQ) vespula vaccine were also built using EMSC data at the entire wavelength window. The PC1 and PC2 score plots are shown in Fig. 7.4. The three different batch samples are almost discriminated from each other.

The predictive ability of the SIMCA model of 450,000 and 45,000 SQ vespula was tested by data set consisting of the calibration set and 6 new samples, respectively. Almost 100% correct prediction results at a confidence level of 95% was obtained in both cases. The detailed information can be seen in Appendix F and Appendix G. However, the correct prediction for low concentrations of vespula (e.g. 45, 450 and 4500 SQ) decreases, since the samples are smiliar, even though different batches can be grouped in the score plots (Fig. 7.4C and Fig. 7.4D).

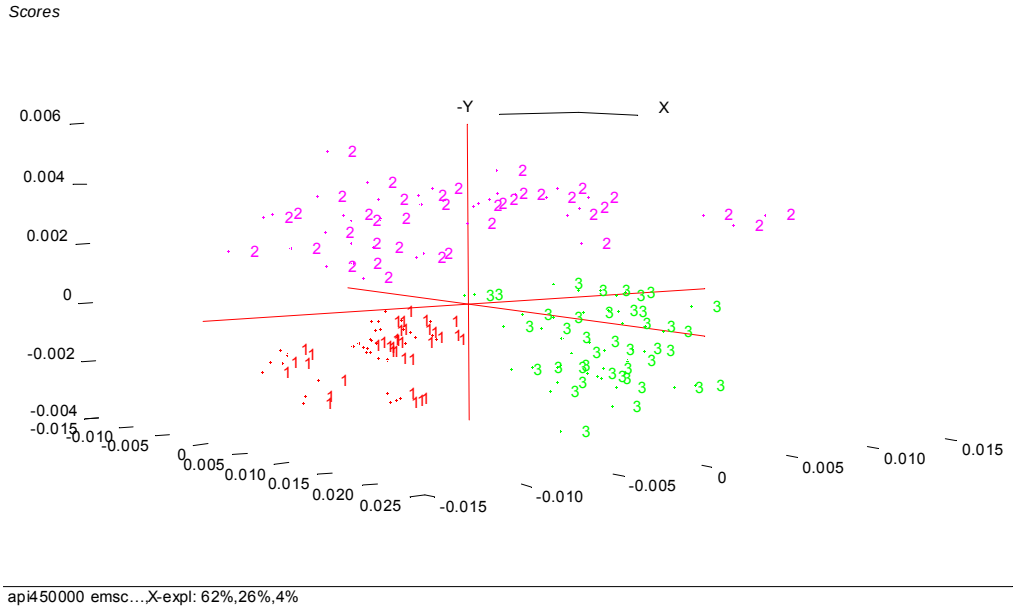

Fig. 7.5 The score plots of three batches of api vaccines at 450,000 SQ. 1—0000030417-21; 2—0000041728-849; 3—0000050932-7

Classification of different batches for api vaccines

A PCA model for api vaccine at 450,000 SQ was constructed using EMSC data at the whole wavelength window. The PC1 and PC2 score plot is shown in Fig. 7.5. Three batch samples are not overlapping after removal of outliers. PC1, PC2 and PC3 explain 62%, 26% and 4% of the variance

respectively. The classification of the SIMCA model is verified by the calibration data and 14 new samples. About 78.5% correct predication result is obtained at a confidence level of 95%. This is an indication that the variable from batch to batch is not so clearly distinguishable in t this case. The detailed information is available in Appendix H. For the low concentration (< 450,000 SQ) api vaccine, the classification for each batch is not possible because of the similarity of the samples.

Classification of different batches for cat vaccines

PCA models were built for cat vaccines for each concentration using EMSC data at the whole wavelength region after removal of a few outliers. The PC1 and PC2 score plots are shown in Fig. 7.6. Two batches were discriminated by PC1 for all five concentrations. Correct predictions results at 95% confidence level were gained for all SIMCA models which were tested using new test set. The detailed results are given in Appendix I to Appendix M.

Classification of different batches for grass vaccines

PCA models of the grass vaccine were constructed for each concentration using EMSC data at whole wavelength window after removal of outliers. The two batches at each concentration were well separated in PC1 and PC2 score plots (Fig. 7.7.), except for the concentration of 4,500 SQ (Fig. 7.7C) which is given in the PC1 versus PC3 plots. PC1 explains most data variance resulting from batch to batch difference. The prediction ability of the SIMCA models is tested using a test date set including calibration data and new samples. The results show correct predictions at a confidence of 95%. The predicted results are shown in Appendix N to Appendix R.

For batch classification, when many batches are involved, the heterogeneity and complexity of the data set will increase, and this may reduce the reliability of the classification. More experiments are required to address this question. On the other hands, batch differences do not constitute a big problem for the allergen vaccines.

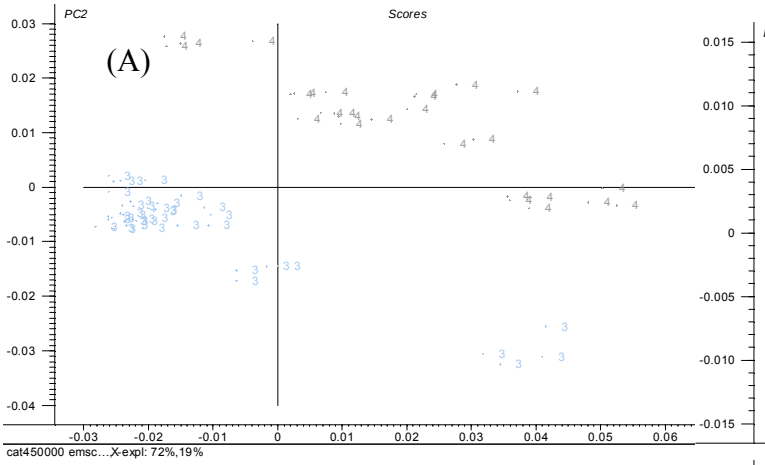

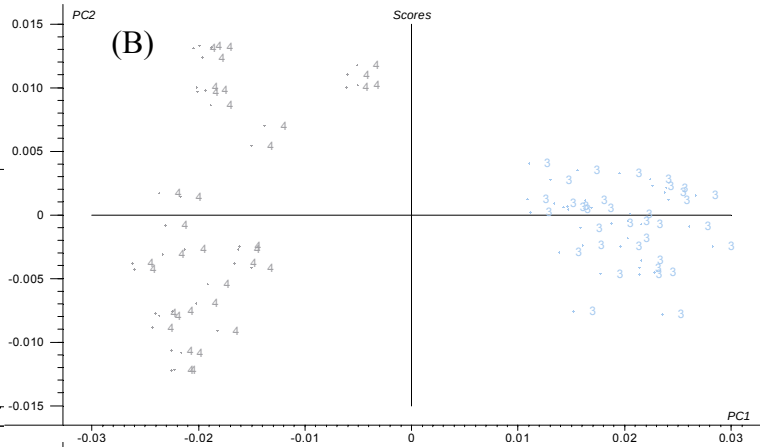

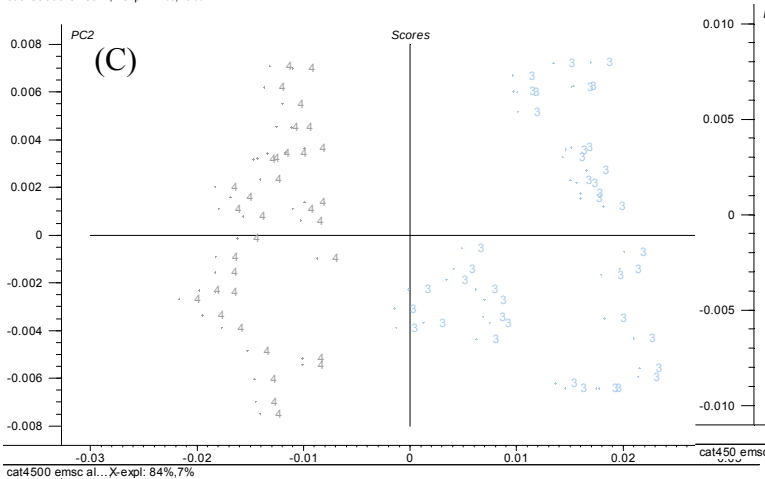

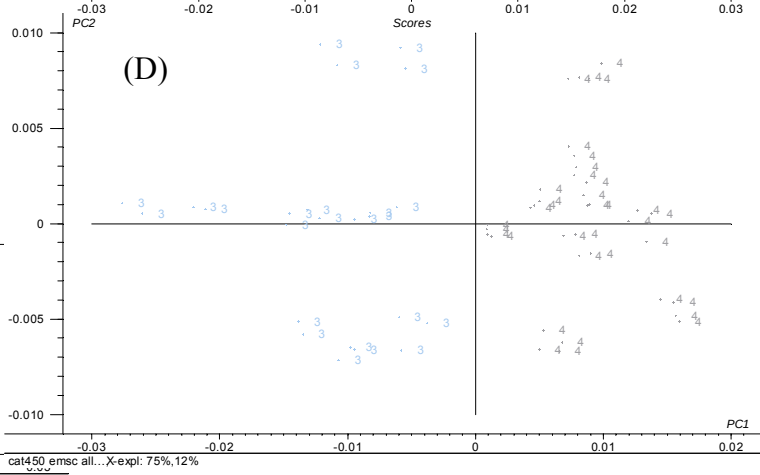

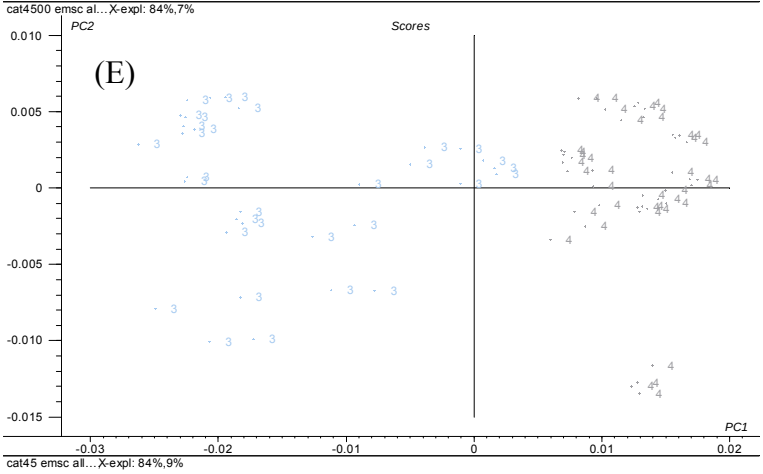

Fig. 7.6 The score plots of two batches of cat vaccines. (A) 450,000 SQ; (B) 45,000 SQ; (C) 4,500 SQ; (D) 450 SQ; (E) 45 SQ; 3—0000032114-9; 4—0000045531-5

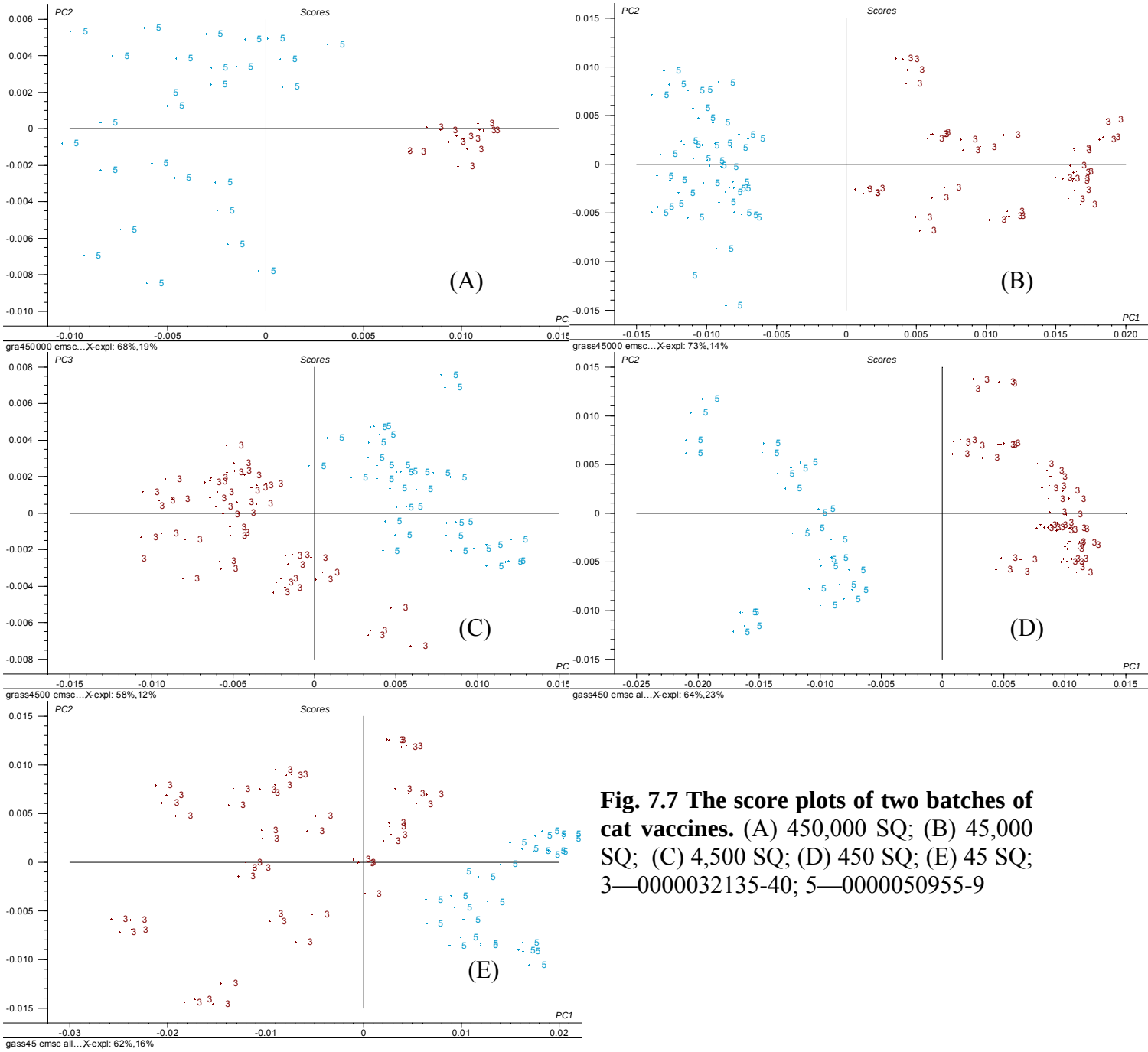

Fig. 7.7 The score plots of two batches of cat vaccines. (A) 450,000 SQ; (B) 45,000 SQ; (C) 4,500 SQ; (D) 450 SQ; (E) 45 SQ; 3—0000032135-40; 5—0000050955-9

4 Conclusion

The potential of NIR spectroscopy and SIMCA as a rapid non-destructive tool to classify and identify allergy vaccines at different concentrations, different species and different batches has been demonstrated in this work. The results indicate that for the highest concentration of vaccines, a successful classification can be preformed from low concentrations (100% at the level of 95% confidence), with the exception of the api samples. Five different vaccine products at the highest

concentration were discriminated from each other by a SIMCA model. The classification of different batches is possible when products at high concentrations are analyzed. However, more experiments are required for the low concentration samples and for analysis including many batches. The results indicate that NIR spectroscopy can be applied as a rapid and non-destructive tool to classify and identify allergy vaccines. If implemented this technique will increases the efficiency and decreases the costs of the quality control procedures in the allergy vaccine manufacturing industry.

Reference

1. Blanco M, Eustaquio A, González JM, Serrano D. Identification and quantitation assays for intact tablets of two related pharmaceutical preparations by reflectance near-infrared spectroscopy: validation of the procedure. Journal of Pharmaceutical and Biomedical Analysis, 2000; 22: 139-148.
2. Sanchez MS, Bertran E, Sarabia LA, Ortiz MC, Blanco M, Coello J. Quality control decisions with near infrared data. Chemometrics and Intelligent Laboratory Systems, 2002; 53: 69-80.
3. Herkert T, Prinz H, Kovar KA. One hundred percent online identity check of pharmaceutical products by near-infrared spectroscopy on the packaging line. European Journal of Pharmaceutics and Biopharmaceutics, 2001; 51: 9-16.
4. Cozzolino D, Chree A, Scaife JR, Murray I. Usefulness of Near-infrared reflectance (NIR) spectroscopy and chemometrics to discriminate fishmeal batches made with different fish species. Journal of Agriculture and Food Chemistry, 2005; 53: 4459-4463.
5. Reich G. Near-infrared spectroscopy and imaging: Basic principle and pharmaceutical application. Advanced Drug Delivery Reviews, 2005: 1109-1143.
6. Mark H. Qualitative near-infrared analysis. In: Williams P, Norris K (Eds.). Near-infrared technology in the agricultural and food industries. American Association of Cereal Chemists, Inc. St. Paul, Minnesota, USA 2001, p233-238.
7. Siesler HW, Ozaki Y, Kawata S, Heise HM (Eds.). Near-infrared spectroscopy—principles, instruments, applications. Wiley-VCH, Weinheim Germany 2002, p2.
8. Bran & Luebbe GmbH. Near infrared spectroscopy for pharmaceuticals validation. Pharmaceutical Manufacturing Review, 1999, 11: 10-11.
9. Martens H, Nielsen JP, Engelsen SB. Light scattering and light absorbance separated by extended multiplicative signal correction application to near-infrared transmission analysis of powder mixtures. Analytical Chemistry, 2003; 75: 394-404.

Chapter VIII: Conclusions and perspectives

Vaccine has had greatest impact on the world's health. It prevents disease and death for millions of individual every year. For allergic diseases, SIT is the only treatment that may affect the course and it also may prevent the development of asthma in patients with allergic rhinitis. A successful SIT is dependent on the use of high quality allergen vaccines that are properly standardized and can be manufactured consistently. Allergen vaccines are produced by adsorption antigens onto ACA to accelerate and prolong the specific immune response towards the desired response. To well understand antigens and vaccines and to produce high quality vaccines and manufacture consistently, this study focuses on the structures of model antigens when they are adsorbed by aluminium hydroxide and when they are subsequently released. In relation this, the mechanism of ACA is also discussed. The stability of vaccines is investigated during storage and under different temperatures. A fast, non-destructive method is introduced for determining the residual moisture content and classification of lyophilized allergy vaccines as well.

In **chapter I**, the background and purposes of the thesis are presented. The brief introductions to NIR, MIR and MVA which are the core technologies in this work are presented. **Chapter II** reviews the protein structures and the current methods for protein structural analysis. The advantages and disadvantages of the methods are presented in addition to whether they are suitable for adsorbed protein analysis, e.g., protein adsorbed by aluminium hydroxide. The technology is especially focused on FTIR-ATR spectroscopy.

The results summarized in **chapter III** suggest that FTIR-ATR spectroscopy provides direct information on the secondary structural changes of the model antigens when adsorbed to aluminium hydroxide and subsequently release. It is shown that the secondary structures of protein antigens change when adsorbed by aluminium hydroxide. The adsorption-induced protein structural changes depend on how much protein is adsorbed by aluminium hydroxide. Maximal adsorption (e.g. achieving adsorption capacity) gives a more native-like structure than low protein adsorption. However, Less protein adsorbed may result in a stronger immune response, since the protein structure becomes more denatural and this modified structure is more easily presented to the immune system. According to Jones *et al.*, protein structure became destabilized upon adsorption by aluminium adjuvant. The physical changes of adsorbed antigens made them more susceptible to proteolytic processing by the immune system, resulting in an enhanced antigen presentation. This may be the reason why different amounts of antigens adsorbed onto same amount aluminium

hydroxide show similar immune response. PBS is a good buffer to release adsorbed protein antigens from aluminium adjuvant. The current experiments showed that recovery is approximate 80% after 40 min in PBS. The released antigens generally refold to their native state. However, released BSA regains its native structure more completely than does BLG.

In **chapter IV**, the structural stability of aluminium-adsorbed model antigens is compared to the antigens in solutions. This study has shown that the structure of an antigen can be stabilized by adsorption onto aluminium hydroxide during exposure to high temperature and/or during storage. It may be one of the reasons why adjuvant can enhance the immune response and/or exert its activities. This phenomenon of structural stabilization is more obvious for BSA than BLG, which may be ascribed to the low protein concentration of BLG. Another explanation is that it may be that there is more free protein which is not adsorbed onto aluminium hydroxide in the BLG model vaccines. The free protein antigens may facilitate the degradation of vaccine, but further experiments are required to confirm this hypothesis.

The changes of model vaccines during the storage at normal vaccine storage temperature and an elevated temperature are systematically monitored see **chapter V**. The data show that the pre-adsorbed antigens are difficult to release from the adjuvant during the storage. It may indicate why vaccine loses or decreases potency during storage. The protein adsorption and pH of vaccine also change during storage, and these two parameters are protein specific. Model vaccines generally undergo rapid modifications with the time upon storage at 37 ºC. Similar changes are seen upon storage at 4 ºC, although at a slower rate. NIR spectroscopy is for the first time used to monitor the aging of vaccine. The results suggest that it is possible to detect the changes of adsorption/desorption of protein antigens, but it is difficult to determine the change of particle size during vaccine storage, even though analyzing the particle size of aluminium adjuvants may be practical. Both BSA and BLG model vaccines as well as aluminium hydroxide are profoundly affected by rotation. Vigorous rotation increases the particle size of aluminium hydroxide and may denature protein antigens. Thus, it should be minimised in vaccine productions.

A general ability of NIR spectroscopy combined with multivariate data analysis to predict RMC for lyophilized vaccines is conducted in **chapter VI**. RMC results obtained from NIR spectroscopy show good agreement with results from KF titration. The acceptable product-specific models and multi-product models indicate that NIR spectroscopy can be used as a quantitative method to determine RMC in lyophilized allergy vaccines. The models based on product-specific data are slightly better than models based on multi-product data; however, a general multi-product model is

more useful, since one model can predict all samples in a pharmaceutical production of allergy vaccines. However, the current models have to be revalidated by new unknown data in the future study.

In **chapter VII**, NIR spectroscopy is applied to classify and identify allergen vaccines at different concentrations, different species and different batches. The vaccines with highest concentration antigens are successfully classified from low concentrations (100% at the level of 95% confidence) without the api samples. Five different vaccine products at the highest concentration are successfully discriminated from each other by a SIMCA model. The classification of different batch is possible for products which are at high concentrations antigens. However, more experiments are required in the future study for low concentration samples and for many batches involved. The results indicate that NIR spectroscopy can be applied as a rapid and non-destructive tool to classify and identify allergy vaccines. If implemented this technique will increases the efficiency and decreases the costs of the quality control procedures in the allergy vaccine manufacturing industry.

Appendices

Appendix A in Chapter VI

The RMC of the calibration samples by KF: The data were used as reference data for calibration models

	vaccines	Concentration of allergy (SQ-U)	Batch No.	KF (µg/vial)
01API06B	api	45	30417	50.9
02API10B	api	45	41849	36.3
03API04B	api	45	50938	39.7
11API04B	api	450	30418	31.1
12API04B	api	450	41848	36
13API05B	api	450	50937	40.6
21API01B	api	4,500	30419	22.9
22API01B	api	4,500	41730	36
23API06B	api	4,500	50934	40.9
31API05B	api	45,000	30420	29.7
33API01B	api	45,000	50933	39.7
41API08B	api	450,000	30421	57.5
41API17B	api	450,000	30421	25.7
42API01B	api	450,000	41728	45.4
42API07B	api	450,000	41728	70.7
43API05B	api	450,000	50932	44.3
01CAT11B	cat	45	32119	28
01CAT19B	cat	45	32119	29.2
01CAT20B	cat	45	32119	35.2
02CAT02B	cat	45	45535	53
02CAT04B	cat	45	45535	32.3
02CAT08B	cat	45	45535	43.8
11CAT05B	cat	450	32118	30.4
11CAT08B	cat	450	32118	10.8
11CAT16B	cat	450	32118	30.1
11CAT21B	cat	450	32118	32.4
12CAT04B	cat	450	45534	47.8
12CAT08B	cat	450	45534	45.1
12CAT10B	cat	450	45534	43.5
21CAT01B	cat	4,500	32117	23.8
21CAT02B	cat	4,500	32117	29
21CAT07B	cat	4,500	32117	16.8
22CAT02B	cat	4,500	45533	56.3
22CAT05B	cat	4,500	45533	66.4
22CAT06B	cat	4,500	45533	73
31CAT01B	cat	45,000	32116	34.7
31CAT03B	cat	45,000	32116	36.3
31CAT09B	cat	45,000	32116	32.7
32CAT03B	cat	45,000	45532	47
32CAT05B	cat	45,000	45532	52.9
32CAT07B	cat	45,000	45532	48.7
41CAT01B	cat	450,000	32115	55.7
41CAT02B	cat	450,000	32115	92.1
41CAT04B	cat	450,000	32115	85.8

41CAT07B	cat	450,000	32115	77
42CAT01B	cat	450,000	45531	122.7
42CAT02B	cat	450,000	45531	98.4
42CAT03B	cat	450,000	45531	112
42CAT06B	cat	450,000	45531	103.5
01DER16B	der	45	30016	24.9
11DER23B	der	450	30019	31.1
21DER08B	der	4,500	30021	48
31DER02B	der	45,000	30023	44.3
41DER01B	der	450,000	30025	74.4
41DER02B	der	450,000	30025	61.5
41DER03B	der	450,000	30025	51.4
01GRA08B	grass	45	32140	43.9
02GRA03B	grass	45	50959	34.2
11GRA06B	grass	450	32138	55
12GRA03B	grass	450	50958	43.3
21GRA12B	grass	4,500	32137	46.8
22GRA04B	grass	4,500	50957	33
31GRA01B	grass	45,000	32136	34.5
31GRA09B	grass	45,000	32136	28.7
31GRA11B	grass	45,000	32136	22.4
32GRA06B	grass	45,000	50956	31
41GRA04B	grass	450,000	32135	58.2
41GRA07B	grass	450,000	32135	61.2
41GRA09B	grass	450,000	32135	63.5
42GRA03B	grass	450,000	50955	55.8
42GRA06B	grass	450,000	50955	66.1
42GRA07B	grass	450,000	50955	65.6
01VES09B	ves	45	31227	38.2
02VES05B	ves	45	41633	27.6
03VES02B	ves	45	52720	33.6
11VES01B	ves	450	31226	37
12VES10B	ves	450	41632	29
13VES09B	ves	450	52719	30.2
21VES07B	ves	4,500	31225	41.6
22VES02B	ves	4,500	41631	32.5
23VES09B	ves	4,500	52718	25.6
31VES04B	ves	45,000	31224	46.5
32VES03B	ves	45,000	41628	50.2
33VES10B	ves	45,000	52717	33.6
41VES03B	ves	450,000	31223	71.5
41VES05B	ves	450,000	31223	87.2
41VES08B	ves	450,000	31223	89.9
41VES11B	ves	450,000	31223	94.4
42VES01B	ves	450,000	40986	97.9
42VES03B	ves	450,000	40986	98.4
42VES06B	ves	450,000	40986	98.7
42VES07B	ves	450,000	40986	151
43VES03B	ves	450,000	52716	47
43VES06B	ves	450,000	52716	59
43VES09B	ves	450,000	52716	61.3

Appendix B in chapter VI

The results of calibration models for each vaccine product: PLS regression with different data pre-treatments and different wavelength windows.

Product	Samples	Wavelength	Data pretreatment	Jack-knifing	Optimum PCs	Correlation	RMSEP
Cat	33	Whole region	None	No	4	0.91	11.85
		Whole region	None	Yes	3	0.91	11.63
		1900-1960	None	No	4	0.93	10.45
		1900-1960	None	Yes	4	0.95	9.20
		Whole region	2nd derivative	No	2	0.91	11.63
		Whole region	2nd derivative	Yes	2	0.91	11.57
		1900-1960	2nd derivative	No	2	0.94	9.78
		1900-1960	2nd derivative	Yes	2	0.95	8.86
		Whole region	EMSC	No	2	0.94	9.73
		Whole region	EMSC	Yes	1	0.94	9.96
		1900-1960	EMSC	No	4	0.92	10.93
		1900-1960	EMSC	Yes	4	0.93	10.31
Grass	16	Whole region	None	No	5	0.93	5.50
		Whole region	None	Yes	4	0.92	5.62
		1900-1960	None	No	4	0.87	7.06
		1900-1960	None	Yes	4	0.88	6.99
		Whole region	2nd derivative	No	1	0.92	5.71
		Whole region	2nd derivative	Yes	1	0.92	5.79
		1900-1960	2nd derivative	No	1	0.89	6.34
		1900-1960	2nd derivative	Yes	1	0.90	6.35
		Whole region	EMSC	No	1	0.92	5.77
		Whole region	EMSC	Yes	1	0.92	5.54
		1900-1960	EMSC	No	4	0.92	5.80
		1900-1960	EMSC	Yes	3	0.90	6.63
Ves	23	Whole region	None	No	12	0.97	6.90
		Whole region	None	Yes	10	0.96	7.66
		1900-1960	None	No	6	0.97	6.42
		1900-1960	None	Yes	1	0.38	24.44
		Whole region	2nd derivative	No	6	0.95	7.84
		Whole region	2nd derivative	Yes	4	0.96	6.83
		1900-1960	2nd derivative	No	2	0.96	6.89
		1900-1960	2nd derivative	Yes	1	0.96	6.96

		derivative				
	Whole region	EMSC	No	5	0.94	8.82
	Whole region	EMSC	Yes	3	0.94	9.23
	1900-1960	EMSC	No	3	0.97	6.67
	1900-1960	EMSC	Yes	2	0.97	6.66

Appendix C in chapter VII

Data set description of the sample collection

Vaccine products	Concentrations (SQ)	Number of batches	Number of vials or samples (total 665)
api	45	3	42
	450	3	39
	4,500	3	41
	45,000	2	30
	450,000	3	44
cat	45	2	21
	450	2	16
	4,500	2	24
	45,000	2	20
	450,000	2	17
der	45	1	17
	450	1	16
	4,500	1	15
	45,000	1	16
	450,000	1	4
grass	45	2	26
	450	2	26
	4,500	2	27
	45,000	2	23
	450,000	2	11
vespula	45	3	42
	450	3	40
	4,500	3	41
	45,000	3	31
	450,000	3	36

Appendix D in chapter VII

Classification of highest concentration (450,000 SQ) vaccines from low concentrations

H = 450,000 SQ and L < 450,000SQ (SIMCA results at 95% confidence level).

Sample	H	L	450 cat		*	4500 cat		*	cat 450000	*	
45 cat		*	450 cat		*	4500 cat		*	cat 450000	*	
45 cat		*	450 cat		*	4500 cat		*	cat 450000	*	
45 cat		*	450 cat		*	4500 cat		*	cat 450000	*	
45 cat		*	450 cat		*	4500 cat		*	cat 450000	*	
45 cat		*	450 cat		*	4500 cat		*	cat 450000	*	
45 cat		*	450 cat		*	4500 cat		*	cat 450000	*	
45 cat		*	450 cat		*	45000 cat			cat 450000	*	
45 cat		*	450 cat		*	45000 cat		*	cat 450000	*	
45 cat		*	450 cat		*	45000 cat		*	cat 450000	*	
45 cat		*	450 cat		*	45000 cat			cat 450000	*	
45 cat		*	450 cat		*	45000 cat		*	cat 450000	*	
45 cat		*	450 cat		*	45000 cat		*	cat 450000	*	
45 cat		*	450 cat		*	45000 cat		*	cat 450000	*	
45 cat		*	4500 cat		*	45000 cat		*	cat 450000	*	
45 cat		*	4500 cat		*	45000 cat			cat 450000	*	
45 cat		*	4500 cat		*	45000 cat		*	cat 450000	*	
45 cat		*	4500 cat		*	45000 cat			cat 450000	*	
45 cat		*	4500 cat		*	45000 cat			cat 450000	*	
45 cat		*	4500 cat		*	45000 cat		*	cat 450000	*	
45 cat		*	4500 cat		*	45000 cat		*	cat 450000	*	
45 cat		*	4500 cat		*	45000 cat		*	cat 450000	*	
45 cat		*	4500 cat		*	45000 cat		*	cat 450000	*	
45 cat		*	4500 cat		*	45000 cat		*	cat 450000	*	
45 cat		*	4500 cat		*	45000 cat		*	cat 450000	*	
45 cat		*	4500 cat		*	45000 cat		*	cat 450000	*	
45 cat		*	4500 cat		*	45000 cat		*	cat 450000	*	
45 cat		*	4500 cat		*	45000 cat		*	cat 450000	*	
45 cat		*	4500 cat		*	45000 cat		*	cat 450000	*	
45 cat		*	4500 cat		*	45000 cat		*	cat 450000	*	
45 cat		*	4500 cat		*	45000 cat			cat 450000	*	
45 cat		*	4500 cat		*	45000 cat		*	cat 450000	*	
45 cat		*	4500 cat		*	45000 cat		*	cat 450000	*	
45 cat		*	4500 cat		*	45000 cat		*	cat 450000	*	
45 cat		*	4500 cat		*	45000 cat		*	cat 450000	*	
45 cat		*	4500 cat		*	45000 cat		*	cat 450000	*	
45 cat		*	4500 cat		*	45000 cat		*	45 cat		*
450 cat		*	4500 cat		*	45000 cat		*	45 cat		*
450 cat		*	4500 cat		*	45000 cat		*	45 cat		*
450 cat		*	4500 cat		*	45000 cat		*	45 cat		*
450 cat		*	4500 cat		*	45000 cat		*	45 cat		*
450 cat		*	4500 cat		*	45000 cat		*	45 cat		*
450 cat		*	4500 cat		*	45000 cat		*	45 cat		*
450 cat		*	4500 cat		*	cat 450000	*		45 cat		*
450 cat		*	4500 cat		*	cat 450000	*		45 cat		*
450 cat		*	4500 cat		*	cat 450000	*		45 cat		*
450 cat		*	4500 cat		*	cat 450000	*		45 cat		*

45 cat		*
45 cat		*
45 cat		*
45 cat		*
45 cat		*
45 cat		*
45 cat		*
45 cat		*
45 cat		*
45 cat		*
45 cat		*
45 cat		*
45 cat		*
45 cat		*
45 cat		*
45 cat		*
45 cat		*
45 cat		*
45 cat		*
45 cat		*
45 cat		*
45 cat		*
45 cat		*
45 cat		*
45 cat		*
45 cat		*
45 cat		*
45 cat		*
45 cat		*
450 cat		*
450 cat		*
450 cat		*
450 cat		*
450 cat		*
450 cat		*
450 cat		*
450 cat		*
450 cat		*
450 cat		*
450 cat		*
450 cat		*
450 cat		*
450 cat		*
450 cat		*
450 cat		*
450 cat		*
450 cat		*
450 cat		*
450 cat		*
450 cat		*

450 cat		*
450 cat		*
450 cat		*
450 cat		*
450 cat		*
450 cat		*
450 cat		*
450 cat		*
450 cat		*
450 cat		*
450 cat		*
450 cat		*
450 cat		*
450 cat		*
450 cat		*
4500 cat		*
4500 cat		*
4500 cat		*
4500 cat		*
4500 cat		*
4500 cat		*
4500 cat		*
4500 cat		*
4500 cat		*
4500 cat		*
4500 cat		*
4500 cat		*
4500 cat		*
4500 cat		*
4500 cat		*
4500 cat		*
4500 cat		*
4500 cat		*
4500 cat		*
4500 cat		*
4500 cat		*
4500 cat		*
4500 cat		*
4500 cat		*
4500 cat		*
4500 cat		*
4500 cat		*
4500 cat		*
4500 cat		*
4500 cat		*
4500 cat		*
4500 cat		*
4500 cat		*
4500 cat		*
4500 cat		*

4500 cat		*
4500 cat		*
4500 cat		*
4500 cat		*
4500 cat		*
45000 cat		*
45000 cat		*
45000 cat		*
45000 cat		*
45000 cat		*
45000 cat		*
45000 cat		*
45000 cat		*
45000 cat		*
45000 cat		*
45000 cat		*
45000 cat		*
45000 cat		*
45000 cat		*
45000 cat		*
45000 cat		*
45000 cat		*
45000 cat		*
45000 cat		*
45000 cat		*
45000 cat		*
45000 cat		*
45000 cat		*
45000 cat		*
45000 cat		*
45000 cat		*
45000 cat		*
45000 cat		*
45000 cat		*
45000 cat		*
45000 cat		*
45000 cat		*
45000 cat		*
45000 cat		*
45000 cat		*
45000 cat		*
45000 cat		*
45000 cat		*
45000 cat		
45000 cat		*
cat 450000	*	
cat 450000	*	
cat 450000	*	
cat 450000	*	
cat 450000	*	

cat 450000	*	
cat 450000	*	
cat 450000	*	
cat 450000	*	
cat 450000	*	
cat 450000	*	
cat 450000	*	
cat 450000	*	
cat 450000	*	
cat 450000	*	
cat 450000	*	
cat 450000	*	
cat 450000	*	
cat 450000	*	
cat 450000	*	
cat 450000	*	
cat 450000	*	
cat 450000	*	
cat 450000	*	
cat 450000	*	
cat 450000	*	
cat 450000	*	
cat 450000	*	
45 der		*
45 der		*
45 der		*
45 der		*
45 der		*
45 der		*
45 der		*
45 der		*
45 der		*
45 der		*
45 der		*
45 der		*
45 der		
45 der		*
45 der		*
45 der		*
45 der		*
45 der		*
45 der		*
45 der		*
45 der		*
45 der		*
45 der		*
45 der		*
45 der		
45 der		*
45 der		*

45 der		*
45 der		*
45 der		*
45 der		*
45 der		*
45 der		*
45 der		*
45 der		*
45 der		*
45 der		*
45 der		*
45 der		*
45 der		*
45 der		*
45 der		*
45 der		
45 der		*
45 der		*
45 der		*
45 der		*
45 der		*
450 der		*
450 der		*
450 der		*
450 der		*
450 der		*
450 der		*
450 der		*
450 der		*
450 der		*
450 der		*
450 der		*
450 der		*
450 der		*
450 der		*
450 der		*
450 der		*
450 der		*
450 der		*
450 der		*
450 der		*
450 der		*
450 der		*
450 der		*
450 der		*
450 der		*
450 der		
450 der		*
450 der		*
450 der		*
450 der		*

450 der		*
450 der		*
450 der		*
450 der		*
450 der		*
450 der		*
450 der		
450 der		*
450 der		*
450 der		*
450 der		*
450 der		*
450 der		*
450 der		*
450 der		*
450 der		*
450 der		*
450 der		*
450 der		*
4500 der		*
4500 der		*
4500 der		*
4500 der		*
4500 der		*
4500 der		*
4500 der		*
4500 der		*
4500 der		*
4500 der		*
4500 der		*
4500 der		*
4500 der		*
4500 der		*
4500 der		*
4500 der		*
4500 der		*
4500 der		*
4500 der		*
4500 der		*
4500 der		*
4500 der		*
4500 der		*
4500 der		*
4500 der		*
4500 der		*
4500 der		*
4500 der		*
4500 der		*
4500 der		*
4500 der		*
4500 der		*

4500 der		*
4500 der		*
4500 der		*
4500 der		*
4500 der		*
4500 der		*
4500 der		*
4500 der		*
4500 der		*
4500 der		*
4500 der		*
4500 der		*
4500 der		*
4500 der		*
4500 der		*
4500 der		*
4500 der		*
45000 der		*
45000 der		*
45000 der		*
45000 der		*
45000 der		*
45000 der		*
45000 der		*
45000 der		*
45000 der		*
45000 der		*
45000 der		*
45000 der		*
45000 der		*
45000 der		*
45000 der		*
45000 der		*
45000 der		*
45000 der		*
45000 der		*
45000 der		*
45000 der		*
45000 der		*
45000 der		*
45000 der		*
45000 der		*
45000 der		*
45000 der		*
45000 der		*
45000 der		*
45000 der		*
45000 der		*
45000 der		*
45000 der		*

45000 der		*
45000 der		*
45000 der		*
45000 der		*
45000 der		*
45000 der		*
45000 der		*
45000 der		*
45000 der		*
45000 der		*
45000 der		*
45000 der		*
45000 der		*
45000 der		*
45000 der		*
der 450000	*	
der 450000	*	
der 450000	*	
der 450000	*	
der 450000	*	
der 450000	*	
der 450000	*	
der 450000	*	
der 450000		
der 450000		
der 450000		
der 450000		
der 450000	*	
der 450000	*	
der 450000	*	
der 450000	*	
45 grass		*
45 grass		*
45 grass		*
45 grass		*
45 grass		*
45 grass		*
45 grass		*
45 grass		*
45 grass		*
45 grass		*
45 grass		*
45 grass		*
45 grass		*
45 grass		*
45 grass		*
45 grass		*
45 grass		*
45 grass		*
45 grass		*

45 grass		*
45 grass		*
45 grass		*
45 grass		*
45 grass		*
45 grass		*
45 grass		*
45 grass		*
45 grass		*
45 grass		*
45 grass		*
45 grass		*
45 grass		*
45 grass		*
45 grass		*
45 grass		*
45 grass		*
45 grass		*
45 grass		*
45 grass		*
45 grass		*
45 grass		*
45 grass		*
45 grass		*
45 grass		*
45 grass		*
45 grass		*
45 grass		*
45 grass		*
450 grass		*
450 grass		*
450 grass		*
450 grass		*
450 grass		*
450 grass		*
450 grass		*
450 grass		*
450 grass		*
450 grass		*
450 grass		*
450 grass		*
450 grass		*
450 grass		*
450 grass		*
450 grass		*
450 grass		*
450 grass		*
450 grass		*
450 grass		*
450 grass		*

450 grass		*
450 grass		*
450 grass		*
450 grass		*
450 grass		*
450 grass		*
450 grass		*
450 grass		*
450 grass		*
450 grass		*
450 grass		*
450 grass		*
450 grass		*
450 grass		*
450 grass		*
450 grass		*
450 grass		*
450 grass		*
450 grass		*
450 grass		*
450 grass		*
450 grass		*
450 grass		*
450 grass		*
450 grass		*
450 grass		*
450 grass		*
4500 grass		*
4500 grass		*
4500 grass		*
4500 grass		*
4500 grass		*
4500 grass		*
4500 grass		*
4500 grass		*
4500 grass		*
4500 grass		*
4500 grass		*
4500 grass		*
4500 grass		*
4500 grass		*
4500 grass		*
4500 grass		*
4500 grass		*
4500 grass		*
4500 grass		*
4500 grass		*
4500 grass		*
4500 grass		*
4500 grass		*

4500 grass		*
4500 grass		*
4500 grass		*
4500 grass		*
4500 grass		*
4500 grass		*
4500 grass		*
4500 grass		*
4500 grass		*
4500 grass		*
4500 grass		*
4500 grass		*
4500 grass		*
4500 grass		*
4500 grass		*
4500 grass		*
4500 grass		*
4500 grass		*
4500 grass		*
4500 grass		*
4500 grass		*
4500 grass		*
4500 grass		*
4500 grass		*
4500 grass		*
45000 grass		
45000 grass		
45000 grass		
45000 grass		
45000 grass		*
45000 grass		*
45000 grass		*
45000 grass		*
45000 grass		*
45000 grass		*
45000 grass		*
45000 grass		
45000 grass		*
45000 grass		*
45000 grass		*
45000 grass		*
45000 grass		*
45000 grass		*
45000 grass		*
45000 grass		*
45000 grass		*
45000 grass		*
45000 grass		*
45000 grass		*
45000 grass		

45000 grass		
45000 grass		
45000 grass		
45000 grass		*
45000 grass		*
45000 grass		*
45000 grass		*
45000 grass		
45000 grass		
45000 grass		
45000 grass		
45000 grass		*
45000 grass		*
45000 grass		*
45000 grass		*
grass 450000	*	
grass 450000	*	
grass 450000	*	
grass 450000	*	
grass 450000	*	
grass 450000	*	
grass 450000	*	
grass 450000	*	
grass 450000	*	
grass 450000	*	
grass 450000	*	
grass 450000	*	
grass 450000	*	
grass 450000	*	
grass 450000	*	
grass 450000	*	
45 grass		*
45 grass		*
45 grass		*
45 grass		*
45 grass		*
45 grass		*
45 grass		*

45 grass		*
45 grass		*
45 grass		*
45 grass		*
45 grass		*
45 grass		
45 grass		
45 grass		
45 grass		
45 grass		*
45 grass		*
45 grass		*
45 grass		*
45 grass		*
45 grass		*
45 grass		*
45 grass		*
45 grass		*
45 grass		*
45 grass		*
45 grass		*
450 grass		*
450 grass		*
450 grass		*
450 grass		*
450 grass		*
450 grass		*
450 grass		*
450 grass		*
450 grass		*
450 grass		*
450 grass		*
450 grass		*
450 grass		*
450 grass		*
450 grass		*
450 grass		*
450 grass		*
450 grass		*
450 grass		*
450 grass		*
450 grass		*
450 grass		*
450 grass		*
450 grass		*
450 grass		*
450 grass		*
450 grass		*
450 grass		*
4500 grass		*

4500 grass		*
4500 grass		*
4500 grass		*
4500 grass		*
4500 grass		*
4500 grass		*
4500 grass		*
4500 grass		*
4500 grass		*
4500 grass		*
4500 grass		*
4500 grass		*
4500 grass		*
4500 grass		*
4500 grass		*
4500 grass		*
4500 grass		*
4500 grass		*
4500 grass		*
4500 grass		*
4500 grass		*
4500 grass		*
4500 grass		*
4500 grass		*
4500 grass		*
4500 grass		*
4500 grass		*
4500 grass		*
4500 grass		*
4500 grass		*
4500 grass		*
4500 grass		*
4500 grass		*
4500 grass		*
4500 grass		*
4500 grass		*
4500 grass		*
4500 grass		*
4500 grass		*
45000 grass		*
45000 grass		*
45000 grass		*
45000 grass		*
45000 grass		*
45000 grass		*
45000 grass		*
45000 grass		*
45000 grass		*
45000 grass		*
45000 grass		*

45000 grass		*
45000 grass		*
45000 grass		*
45000 grass		*
45000 grass		*
45000 grass		*
45000 grass		*
45000 grass		*
45000 grass		*
45000 grass		*
45000 grass		*
45000 grass		*
45000 grass		*
45000 grass		*
45000 grass		*
45000 grass		*
45000 grass		*
45000 grass		*
45000 grass		*
45000 grass		*
45000 grass		*
45000 grass		*
45000 grass		*
45000 grass		*
45000 grass		*
45000 grass		*
45000 grass		*
45000 grass		*
45000 grass		*
grass 450000	*	
grass 450000	*	
grass 450000	*	
grass 450000	*	
grass 450000	*	
grass 450000	*	
grass 450000	*	
grass 450000	*	
grass 450000	*	
grass 450000	*	
grass 450000	*	
grass 450000	*	

grass 450000	*	
grass 450000	*	
grass 450000	*	
grass 450000	*	
grass 450000	*	
grass 450000	*	
grass 450000	*	
grass 450000	*	
grass 450000	*	
grass 450000	*	
grass 450000	*	
grass 450000	*	
grass 450000	*	
grass 450000	*	
grass 450000	*	
grass 450000	*	
45 ves		*
45 ves		*
45 ves		*
45 ves		*
45 ves		*
45 ves		*
45 ves		*
45 ves		*
45 ves		*
45 ves		*
45 ves		*
45 ves		*
45 ves		*
45 ves		*
45 ves		*
45 ves		*
45 ves		*
45 ves		*
45 ves		*
45 ves		*
45 ves		*
45 ves		*

45 ves		*
45 ves		*
45 ves		*
45 ves		*
45 ves		*
45 ves		*
45 ves		*
45 ves		*
45 ves		*
45 ves		*
45 ves		*
45 ves		*
45 ves		*
45 ves		*
45 ves		*
45 ves		*
45 ves		*
45 ves		*
45 ves		*
45 ves		*
45 ves		*
45 ves		*
45 ves		
45 ves		
45 ves		
45 ves		
450 ves		*
450 ves		*
450 ves		*
450 ves		*
450 ves		*
450 ves		*
450 ves		*
450 ves		*
450 ves		*
450 ves		*
450 ves		*
450 ves		*
450 ves		*
450 ves		*
450 ves		*
450 ves		*
450 ves		*
450 ves		*
450 ves		*
450 ves		*
450 ves		*
450 ves		*
450 ves		*
450 ves		*

450 ves		*
450 ves		*
450 ves		*
450 ves		*
450 ves		*
450 ves		*
450 ves		*
450 ves		*
450 ves		*
450 ves		*
450 ves		*
450 ves		*
450 ves		*
450 ves		*
450 ves		*
450 ves		*
450 ves		*
450 ves		*
450 ves		*
450 ves		*
450 ves		*
450 ves		*
450 ves		*
450 ves		*
4500 ves		*
4500 ves		*
4500 ves		*
4500 ves		*
4500 ves		*
4500 ves		*
4500 ves		*
4500 ves		*
4500 ves		*
4500 ves		*
4500 ves		*
4500 ves		*
4500 ves		*
4500 ves		*
4500 ves		*
4500 ves		*
4500 ves		*
4500 ves		*
4500 ves		*
4500 ves		*
4500 ves		*
4500 ves		*
4500 ves		*
4500 ves		*
4500 ves		*
4500 ves		*

4500 ves		*
4500 ves		*
4500 ves		*
4500 ves		*
4500 ves		*
4500 ves		*
4500 ves		*
4500 ves		*
4500 ves		*
4500 ves		*
4500 ves		*
4500 ves		*
4500 ves		*
4500 ves		*
4500 ves		*
4500 ves		*
4500 ves		*
4500 ves		*
4500 ves		*
4500 ves		*
4500 ves		*
4500 ves		*
45000 ves		*
45000 ves		*
45000 ves		*
45000 ves		*
45000 ves		*
45000 ves		*
45000 ves		*
45000 ves		*
45000 ves		*
45000 ves		*
45000 ves		*
45000 ves		*
45000 ves		*
45000 ves		*
45000 ves		*
45000 ves		*
45000 ves		*
45000 ves		*
45000 ves		*
45000 ves		*
45000 ves		*
45000 ves		*
45000 ves		*
45000 ves		*
45000 ves		*
45000 ves		*
45000 ves		*
45000 ves		*

45000 ves		*
45000 ves		*
45000 ves		*
45000 ves		*
45000 ves		*
45000 ves		*
45000 ves		*
45000 ves		*
45000 ves		*
45000 ves		*
45000 ves		*
45000 ves		*
ves 450000	*	
ves 450000	*	
ves 450000	*	
ves 450000	*	
ves 450000	*	
ves 450000	*	
ves 450000	*	
ves 450000	*	
ves 450000	*	
ves 450000	*	
ves 450000	*	
ves 450000	*	
ves 450000	*	
ves 450000	*	
ves 450000	*	
ves 450000	*	
ves 450000	*	
ves 450000	*	
ves 450000	*	
ves 450000	*	
ves 450000	*	
ves 450000	*	
ves 450000	*	
ves 450000	*	
ves 450000	*	
ves 450000	*	
ves 450000	*	
ves 450000	*	
ves 450000	*	
ves 450000	*	
ves 450000	*	
ves 450000	*	
ves 450000	*	
ves 450000	*	
ves 450000	*	
ves 450000	*	
ves 450000	*	
ves 450000	*	

ves 450000	*	
ves 450000	*	
45 ves		*
45 ves		*
45 ves		*
45 ves		*
45 ves		*
45 ves		*
45 ves		*
45 ves		*
45 ves		*
45 ves		*
45 ves		*
45 ves		*
45 ves		*
45 ves		*
45 ves		*
45 ves		*
45 ves		*
45 ves		*
45 ves		*
45 ves		*
45 ves		*
45 ves		*
45 ves		*
45 ves		*
45 ves		*
45 ves		*
45 ves		*
45 ves		*
45 ves		*
45 ves		*
45 ves		*
45 ves		*
45 ves		*
45 ves		*
45 ves		*
45 ves		*
45 ves		*
45 ves		*
45 ves		*
45 ves		*
450 ves		*
450 ves		*
450 ves		*
450 ves		*
450 ves		*
450 ves		*
450 ves		*
450 ves		*

450 ves		
450 ves		
450 ves		
450 ves		
450 ves		*
450 ves		*
450 ves		*
450 ves		*
450 ves		*
450 ves		*
450 ves		*
450 ves		*
450 ves		*
450 ves		*
450 ves		*
450 ves		*
450 ves		*
450 ves		*
450 ves		*
450 ves		*
450 ves		
450 ves		*
450 ves		
450 ves		*
450 ves		
450 ves		
450 ves		
450 ves		
450 ves		*
450 ves		*
450 ves		*
450 ves		*
4500 ves		*
4500 ves		*
4500 ves		*
4500 ves		*
4500 ves		*
4500 ves		*
4500 ves		*
4500 ves		*
4500 ves		*
4500 ves		*
4500 ves		*
4500 ves		*
4500 ves		*
4500 ves		*
4500 ves		*
4500 ves		*
4500 ves		*
4500 ves		*

4500 ves		*
4500 ves		*
4500 ves		*
4500 ves		*
4500 ves		*
4500 ves		*
4500 ves		*
4500 ves		*
4500 ves		*
4500 ves		*
4500 ves		*
4500 ves		*
4500 ves		*
4500 ves		*
4500 ves		*
4500 ves		*
4500 ves		*
4500 ves		*
4500 ves		*
4500 ves		*
4500 ves		*
4500 ves		*
45000 ves		*
45000 ves		*
45000 ves		*
45000 ves		*
45000 ves		*
45000 ves		*
45000 ves		*
45000 ves		*
45000 ves		*
45000 ves		*
45000 ves		*
45000 ves		*
45000 ves		*
45000 ves		*
45000 ves		*
45000 ves		*
45000 ves		*
45000 ves		*
45000 ves		*
45000 ves		*
ves 450000		
ves 450000		
ves 450000	*	
ves 450000		
ves 450000	*	
ves 450000	*	
ves 450000	*	
ves 450000	*	

ves 450000	*	
ves 450000	*	
ves 450000	*	
ves 450000	*	
ves 450000	*	
ves 450000	*	
ves 450000	*	
ves 450000	*	
ves 450000	*	
ves 450000	*	
ves 450000	*	
ves 450000	*	
ves 450000	*	
ves 450000	*	
ves 450000	*	
ves 450000	*	
ves 450000	*	
ves 450000	*	
ves 450000	*	
ves 450000	*	
ves 450000	*	
ves 450000	*	
ves 450000	*	
ves 450000	*	
ves 450000	*	
ves 450000	*	
ves 450000	*	
ves 450000	*	
ves 450000	*	
ves 450000	*	
ves 450000	*	
ves 450000	*	
45 ves		*
45 ves		*
45 ves		*
45 ves		*
45 ves		*
45 ves		*
45 ves		*
45 ves		*
45 ves		*
45 ves		*
45 ves		*
45 ves		*
45 ves		*
45 ves		*
45 ves		*
45 ves		*
45 ves		*
45 ves		*

45 ves		*
45 ves		*
45 ves		*
45 ves		*
45 ves		*
45 ves		*
45 ves		*
45 ves		*
45 ves		*
45 ves		*
45 ves		
45 ves		*
45 ves		
45 ves		
45 ves		*
45 ves		*
45 ves		*
45 ves		*
45 ves		*
45 ves		*
45 ves		*
45 ves		*
450 ves		*
450 ves		*
450 ves		*
450 ves		*
450 ves		*
450 ves		*
450 ves		*
450 ves		*
450 ves		*
450 ves		*
450 ves		*
450 ves		*
450 ves		*
450 ves		*
450 ves		*
450 ves		*
450 ves		*
450 ves		*
450 ves		*
450 ves		*
450 ves		*
450 ves		*
450 ves		*
450 ves		*
450 ves		*
450 ves		*
450 ves		*
450 ves		*

450 ves		*
450 ves		*
450 ves		*
450 ves		*
450 ves		*
450 ves		*
450 ves		*
450 ves		*
450 ves		*
450 ves		*
450 ves		*
450 ves		*
4500 ves		*
4500 ves		*
4500 ves		*
4500 ves		*
4500 ves		*
4500 ves		*
4500 ves		*
4500 ves		*
4500 ves		*
4500 ves		*
4500 ves		*
4500 ves		*
4500 ves		*
4500 ves		*
4500 ves		*
4500 ves		*
4500 ves		*
4500 ves		*
4500 ves		*
4500 ves		*
4500 ves		*
4500 ves		*
4500 ves		*
4500 ves		*
4500 ves		*
4500 ves		*
4500 ves		*
4500 ves		*
4500 ves		*
4500 ves		*
4500 ves		*
4500 ves		*
4500 ves		*
4500 ves		*
4500 ves		*
4500 ves		*
4500 ves		*
4500 ves		*

4500 ves		*
4500 ves		*
45000 ves		*
45000 ves		*
45000 ves		*
45000 ves		*
45000 ves		*
45000 ves		*
45000 ves		*
45000 ves		*
45000 ves		*
45000 ves		*
45000 ves		*
45000 ves		*
45000 ves		*
45000 ves		*
45000 ves		*
45000 ves		*
45000 ves		*
45000 ves		*
45000 ves		*
45000 ves		*
45000 ves		*
45000 ves		*
45000 ves		*
45000 ves		*
45000 ves		*
45000 ves		*
45000 ves		*
45000 ves		*
45000 ves		*
45000 ves		*
45000 ves		*
45000 ves		*
45000 ves		*
45000 ves		*
45000 ves		*
45000 ves		*
45000 ves		*
45000 ves		*
45000 ves		*
45000 ves		*
ves 450000	*	
ves 450000	*	
ves 450000	*	
ves 450000	*	
ves 450000	*	
ves 450000	*	
ves 450000	*	
ves 450000	*	

ves 450000	*	
ves 450000	*	
ves 450000	*	
ves 450000	*	
ves 450000	*	
ves 450000	*	
ves 450000	*	
ves 450000	*	
ves 450000	*	
ves 450000	*	
ves 450000	*	
ves 450000	*	
ves 450000	*	
ves 450000	*	
ves 450000	*	
ves 450000	*	
ves 450000	*	
ves 450000	*	
ves 450000	*	
ves 450000	*	
ves 450000	*	
ves 450000	*	
ves 450000	*	
ves 450000	*	
ves 450000	*	
ves 450000	*	
ves 450000	*	
ves 450000	*	
ves 450000	*	
ves 450000	*	
ves 450000	*	
ves 450000	*	
4500 cat		*
4500 cat		*
4500 cat		*
4500 cat		*
4500 cat		*
4500 cat		*
4500 cat		*
4500 cat		*
45 cat		*
45 cat		*
45 cat		*
45 cat		*
45 cat		*
45 cat		*
45 cat		*
45 cat		*
450 cat		*
450 cat		*

450 cat		*
450 cat		*
4500 cat		*
4500 cat		*
4500 cat		*
4500 cat		*
4500 cat		*
4500 cat		*
4500 cat		*
4500 cat		*
45000 cat		*
45000 cat		*
45000 cat		*
45000 cat		*
45 der		*
45 der		*
45 der		*
45 der		*
45 der		*
45 der		*
45 der		*
45 der		*
45 der		*
45 der		*
45 der		*
45 der		*
45 der		*
45 der		*
45 der		*
45 der		*
45 der		*
45 der		*
45 der		*
45 der		*
450 der		*
450 der		*
450 der		*
450 der		*
450 der		
450 der		*
450 der		*
450 der		*
450 der		
450 der		*
450 der		*
450 der		*
450 der		*
450 der		*
450 der		*
450 der		*

4500 der		*
4500 der		*
4500 der		*
4500 der		*
4500 der		*
4500 der		*
4500 der		*
4500 der		*
4500 der		*
4500 der		*
4500 der		*
4500 der		
45000 der		*
45000 der		*
45000 der		*
45000 der		*
45000 der		*
45000 der		*
45000 der		
45000 der		*
45000 der		*
45000 der		*
45000 der		*
45000 der		*
45000 der		*
45000 der		*
45000 der		*
45000 der		*
45 grass		*
45 grass		*
45 grass		*
45 grass		*
45 grass		*
45 grass		*
45 grass		*
45 grass		*
45 grass		*
45 grass		*
45 grass		*
45 grass		*
45 grass		*
45 grass		*
45 grass		*
45 grass		*
45 grass		*
45 grass		*
45 grass		*
45 grass		*
45 grass		*
45 grass		*

45 grass		*
45 grass		*
45 grass		*
45 grass		*
45 grass		*
45 grass		*
450 grass		*
450 grass		*
450 grass		*
450 grass		*
450 grass		*
450 grass		*
450 grass		*
450 grass		*
450 grass		*
450 grass		*
450 grass		*
450 grass		*
450 grass		*
450 grass		*
450 grass		*
450 grass		*
450 grass		*
450 grass		*
450 grass		*
450 grass		*
450 grass		*
450 grass		*
450 grass		*
450 grass		*
450 grass		*
450 grass		*
450 grass		*
450 grass		*
4500 grass		*
4500 grass		*
4500 grass		*
4500 grass		*
4500 grass		*
4500 grass		*
4500 grass		*
4500 grass		*
4500 grass		*
4500 grass		*
4500 grass		*
4500 grass		*
4500 grass		*
4500 grass		*
4500 grass		*
4500 grass		*

4500 grass		*
4500 grass		*
4500 grass		*
4500 grass		*
4500 grass		*
4500 grass		*
4500 grass		*
4500 grass		*
45000 grass		*
45000 grass		*
45000 grass		*
45000 grass		*
45000 grass		*
45000 grass		*
45000 grass		*
45000 grass		*
45 ves		*
45 ves		*
45 ves		*
45 ves		*
45 ves		*
45 ves		*
45 ves		*
45 ves		*
45 ves		*
45 ves		*
45 ves		*
45 ves		*
45 ves		*
45 ves		*
45 ves		*
45 ves		*
45 ves		*
45 ves		*
45 ves		*
45 ves		*
45 ves		*
45 ves		*
45 ves		*
45 ves		*
450 ves		*
450 ves		*
450 ves		*
450 ves		*
450 ves		*
450 ves		*
450 ves		*
450 ves		*
450 ves		*
450 ves		*

450 ves		*
450 ves		*
450 ves		*
450 ves		*
450 ves		*
450 ves		*
4500 ves		*
4500 ves		*
4500 ves		*
4500 ves		*
4500 ves		*
4500 ves		*
4500 ves		*
4500 ves		*
4500 ves		*
4500 ves		*
4500 ves		*
4500 ves		*
4500 ves		*
4500 ves		*
4500 ves		*
4500 ves		*
4500 ves		*
4500 ves		*
4500 ves		*
4500 ves		*
4500 ves		*
4500 ves		*
4500 ves		*
4500 ves		*
45000 ves		*
45000 ves		*
45000 ves		*
45000 ves		*

45000 ves		*
45000 ves		*
45000 ves		*
45000 ves		*
45000 ves		*
45000 ves		*
45000 ves		*
45000 ves		*
45000 ves		*
45000 ves		*
45000 ves		*
ves 450000	*	
ves 450000	*	
ves 450000	*	
ves 450000	*	
ves 450000	*	
ves 450000	*	
ves 450000	*	
ves 450000	*	
ves 450000	*	
ves 450000	*	
ves 450000	*	
ves 450000	*	
ves 450000	*	
ves 450000	*	
ves 450000	*	
ves 450000	*	
ves 450000	*	
ves 450000	*	
45 ves		*
45 ves		*
45 ves		*
45 ves		*

45 ves		*
45 ves		*
45 ves		*
45 ves		*
450 ves		*
450 ves		*
450 ves		*
450 ves		*
450 ves		*
450 ves		*
450 ves		*
450 ves		*
450 ves		*
450 ves		*
4500 ves		*
4500 ves		*
4500 ves		*
4500 ves		*
4500 ves		*
4500 ves		*
4500 ves		*
4500 ves		*
4500 ves		*
ves 450000	*	
ves 450000	*	
ves 450000	*	
ves 450000	*	
ves 450000	*	
ves 450000	*	
ves 450000	*	
ves 450000	*	
ves 450000	*	
45 ves		
45 ves		
45 ves		

45 ves		
45 ves		*
45 ves		*
45 ves		*
45 ves		*
450 ves		*
450 ves		*
450 ves		*
450 ves		*
450 ves		*
450 ves		*
450 ves		*
450 ves		*
450 ves		*
4500 ves		*
4500 ves		*
4500 ves		*
4500 ves		*
4500 ves		*
4500 ves		*
4500 ves		*
4500 ves		*
4500 ves		*
45000 ves		*
45000 ves		*
45000 ves		*
45000 ves		*
45000 ves		*
45000 ves		*
45000 ves		*
45000 ves		*
45000 ves		*

Appendix E in chapter VII

Classification of different vaccines at concentration of 450,000 SQ

A—api, C—cat, D—der, G—grass, and V—vespula, (SIMCA results at 95% confidence level).

Sample	A	C	D	G	V	API	*					API	*					CAT		*			
API	*					API	*					API	*					CAT		*			
API	*					API	*					API	*					CAT		*			
API	*					API	*					API	*					CAT		*			
API	*					API	*					API	*					CAT		*			
API	*					API						API	*					CAT		*			
API	*					API	*					API	*					CAT		*			
API	*					API	*					API	*					CAT		*			
API	*					API	*					API	*					CAT		*			
API	*					API	*					API	*					CAT		*			
API	*					API	*					API	*					CAT		*			
API	*					API	*					API	*					CAT		*			
API	*					API	*					API	*					CAT		*			
API	*					API	*					API	*					CAT		*			
API	*					API	*					API	*					CAT		*			
API	*					API	*					API						CAT		*			
API	*					API	*					API	*					CAT		*			
API	*					API	*					API	*					CAT		*			
API	*					API	*					API	*					CAT		*			
API	*					API	*					API	*					CAT		*			
API	*					API	*					API	*					CAT		*			
API	*					API	*					API	*					CAT		*			
API	*					API	*					API	*					CAT		*			
API	*					API	*					API	*					CAT		*			
API	*					API						API	*					CAT		*			
API	*					API						API	*					CAT		*			
API	*					API	*					API	*					CAT		*			
API	*					API	*					API	*					CAT		*			
API	*					API	*					API	*					CAT		*			
API	*					API	*					API	*					CAT					
API	*					API	*					API	*					CAT		*			
API	*					API	*					API	*					CAT		*			
API	*					API	*					API	*					CAT		*			
API	*					API	*					API	*					CAT		*			
API	*					API						API	*					CAT		*			
API	*					API	*					CAT		*				CAT		*			
API	*					API	*					CAT		*				CAT		*			
API	*					API	*					CAT		*				CAT		*			
API	*					API	*					CAT		*				CAT		*			
API	*					API	*					CAT		*				CAT		*			
API	*					API	*					CAT		*				CAT		*			
API	*					API	*					CAT		*				CAT		*			
API	*					API	*					CAT		*				CAT		*			
API	*					API	*					CAT		*				CAT		*			
API	*					API	*					CAT		*				CAT		*			
API	*					API	*					CAT		*				CAT		*			
API	*					API	*					CAT		*				CAT		*			

CAT		*			
CAT		*			
CAT		*			
CAT		*			
CAT		*			
CAT		*			
CAT		*			
CAT		*			
CAT		*			
DER			*		
DER			*		
DER			*		
DER			*		
DER			*		
DER			*		
DER			*		
DER			*		
DER			*		
DER			*		
DER			*		
DER			*		
DER			*		
DER			*		
DER			*		
DER			*		
GRA					
GRA				*	
GRA				*	
GRA					
GRA				*	
GRA				*	
GRA				*	
GRA				*	
GRA				*	
GRA				*	
GRA				*	
GRA				*	
GRA				*	
GRA				*	
GRA				*	
GRA				*	
GRA				*	
GRA				*	
GRA				*	
GRA				*	
GRA				*	
GRA				*	
GRA				*	
GRA				*	

GRA				*	
GRA				*	
GRA				*	
GRA				*	
GRA				*	
GRA				*	
GRA				*	
GRA				*	
GRA				*	
GRA					
GRA				*	
GRA				*	
GRA				*	
GRA				*	
GRA				*	
GRA				*	
GRA				*	
GRA				*	
GRA				*	
VES					*
VES					*
VES					*
VES					*
VES					*
VES					*
VES					*
VES					*
VES					*
VES					*
VES					*
VES					*
VES					*
VES					*
VES					*
VES					*
VES					*
VES					*
VES					*
VES					*
VES					*
VES					*
VES					*
VES					*
VES					*
VES					*
VES					*
VES					*
VES					*
VES					*
VES					*

VES					*
VES					*
VES					*
VES					*
VES					*
VES					*
VES					*
VES					*
VES					*
VES					*
VES					*
VES					*
VES					*
VES					*
VES					*
VES					*
VES					*
VES					*
VES					*
VES					*
VES					*
VES					*
VES					*
VES					*
VES					*
VES					*
VES					*
VES					*
VES					*
VES					*
VES					*
VES					*
VES					*
VES					*
VES					*
VES					*
VES					*
VES					*
VES					*
VES					*
VES					*
VES					*
VES					*
VES					*
VES					*
VES					*
VES					*
VES					*
VES					*
VES					*

VES					*
VES					*
VES					*
VES					*
VES					*
VES					*
VES					*
VES					*
VES					*
VES					*
VES					*
VES					*
VES					*
VES					*
VES					*
VES					*
VES					*
VES					*
VES					*
VES					*
VES					*
VES					*
VES					*
VES					*
VES					*
VES					*
VES					*
VES					*
VES					*
VES					*
VES					*
VES					*
VES					*
VES					*
VES					*
VES					*
VES					*
VES					*
VES					*
VES	*				
API	*				
API	*				
API	*				
API	*				
API	*				
API	*				
API	*				
API	*				
API	*				
API	*				

API	*				
API					
API					
API	*				
API					
API	*				
API	*				
API	*				
API	*				
API	*				
API	*				
API	*				
API	*				
API	*				
API	*				
API	*				
API	*				
API	*				
API	*				
API	*				
API	*				
API	*				
API	*				
API	*				
API	*				
API	*				
API	*				
API	*				
API	*				
API	*				
API	*				
API	*				
API	*				
API	*				
API	*				
API	*				
API	*				
VES					*
VES					*
VES					*
VES					*
VES					*
VES					*
VES					*
VES					*
VES					*
VES					*
VES					*
VES					*
VES					*

VES					*
VES					*
VES					*
VES					*
VES					*
VES					*
VES					*
VES					*
VES					*
VES					*
VES					*

Appendix F in chapter VII

Classification of three batches of vespula vaccines at concentration 450,000 SQ

The second number in the sample names indicates batch number: 1—0000031223-7; 2—0000040986-1633; 3—0000052716-20. (SIMCA results at 95% confidence level).

Samples	Batch numbers		
	1	2	3
41VES1A	*		
41VES1B	*		
41VES1C	*		
41VES1D	*		
41VES2A	*		
41VES2B	*		
41VES2C	*		
41VES2D	*		
41VES3A	*		
41VES3B	*		
41VES3C	*		
41VES3D	*		
41VES4A	*		
41VES4B	*		
41VES4C	*		
41VES4D	*		
41VES5A	*		
41VES5B	*		
41VES5C	*		
41VES5D	*		
41VES6A	*		
41VES6B	*		
41VES6C	*		
41VES6D	*		
41VES7A	*		
41VES7B	*		
41VES7C	*		
41VES7D	*		
41VES8A	*		
41VES8B	*		
41VES8C	*		
41VES8D	*		
41VES9A	*		
41VES9B	*		
41VES9C	*		
41VES9D	*		
41VES10A	*		
41VES10B			
41VES10C	*		
41VES10D	*		
42VES1A		*	
42VES1B		*	
42VES1C		*	
42VES1D		*	
42VES2A		*	
42VES2B		*	
42VES2C		*	
42VES2D		*	
42VES3A		*	
42VES3B		*	
42VES3C		*	
42VES3D		*	
42VES4A		*	
42VES4B		*	
42VES4C		*	
42VES4D		*	
42VES5A		*	
42VES5B		*	
42VES5C		*	
42VES5D		*	
42VES6A		*	
42VES6B		*	
42VES6C		*	
42VES6D		*	
42VES7A		*	
42VES7B		*	
42VES7C		*	
42VES7D		*	
42VES8A		*	
42VES8B		*	
42VES8C		*	
42VES8D		*	
42VES10A		*	
42VES10B		*	
42VES10C		*	
42VES10D		*	
43VES1A			*
43VES1B			*
43VES1C			*
43VES1D			*
43VES2A			*
43VES2B			*
43VES2C			*
43VES2D			*
43VES3A			*
43VES3B			*
43VES3C			*
43VES3D			*
43VES4A			*
43VES4B			*
43VES4C			*
43VES4D			*
43VES5A			*
43VES5B			*
43VES5C			*
43VES5D			*
43VES6A			*
43VES6B			*
43VES6C			*
43VES6D			*
43VES7A			*
43VES7B			*
43VES7C			*
43VES7D			*
43VES8A			*
43VES8B			*
43VES8C			*
43VES8D			*
43VES9A			*
43VES9B			*
43VES9C			*
43VES9D			*
43VES10A			*
43VES10B			*
43VES10C			*
43VES10D			*
41VES11A	*		
41VES11B	*		
41VES11C	*		
41VES11D	*		
41VES12A	*		
41VES12B	*		
41VES12C	*		
41VES12D	*		
41VES13A	*		
41VES13B	*		
41VES13C	*		
41VES13D	*		
41VES14A			
41VES14B	*		
41VES14C	*		
41VES14D	*		
42VES11A		*	
42VES11B		*	
42VES11C		*	

42VES11D		*	
42VES12A		*	
42VES12B		*	
42VES12C		*	
42VES12D		*	

Appendix G in chapter VII

Classification of three batches of vespula vaccines at concentration of 45,000 SQ

The second number in the sample names indicates batch number: 1—0000031223-7; 2—0000040986-1633; 3—0000052716-20. (SIMCA results at 95% confidence level).

Samples	Batch numbers		
	1	2	3
31VES1A	*		
31VES1B	*		
31VES1C	*		
31VES1D	*		
31VES2A	*		
31VES2B	*		
31VES2C	*		
31VES2D	*		
31VES3A	*		
31VES3B	*		
31VES3C	*		
31VES3D	*		
31VES4A	*		
31VES4B	*		
31VES4C	*		
31VES4D	*		
31VES5A	*		
31VES5B	*		
31VES5C	*		
31VES5D	*		
31VES6A	*		
31VES6B	*		
31VES6C	*		
31VES6D	*		
31VES7A	*		
31VES7B	*		
31VES7C	*		
31VES7D	*		
31VES8A	*		
31VES8B	*		
31VES8C	*		
31VES8D	*		
31VES9A	*		
31VES9B	*		
31VES9C	*		
31VES9D	*		
31VES10A	*		
31VES10B	*		
31VES10C	*		
31VES10D	*		
32VES1A			
32VES1B		*	
32VES1C		*	
32VES1D		*	
32VES2A		*	
32VES2B		*	
32VES2C		*	
32VES2D		*	
32VES3A		*	
32VES3B		*	
32VES3C		*	
32VES3D		*	
32VES4A		*	
32VES4B		*	
32VES4C		*	
32VES4D		*	
32VES5A		*	
32VES5B		*	
32VES5C			
32VES5D		*	
33VES1A			*
33VES1B			*
33VES1C			*
33VES1D			*
33VES2A			*
33VES2B			*
33VES2C			*
33VES2D			*
33VES3A			*
33VES3B			*
33VES3C			*
33VES3D			*
33VES4A			*
33VES4B			*
33VES4C			*
33VES4D			*
33VES5A			*
33VES5B			*
33VES5C			*
33VES5D			*
33VES6A			*
33VES6B			*
33VES6C			*
33VES6D			*
33VES7A			*
33VES7B			*
33VES7C			*
33VES7D			*
33VES8A			*
33VES8B			*
33VES8C			*
33VES8D			*
33VES9A			*
33VES9B			*
33VES9C			*
33VES9D			*
33VES10A			*
33VES10B			*
33VES10C			*
33VES10D			*

Appendix H in chapter VII

Classification of three batches of api vaccines at 450, 000 SQ

The second number in the sample names indicates batch number: 1—0000030417-21; 2—0000041728-849; 3—0000050932-7. (SIMCA results at 95% confidence level).

Samples	Batch		
	1	2	3
41API1A	*		
41API1B	*		
41API1C	*		
41API1D	*		
41API2A			
41API2B			
41API2C			
41API2D			
41API3A			*
41API3B			*
41API3C			*
41API3D			*
41API4A	*		
41API4B	*		
41API4C	*		
41API4D	*		
41API5A	*		
41API5B	*		
41API5C	*		
41API5D	*		
41API6A	*	*	
41API6B	*		
41API6C	*		
41API6D	*	*	
41API7A	*	*	
41API7B	*	*	
41API7C	*	*	
41API7D	*	*	
41API8A	*		
41API8B	*		
41API8C	*		
41API8D	*		
41API9A			
41API9B			
41API9C			
41API9D			
41API10A	*		
41API10B	*		
41API10C	*		
41API10D	*		
41API11A	*	*	
41API11B	*	*	
41API11C	*	*	
41API11D	*	*	
41API12A	*	*	
41API12B	*		
41API12C	*	*	
41API12D	*	*	
42API1A		*	
42API1B		*	
42API1C		*	
42API1D		*	
42API2A		*	
42API2B		*	
42API2C		*	
42API2D		*	
42API3A		*	
42API3B		*	
42API3C		*	
42API3D		*	
42API4A		*	
42API4B		*	
42API4C		*	
42API4D		*	
42API5A		*	
42API5B		*	
42API5C		*	
42API5D		*	
42API6A		*	
42API6B		*	
42API6C			
42API6D			
42API7A		*	
42API7B		*	
42API7C	*	*	
42API7D		*	
42API8A		*	
42API8B		*	
42API8C		*	
42API8D		*	
42API9A		*	
42API9B		*	
42API9C		*	
42API9D		*	
42API10A		*	
42API10B		*	
42API10C		*	
42API10D		*	
43API1A			*
43API1B			*
43API1C			*
43API1D			*
43API2A			*
43API2B			*
43API2C			*
43API2D			*
43API3A			*
43API3B			*
43API3C			*
43API3D			*
43API4A			*
43API4B			*
43API4C			*
43API4D			*
43API5A			*
43API5B			*
43API5C			*
43API5D			*
43API6A			*
43API6B			*
43API6C			*
43API6D			*
43API7A			*
43API7B			*
43API7C			*
43API7D			*
43API8A			*
43API8B			*
43API8C			*
43API8D			*
43API9A			*
43API9B			*
43API9C			*
43API9D			*
43API10A			*
43API10B			*
43API10C			*
43API10D			*
41API13A	*	*	
41API13B	*	*	
41API13C	*	*	
41API13D	*	*	
41API14A			
41API14B	*	*	
41API14C	*		
41API14D	*		
41API15A			
41API15B			
41API15C	*		
41API15D	*		
41API16A		*	
41API16B		*	
41API16C		*	
41API16D		*	
41API17A	*		
41API17B	*		
41API17C	*		
41API17D	*		
41API18A	*		
41API18B	*		
41API18C	*		
41API18D	*		
41API19A	*		
41API19B	*		
41API19C	*		
41API19D	*		
41API20A	*		
41API20B	*		
41API20C	*		
41API20D	*	*	
41API21A			
41API21B	*		
41API21C	*		
41API21D			
41API22A			
41API22B			
41API22C	*		
41API22D	*		
42API11A		*	
42API11B		*	
42API11C		*	
42API11D		*	
42API12A		*	
42API12B		*	
42API12C			
42API12D		*	
43API11A			*
43API11B			*
43API11C			*
43API11D			*
43API12A			

43API12B			
43API12C			
43API12D			

Appendix I in chapter VII

Classification of two batches of cat vaccines at concentration of 450,000 SQ

The second number in the sample names indicates batch number: 1—0000032114-9; 2—0000045531-5. (SIMCA results at 95% confidence level).

Samples	Batch number	
	00000 32114-9	00000 45531-5
41CAT1-0	*	
41CAT1-1	*	
41CAT1-2	*	
41CAT1-9	*	
41CAT2-0	*	
41CAT2-1	*	
41CAT2-2	*	
41CAT2-9	*	
41CAT3-0		
41CAT3-1		
41CAT3-2		
41CAT3-9		
41CAT4-0	*	
41CAT4-1	*	
41CAT4-2	*	
41CAT4-9	*	
41CAT5-0	*	
41CAT5-1	*	
41CAT5-2	*	
41CAT5-9	*	
41CAT6-0	*	
41CAT6-1	*	
41CAT6-2	*	
41CAT6-9	*	
41CAT7-0	*	
41CAT7-1	*	
41CAT7-2	*	
41CAT7-9	*	
41CAT8-0	*	
41CAT8-1	*	
41CAT8-2	*	
41CAT8-9	*	
41CAT9-0	*	
41CAT9-1	*	
41CAT9-2	*	
41CAT9-9	*	
41CAT100	*	
41CAT101	*	
41CAT102	*	
41CAT109	*	
42CAT1-0		*
42CAT1-1		*
42CAT1-2		*
42CAT1-9		*
42CAT2-0		*
42CAT2-1		*
42CAT2-2		*
42CAT2-9		*
42CAT3-0		*
42CAT3-1		*
42CAT3-2		*
42CAT3-9		*
42CAT4-0		*
42CAT4-1		*
42CAT4-2		*
42CAT4-9		*
42CAT5-0		*
42CAT5-1		*
42CAT5-2		*
42CAT5-9		*
42CAT6-0		*
42CAT6-1		*
42CAT6-2		*
42CAT6-9		*
42CAT7-0		*
42CAT7-1		*
42CAT7-2		*
42CAT7-9		*

Appendix J in chapter VII

Classification of two batches of cat vaccines at concentration of 45,000 SQ

The second number in the sample names indicates batch number: 1—0000032114-9; 2—0000045531-5. (SIMCA results at 95% confidence level).

Samples	Batch numbers	
	00000 332115-9	00000 45531-5
31CAT1-0	*	
31CAT1-1	*	
31CAT1-2	*	
31CAT1-9	*	
31CAT2-0	*	
31CAT2-1	*	
31CAT2-2	*	
31CAT2-9	*	
31CAT3-0	*	
31CAT3-1	*	
31CAT3-2	*	
31CAT3-9	*	
31CAT4-0	*	
31CAT4-1	*	
31CAT4-2	*	
31CAT4-9	*	
31CAT5-0	*	
31CAT5-1	*	
31CAT5-2	*	
31CAT5-9	*	
31CAT6-0	*	
31CAT6-1	*	
31CAT6-2	*	
31CAT6-9	*	
31CAT7-0	*	
31CAT7-1	*	
31CAT7-2	*	
31CAT7-9	*	
31CAT8-0	*	
31CAT8-1	*	
31CAT8-2	*	
31CAT8-9	*	
31CAT9-0	*	
31CAT9-1	*	
31CAT9-2	*	
31CAT9-9	*	
32CAT1-0		*
32CAT1-1		*
32CAT1-2		*
32CAT1-9		*
32CAT2-0		*
32CAT2-1		*
32CAT2-2		*
32CAT2-9		*
32CAT3-0		*
32CAT3-1		*
32CAT3-2		*
32CAT3-9		*
32CAT4-0		*
32CAT4-1		*
32CAT4-2		*
32CAT4-9		*
32CAT5-0		*
32CAT5-1		*
32CAT5-2		*
32CAT5-9		*
32CAT6-0		*
32CAT6-1		*
32CAT6-2		*
32CAT6-9		*
32CAT7-0		*
32CAT7-1		*
32CAT7-2		*
32CAT7-9		*
32CAT8-0		*
32CAT8-1		
32CAT8-2		
32CAT8-9		*
32CAT9-0		*
32CAT9-1		*
32CAT9-2		*
32CAT9-9		*
32CAT100		*
32CAT101		*
32CAT102		
32CAT109		*
32CAT110		*
32CAT111		*
32CAT112		*
32CAT119		*

Appendix K in chapter VII

Classification of two batches of cat vaccines at concentration of 4,500 SQ

The second number in the sample names indicates batch number: 1—0000032114-9; 2—0000045531-5. (SIMCA results at 95% confidence level).

Samples	Batch numbers	
	00000 32114-9	00000 45531-5
21CAT1-0	*	
21CAT1-1	*	
21CAT1-2	*	
21CAT1-9	*	
21CAT2-0	*	
21CAT2-1	*	
21CAT2-2	*	
21CAT2-9	*	
21CAT3-0	*	
21CAT3-1	*	
21CAT3-2	*	
21CAT3-9	*	*
21CAT4-0	*	
21CAT4-1	*	
21CAT4-2	*	
21CAT4-9	*	
21CAT5-0	*	
21CAT5-1	*	
21CAT5-2	*	
21CAT5-9	*	
21CAT6-0	*	
21CAT6-1	*	
21CAT6-2	*	
21CAT6-9	*	
21CAT7-0	*	
21CAT7-1	*	
21CAT7-2	*	
21CAT7-9	*	
21CAT8-0	*	
21CAT8-1	*	
21CAT8-2	*	
21CAT8-9	*	
21CAT9-0	*	
21CAT9-1	*	
21CAT9-2	*	
21CAT9-9	*	
21CAT100	*	
21CAT101	*	
21CAT102	*	
21CAT109	*	
22CAT1-0		
22CAT1-1		*
22CAT1-2		*
22CAT1-9		*
22CAT2-0		*
22CAT2-1		*
22CAT2-2		*
22CAT2-9		
22CAT3-0		*
22CAT3-1		*
22CAT3-2		*
22CAT3-9		*
22CAT4-0		*
22CAT4-1		*
22CAT4-2		*
22CAT4-9		*
22CAT5-0		*
22CAT5-1		*
22CAT5-2		*
22CAT5-9		*
22CAT6-0		*
22CAT6-1		*
22CAT6-2		*
22CAT6-9		*
22CAT7-0		*
22CAT7-1		*
22CAT7-2		*
22CAT7-9		*
22CAT8-0		*
22CAT8-1		*
22CAT8-2		*
22CAT8-9		*
22CAT9-0		
22CAT9-1		
22CAT9-2		
22CAT9-9		
22CAT100		*
22CAT101		*
22CAT102		*
22CAT109		*
21CAT110	*	
21CAT111	*	
21CAT112	*	
21CAT119	*	
21CAT120	*	
21CAT121	*	
21CAT122	*	
21CAT129	*	
22CAT110	*	*
22CAT111		*
22CAT112		*
22CAT119		*
22CAT120		
22CAT121		
22CAT122		
22CAT129		

Appendix L in chapter VII

Classification of two batches of cat vaccines at concentration of 450 SQ

The second number in the sample names indicates batch number: 1—0000032114-9; 2—0000045531-5. (SIMCA results at 95% confidence level).

Samples	Batch number	
	00000 32115-9	00000 45531-5
11CAT1-0	*	
11CAT1-1	*	
11CAT1-2	*	
11CAT1-9	*	
11CAT2-0	*	
11CAT2-1	*	
11CAT2-2	*	
11CAT2-9	*	
11CAT3-0	*	
11CAT3-1	*	
11CAT3-2	*	
11CAT3-9	*	
11CAT4-0	*	
11CAT4-1	*	
11CAT4-2	*	
11CAT4-9	*	
11CAT5-0	*	
11CAT5-1	*	
11CAT5-2	*	
11CAT5-9	*	
11CAT6-0	*	
11CAT6-1	*	
11CAT6-2	*	*
11CAT6-9	*	
12CAT1-0		*
12CAT1-1		*
12CAT1-2		*
12CAT1-9		*
12CAT2-0		*
12CAT2-1		*
12CAT2-2		*
12CAT2-9		*
12CAT4-0		*
12CAT4-1		*
12CAT4-2		*
12CAT4-9		*
12CAT5-0		*
12CAT5-1		*
12CAT5-2		*
12CAT5-9		*
12CAT6-0		*
12CAT6-1		*
12CAT6-2		*
12CAT6-9		*
12CAT7-0		*
12CAT7-1		*
12CAT7-2		*
12CAT7-9		*
12CAT8-0		*
12CAT8-1		*
12CAT8-2		*
12CAT8-9		*
12CAT9-0		*
12CAT9-1		*
12CAT9-2		*
12CAT9-9		*
12CAT100		*
12CAT101		*
12CAT102		*
12CAT109		*
12CAT120		*
12CAT121		*
12CAT122		*
12CAT129		*

Appendix M in chapter VII

Classification of two batches of cat vaccines at concentration of 45 SQ

The second number in the sample names indicates batch number: 1—0000032114-9; 2—0000045531-5. (SIMCA results at 95% confidence level).

Samples	Batch number	
	00000 32115-9	00000 45531-5
01CAT1-0	*	
01CAT1-1	*	
01CAT1-2	*	
01CAT1-9	*	
01CAT2-0	*	
01CAT2-1	*	
01CAT2-2	*	
01CAT2-9	*	
01CAT3-0	*	
01CAT3-1	*	
01CAT3-2	*	
01CAT3-9	*	
01CAT4-0	*	
01CAT4-1	*	
01CAT4-2	*	
01CAT4-9	*	
01CAT5-0	*	
01CAT5-1	*	
01CAT5-2	*	
01CAT5-9	*	
01CAT6-0	*	
01CAT6-1	*	
01CAT6-2	*	
01CAT6-9	*	
01CAT7-0	*	
01CAT7-1	*	
01CAT7-2	*	
01CAT7-9	*	
01CAT8-0	*	
01CAT8-1	*	
01CAT8-2	*	
01CAT8-9	*	
01CAT9-0	*	
01CAT9-1	*	
01CAT9-2	*	
01CAT9-9	*	
02CAT1-0	*	*
02CAT1-1	*	*
02CAT1-2	*	*
02CAT1-9	*	*
02CAT2-0		*
02CAT2-1		*
02CAT2-2		*
02CAT2-9		*
02CAT3-0	*	*
02CAT3-1		*
02CAT3-2		*
02CAT3-9	*	*
02CAT4-0	*	*
02CAT4-1	*	*
02CAT4-2	*	*
02CAT4-9	*	*
02CAT5-0		*
02CAT5-1		*
02CAT5-2		*
02CAT5-9		*
02CAT6-0	*	*
02CAT6-1	*	*
02CAT6-2	*	*
02CAT6-9	*	*
02CAT7-0	*	*
02CAT7-1		*
02CAT7-2		*
02CAT7-9		*
02CAT8-0		*
02CAT8-1		*
02CAT8-2		*
02CAT8-9		*
02CAT9-0		*
02CAT9-1		*
02CAT9-2		*
02CAT9-9		*
02CAT100		*
02CAT101		*
02CAT102		*
02CAT109		*
02CAT110		*
02CAT111		*
02CAT112		*
02CAT119		*
02CAT120	*	*
02CAT121		*
02CAT122		*
02CAT129		*

Appendix N in chapter VII

Classification of two batches of grass vaccines at concentration 450,000 SQ

The second number in the sample names indicates batch number: 1—0000032135-40; 3—0000050955-9. (SIMCA results at 95% confidence level).

Sample	Batch number	
	0000032135-40	00000-50955-9
41GRA1A		
41GRA1B		
41GRA1C		
41GRA1D		
41GRA2A	*	
41GRA2B	*	
41GRA2C	*	
41GRA2D	*	
41GRA3A	*	
41GRA3B	*	
41GRA3C	*	
41GRA3D	*	
41GRA4A	*	
41GRA4B	*	
41GRA4C	*	
41GRA4D	*	
42GRA1A		*
42GRA1B		*
42GRA1C		*
42GRA1D		*
42GRA2A		*
42GRA2B		*
42GRA2C		*
42GRA2D		*
42GRA3A		*
42GRA3B		*
42GRA3C		*
42GRA3D		*
42GRA4A		*
42GRA4B		*
42GRA4C		*
42GRA4D		*
42GRA5A		*
42GRA5B		*
42GRA5C		
42GRA5D		*
42GRA6A		*
42GRA6B		*
42GRA6C		*
42GRA6D		*
42GRA7A		*
42GRA7B		*
42GRA7C		*
42GRA7D		*

Appendix O in chapter VII

Classification of two batches of grass vaccines at concentration of 45,000 SQ

The second number in the sample names indicates batch number: 1—0000032135-40; 3—0000050955-9. (SIMCA results at 95% confidence level).

Samples	Batch number	
	00000 32135-40	00000 50955-9
31GRA1A	*	
31GRA1B	*	
31GRA1C	*	
31GRA1D	*	
31GRA2A	*	
31GRA2B	*	
31GRA2C	*	
31GRA2D	*	
31GRA3A	*	
31GRA3B	*	
31GRA3C	*	
31GRA3D	*	
31GRA4A	*	
31GRA4B	*	
31GRA4C	*	
31GRA4D	*	
31GRA5	*	
31GRA5A	*	
31GRA5C	*	
31GRA5D	*	
31GRA6A	*	
31GRA6B	*	
31GRA6C	*	
31GRA6D	*	
31GRA7A	*	
31GRA7B	*	
31GRA7C	*	
31GRA7D	*	
31GRA8A	*	
31GRA8B	*	
31GRA8C	*	
31GRA8D	*	
31GRA9A	*	
31GRA9B	*	
31GRA9C	*	
31GRA9D	*	
31GRA10A	*	
31GRA10B	*	
31GRA10C	*	
31GRA10D	*	
32GRA1A		*
32GRA1B		*
32GRA1C		*
32GRA1D		*
32GRA2A		*
32GRA2B		*
32GRA2C		*
32GRA2D		*
32GRA3A		*
32GRA3B		*
32GRA3C		*
32GRA3D		*
32GRA4A		*
32GRA4B		*
32GRA4C		*
32GRA4D		*
32GRA5A		*
32GRA5B		*
32GRA5C		*
32GRA5D		*
32GRA6A		*
32GRA6B		*
32GRA6C		*
32GRA6D		*
32GRA7A		*
32GRA7B		*
32GRA7C		*
32GRA7D		*
32GRA8A		*
32GRA8B		*
32GRA8C		*
32GRA8D		*
32GRA9A		*
32GRA9B		*
32GRA9C		*
32GRA9D		*
32GRA10A		*
32GRA10B		*
32GRA10C		*
32GRA10D		*
31GRA11A	*	
31GRA11B	*	
31GRA11C	*	
31GRA11D	*	
32GRA11A		*
32GRA11B		*
32GRA11C		*
32GRA11D		*
32GRA12A		*

32GRA12B		*
32GRA12C		
32GRA12D		*

Appendix P in chapter VII

Classification of two batches of grass vaccines at concentration of 4,500 SQ

The second number in the sample names indicates batch number: 1—0000032135-40; 3—0000050955-9. (SIMCA results at 95% confidence level).

Samples	Batch numbers	
	00000 32135-40	00000 50955-9
21GRA1A	*	
21GRA1B	*	
21GRA1C	*	
21GRA1D	*	
21GRA2A	*	
21GRA2B	*	
21GRA2C	*	
21GRA2D	*	
21GRA3A	*	
21GRA3B	*	
21GRA3C	*	
21GRA3D	*	
21GRA4A	*	
21GRA4B	*	
21GRA4C	*	
21GRA4D	*	
21GRA5A	*	
21GRA5B	*	
21GRA5C	*	
21GRA5D	*	
21GRA6A	*	
21GRA6B	*	
21GRA6C	*	
21GRA6D	*	
21GRA7A	*	
21GRA7B	*	
21GRA7C	*	
21GRA7D	*	*
21GRA8A	*	*
21GRA8B	*	*
21GRA8C	*	*
21GRA8D	*	*
21GRA9A	*	
21GRA9B	*	
21GRA9C	*	
21GRA9D	*	
21GRA10A	*	
21GRA10B	*	
21GRA10C	*	
21GRA10D	*	
21GRA11A	*	
21GRA11B	*	
21GRA11C	*	
21GRA11D	*	
21GRA12A	*	
21GRA12B	*	
21GRA12C	*	
21GRA12D	*	
22GRA1A		*
22GRA1B		*
22GRA1C		*
22GRA1D		*
22GRA2A		
22GRA2B		
22GRA2C		
22GRA2D		
22GRA3A		*
22GRA3B		*
22GRA3C		*
22GRA3D		*
22GRA4A		*
22GRA4B		*
22GRA4C		*
22GRA4D		*
22GRA5A		*
22GRA5B		*
22GRA5C		*
22GRA5D		*
22GRA6A		*
22GRA6B		*
22GRA6C		
22GRA6D		*
22GRA7A		*
22GRA7B		*
22GRA7C		*
22GRA7D		*
22GRA8A		*
22GRA8B		*
22GRA8C		*
22GRA8D		*
22GRA9A		*
22GRA9B		*
22GRA9C		*
22GRA9D	*	*
22GRA10A		*
22GRA10B		*
22GRA10C		*
22GRA10D		*
21GRA13A	*	
21GRA13B	*	
21GRA13C	*	
21GRA13D	*	
21GRA14A	*	
21GRA14B	*	
21GRA14C	*	
21GRA14D	*	
21GRA15A	*	
21GRA15B	*	
21GRA15C	*	
21GRA15D	*	
22GRA12A		*
22GRA12B		*
22GRA12C		*
22GRA12D		*

Appendix Q in chapter VII

Classification of two batches of grass vaccines at concentration of 450 SQ

The second number in the sample names indicates batch number: 1—0000032135-40; 3—0000050955-9. (SIMCA results at 95% confidence level).

Samples	Batch numbers	
	00000 32135-40	00000 50955-9
11GRA1A	*	
11GRA1B	*	
11GRA1C	*	
11GRA1D	*	
11GRA2A	*	
11GRA2B	*	
11GRA2C	*	
11GRA2D	*	
11GRA3A	*	
11GRA3B	*	
11GRA3C	*	
11GRA3D	*	
11GRA4A	*	
11GRA4B	*	
11GRA4C	*	
11GRA4D	*	
11GRA5A	*	
11GRA5B	*	
11GRA5C	*	
11GRA5D	*	
11GRA6A	*	
11GRA6B	*	
11GRA6C	*	
11GRA6D	*	
11GRA7A	*	
11GRA7B	*	
11GRA7C	*	
11GRA7D	*	
11GRA8A	*	
11GRA8B	*	
11GRA8C	*	
11GRA8D	*	
11GRA9A	*	
11GRA9B	*	
11GRA9C	*	
11GRA9D	*	
11GRA10A	*	
11GRA10B	*	
11GRA10C	*	
11GRA10D	*	
11GRA11A	*	
11GRA11B	*	
11GRA11C	*	
11GRA11D	*	
11GRA12A	*	
11GRA12B	*	
11GRA12C	*	
11GRA12D	*	
12GRA1A		*
12GRA1B		*
12GRA1C		*
12GRA1D		*
12GRA2A		*
12GRA2B		*
12GRA2C		*
12GRA2D		*
12GRA3A		*
12GRA3B		*
12GRA3C		*
12GRA3D		*
12GRA4A		*
12GRA4B		*
12GRA4C		*
12GRA4D		*
12GRA5A		*
12GRA5B		*
12GRA5C		*
12GRA5D		*
12GRA6A		*
12GRA6B		*
12GRA6C		*
12GRA6D		*
12GRA7A		*
12GRA7B		*
12GRA7C		*
12GRA7D		*
11GRA13A	*	
11GRA13B	*	
11GRA13C	*	
11GRA13D	*	
11GRA14A	*	
11GRA14B	*	
11GRA14C		
11GRA14D		
11GRA15A	*	
11GRA15B	*	
11GRA15C	*	
11GRA15D	*	
11GRA16A	*	
11GRA16B	*	
11GRA16C	*	
11GRA16D	*	
11GRA17A	*	
11GRA17B	*	
11GRA17C	*	
11GRA17D	*	
11GRA18A	*	
11GRA18B	*	
11GRA18C	*	
11GRA18D	*	
11GRA19A	*	
11GRA19B	*	
11GRA19C	*	
11GRA19D	*	
11VES13A		*
11VES13B		*
11VES13C		*
11VES13D		*
11VES14A		*
11VES14B		*
11VES14C		*
11VES14D		*
11VES15A		
11VES15B		
11VES15C		
11VES15D		
11VES16A		
11VES16B		
11VES16C		
11VES16D		

Appendix R in chapter VII

Classification of two batches of grass vaccines at concentration of 45 SQ

The second number in the sample names indicates batch number: 1—0000032135-40; 3—0000050955-9. (SIMCA results at 95% confidence level).

Samples	Batch numbers	
	00000 32135-40	00000 50955-9
01GRA19D	*	
01GRA19C	*	
01GRA19B	*	
01GRA19A	*	
01GRA18D	*	
01GRA18C	*	
01GRA18B	*	
01GRA18A	*	
01GRA17D	*	
01GRA17C	*	
01GRA17B	*	
01GRA17A	*	
01GRA16D	*	
01GRA16C	*	
01GRA16B	*	
01GRA16A	*	
01GRA15D	*	
01GRA15C	*	
01GRA15B	*	
01GRA15A	*	
01GRA14D	*	
01GRA14C	*	
01GRA14B	*	
01GRA14A	*	
01GRA13D	*	
01GRA13C	*	
01GRA13B	*	
01GRA13A	*	
02GRA7D	*	*
02GRA7C	*	*
02GRA7B	*	*
02GRA7A	*	*
02GRA6D	*	*
02GRA6C		*
02GRA6B		*
02GRA6A	*	*
02GRA5D		*
02GRA5C		*
02GRA5B		*
02GRA5A		*
02GRA4D		*
02GRA4C		*
02GRA4B		*
02GRA4A		*
02GRA3D	*	*
02GRA3C	*	*
02GRA3B	*	*
02GRA3A	*	*
02GRA2D		*
02GRA2C		*
02GRA2B		*
02GRA2A		*
02GRA1D		*
02GRA1C		*
02GRA1B		*
02GRA1A		*
01GRA12D	*	
01GRA12C	*	
01GRA12B	*	
01GRA12A	*	
01GRA11D	*	
01GRA11C	*	
01GRA11B	*	
01GRA11A	*	
01GRA10D	*	
01GRA10C	*	
01GRA10B	*	
01GRA10A	*	
01GRA9D	*	
01GRA9C	*	
01GRA9B	*	
01GRA9A	*	
01GRA8D	*	
01GRA8C	*	
01GRA8B	*	
01GRA8A	*	
01GRA7D	*	
01GRA7C	*	
01GRA7B	*	
01GRA7A	*	
01GRA6D	*	
01GRA6C	*	
01GRA6B	*	
01GRA6A	*	
01GRA5D	*	
01GRA5C	*	
01GRA5B	*	
01GRA5A	*	
01GRA4D	*	
01GRA4C	*	
01GRA4B	*	
01GRA4A	*	
01GRA3D	*	
01GRA3C	*	
01GRA3B	*	
01GRA3A	*	
01GRA2D	*	
01GRA2C	*	
01GRA2B	*	
01GRA2A	*	
01GRA1D	*	
01GRA1C	*	
01GRA1B	*	
01GRA1A	*	